ATMOSPHERIC AEROSOL AGING INVOLVING ORGANIC COMPOUNDS AND IMPACTS ON PARTICLE PROPERTIES

A Dissertation

by

CHONG QIU

Submitted to the Office of Graduate Studies of
Texas A&M University
in partial fulfillment of the requirements for the degree of

DOCTOR OF PHILOSOPHY

Approved by:

Chair of Committee,	Renyi Zhang
Committee Members,	Don Collins
	Robert R. Lucchese
	Emile A. Schweikert
Head of Department,	David H. Russell

May 2013

Major Subject: Chemistry

ABSTRACT

In the first part of this dissertation, we study the aging of soot, a representative type of primary aerosols, in the presence of OH-initiated oxidation products of toluene. Monodisperse soot particles are introduced into an environmental chamber where toluene is oxidized by OH radicals. The variations in soot particle properties are simultaneously monitored, including particle size, mass, organic mass faction, hygroscopicity, and optical properties. The changes in particle properties are found to be largely governed by the thickness of the organic coating that is closely related to reaction time and initial reactant concentrations. Derived from particle size and mass, the effective density increases while dynamic shape factor decreases as the organic coating grows, suggesting a compaction of the soot morphology. As the organic coating grows, the particles become more hygroscopic and have enhanced light scattering and absorption.

The second part discusses the potential reactions between amines and some aerosol constituents and alteration of aerosol properties. The reactions between alkylamines and ammonium sulfate/bisulfate have been studied using a low-pressure fast flow reactor coupled to a mass spectrometer at 293 K. Alkylamines react with ammonium sulfate/bisulfate to form alkylaminium sulfates, suggesting the existence of alkylaminium salts in particle phase. We have extended our study to characterize the physicochemical properties of alkylaminium sulfates. The hygroscopicity, thermostability, and density of five representative alkylaminium sulfates have been

measured by an integrated aerosol analytical system. All alkylaminium sulfate aerosols show monotonic size growth when exposed to increasing relative humidity. Mixing ammonium sulfate with alkylaminium sulfates lowers the deliquescence point corresponding to ammonium sulfate. Alkylaminium sulfates are thermally comparable to or more stable than ammonium sulfate. The densities of alkylaminium sulfate particles are lower than that of ammonium sulfate.

Our results suggest that the organic compounds can effectively alter the composition and properties of atmospheric aerosols, considerably influencing the impacts of aerosols on air quality, climate forcing, and human health.

DEDICATION

To my family and friends

ACKNOWLEDGEMENTS

I would like to acknowledge my research advisor and committee chair, Dr. Renyi Zhang, for the opportunity to join his research group and accomplish interesting yet challenging projects. I also wish to thank my committee members, Dr. Don Collins, Dr. Robert Lucchese, and Dr. Emile Schweikert, for their guidance and support during my graduate studies. In addition, I wish to thank the Graduate Advisor, Dr. Simon North, for his help.

I also wish to acknowledge several funding agencies, including the National Science Foundation, the Robert Welch Foundation, and the Texas A&M Research Foundation, for their financial support. Additional support from both the Department of Chemistry and Department of Atmospheric Sciences is also acknowledged.

Special thanks also go to my friend and colleague, Dr. Alexei F. Khalizov, for his help and support. The staff members from both the Chemistry and the Atmospheric Sciences Departments have been very friendly and helpful, making my study at Texas A&M University a great experience.

Finally, I would like to thank to my family for their encouragement and support.

NOMENCLATURE

AS	Ammonium Sulfate
AAS	Alkylaminium Sulfate
ABS	Ammonium Bisulfate
AN	Ammonium Nitrate
APM	Aerosol Particle Mass Analyzer
CPC	Condensation Particle Counter
D_p	Mobility Diameter
D_{ve}	Volume Equivalent Diameter
DEA	Diethylamine
DEAS	Diethylaminium Sulfate
DMAS	Dimethylaminium Sulfate
MMA	Monomethylamine
MMAS	Monomethylaminium Sulfate
SMPS	Scanning Mobility Particle Sizer
TDMA	Tandem Differential Mobility Analyzer
TEA	Triethylamine
TEAS	Triethylaminium Sulfate
TMA	Trimethylamine
TMAS	Trimethylaminium Sulfate
VOC	Volatile Organic Compound

TABLE OF CONTENTS

Page

LIST OF FIGURES

Page

Page

LIST OF TABLES

Page

CHAPTER I

INTRODUCTION

Atmospheric aerosols are microscopic solid/liquid particles suspended in the air.[1] The aerosol size ranges from 3 nm to 10 microns, spanning four orders of magnitudes.[2] It is still unclear about the smallest size of ambient particles, especially those formed from nucleation of gas-phase molecules (critical clusters).[3] For particles larger than 10 microns, the gravitation force becomes too large and the particles are lost through sedimentation process.[2]

Based on their sources of origin, ambient aerosols can be divided in two categories: primary and secondary particles.[4,5] Primary aerosol is emitted into the atmosphere directly from the sources, including natural processes (biogenic sources) and human activities (anthropogenic sources). Particles from biogenic sources include sea salt aerosols from the sprays of the ocean and sea, wax particles from plants and animals, and mineral dust brought up into the air through sandstorm.[2] Examples of anthropogenic sources are vehicle exhaust, plant emission, and construction sites. Some aerosols may have both biogenic and anthropogenic sources. For example, soot aerosols, also known as black carbon, can be produced from wildfire (natural sources) and fossil fuel burning (human activities).[4,6] Secondary aerosols are formed in the gas phase through the nucleation of gaseous molecules, normally including sulfuric acid, water, ammonia, iodine oxides and many other species.[3,7-9] Ammonium nitrate, sulfate and bisulfate are common secondary aerosol constituents.

Once emitted to or formed in the atmosphere, aerosol particles constantly interact with solar radiation, gas-phase molecules and each other, resulting in changes in particle size and composition, which would alter the aerosol properties.[10,11] Several types of interactions between gas molecules and particles have been identified, including physical transformations (condensation and partitioning) and chemical reactions (oxidation of particles by gas-phase oxidants and heterogeneous reactions between gas molecules and particles).[5] For example, when initially formed, soot particles are hydrophobic and fractal in morphology, with low effective density and strong light absorption cross-section.[6] It has been shown that the condensation of gas-phase inorganic and/or organic species on soot aerosols can effectively change the particle composition, significantly increase the particle size, and substantially alter the aerosol hygroscopicity and light absorption.[12,13]

Due to the diverse sources and complicated transformation of atmospheric aerosols, the particle compositions are fairly complex and depend highly on the sources and the aging processes. Sea-salt aerosols are primarily consisted of inorganic salts like sodium chloride, while metal oxides are often found in mineral dusts.[2] Freshly nucleated nanoparticles often contain sulfuric acid and water; other species, such as ammonia, organic acids, and amines can also contribute to the process.[3]

Organic compounds are commonly observed in ambient aerosols, and the mass fraction of particle-phase organics can be as high as 50 wt %.[5] Large quantities of volatile organic compounds (VOCs) are emitted into the atmosphere where they are oxidized further into oxygenated organics, often with lower vapor pressures and ready to

condense or partition into particle phase.[4] Heterogeneous reactions between gas-phase organics and aerosol particles are also observed. Primary and secondary aerosols can interact with the VOCs and their oxidation products, yielding particles with higher organic contents and changed physical/chemical properties. Due to the compliex emission inventory and product matrix of VOCs, it is extremely difficult to identify all the organic species in ambient aerosols by field measurements or modeling work. Accurate determination of ambient aerosol composition remains one of the biggest challenges.[5]

Atmospheric aerosols have significant influence on human health. Aerosols, especially those smaller than 100 nm, can penetrate deeply into human lungs[14] and may effectively deliver toxic chemicals into human body. For example, polyaromatic hydrocarbons (PAHs), often found in the soot particles, are known carcinogens produced from the combustion of hydrocarbons fuels.[2] Incorporation of PAHs in particle phase may facilitate the delivery of these carcinogens into human body. Epidemic studies have suggested that reduction in ambient aerosols loading can effectively reduce the mortality rate and improve the human longevity.[15]

Aerosol particles also have profound impacts on the climate. Particles can affect the climate directly by effectively scattering and absorption of solar radiation.[2] Changes in particle composition may alter the aerosol optical properties and directly disturb the Earth's energy balance. On the other hand, aerosols can also serve as cloud condensation nuclei, facilitating the cloud formation.[16] Modification in aerosol composition can affect the contribution of aerosol particles to the cloud formation and the lifetime and albedo of

clouds, indirectly perturb the global radiation budget (Figure 1). In addition, aerosols also have impacts on atmospheric multi-phase chemical processes and photochemistry.[17] The uncertainty of the contribution of aerosols to the climate change remains the largest among all the factors identified by the Intergovernmental Panel on Climate Change (IPCC).[18]

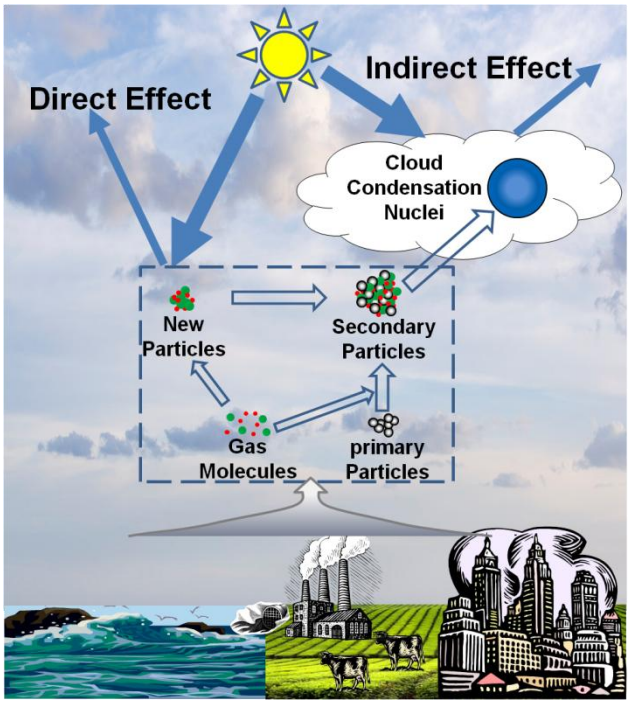

Figure 1. Schematic representation of atmospheric aerosols, their interactions with gas molecules, and contribution to environment and climate.

This dissertation attempts to investigate the physical and chemical interactions between aerosol particles and gas-phase organic compounds. The consequential changes

in aerosol properties and the potential impacts on the environment and climate are also evaluated. The organic compounds selected for this study are toluene and alkylamines. Toluene is a representative secondary organic aerosol precursor, i.e., a compound that does not interact with aerosols directly but its atmospheric degradation products can contribute significantly to the formation of secondary aerosols. Alkylamines, on the other hand, may directly react with aerosols constituents and form new compounds in the particle phase. Two model aerosols are used, namely soot (black carbon) and ammonium salt particles. Soot particles are primary particles that are chemical inert to most of the organic compounds in the atmosphere. As a result, our study on the aging of soot represents the aging processes that primarily involve physical condensation and partitioning. Ammonium salt aerosols, on the contrary, are normally formed in the air and may react with certain types of organic compounds. This dissertation probes the potential chemical aging processes of ammonium salts in the presence of amines, emphasizing the reactions between amines and ammonium sulfate/bisulfate.

In Chapter II, the aging of soot particles in the presence of VOC oxidation products is investigated. The interaction between ammonium sulfate/bisulfate aerosols and alkylamines is discussed in Chapter III, and Chapter IV describes the impacts of particle-phase amines on aerosols properties. Chapter V concludes the results in Chapter II–IV.

CHAPTER II

AGING OF SOOT FROM OH-INITIATED OXIDATION OF TOLUENE[*]

Introduction

Soot aerosols are emitted into the atmosphere from fossil fuel combustion and biomass burning, with an estimated annual emission of ~12 Tg.[4] Fresh soot is hydrophobic and light-absorptive, consisting of chain-like aggregates of spherical primary particles with elemental carbon as the major component.[2,6] Soot undergoes transformation in the atmosphere when exposed to gaseous species, resulting in a dramatic change in their properties. For example, condensation of sulfuric acid on fresh soot has been shown to change the particle morphology, enhance light scattering and absorption, and increase hygroscopicity.[6,13,19,20] Coating of soot with materials that are not light-absorptive has been suggested to enhance single scattering albedo (SSA), light scattering and absorption coefficients in theoretical simulations,[21-24] laboratory experiments,[12,20,25,26] and field observations.[27,28] Also, the changes in the optical properties of soot particles during aging may impact on air photochemistry.[17] Furthermore, increase in hygroscopicity of soot aerosols can significantly modify their potentials to serve as cloud condensation nuclei (CCN).[13] Consequently, aging of soot particles in the atmosphere not only modifies their atmospheric residence time and air chemistry, but also impacts climate directly by scattering and absorbing solar radiation

[*] This chapter is reprinted with permission from Qiu, C.; Khalizov, A. F.; Zhang, R. Soot Aging from OH-Initiated Oxidation of Toluene. *Environmental Science & Technology* **2012**, *46*, 9464. Copyright 2012 American Chemical Society.

and indirectly by influencing cloud formation.[18,29,30] Hence, it is of critical importance to evaluate the aging process of soot particles in the atmosphere to better assess their impacts on air quality, climate forcing, and human health.

VOCs are emitted into the atmosphere in large quantities from both biogenic and anthropogenic sources.[2] Reactions between VOCs and atmospheric oxidants, such as OH and O_3, form products (secondary organic materials, SOMs)[31-33] that may participate in nucleation, condensation, partitioning, and heterogeneous reactions to contribute to the formation of secondary organic aerosol (SOA).[4,5] Because of the ubiquity of soot and SOMs in the atmosphere, it is important to understand their interactions to better evaluate the impacts of SOA formation on soot particle properties. Efforts have been made to evaluate the effects of condensed organics on soot properties by exposing soot aerosols to model compounds, including oleic acid and anthracene,[34] succinic and glutaric acids,[35] and dibutyl phthalate,[26] showing that small structural differences in organic compounds can lead to significant differences in the properties of coated soot.

The environmental chamber has been widely adopted to investigate SOA formation under controllable conditions,[5,36] including several studies using pre-existing poly-disperse soot particles.[37-39] For example, coating on soot particles by α-pinene ozonolysis products has been shown to increase hygroscopicity and restructure the soot core, leading to enhanced optical properties, i.e., higher light scattering and absorption coefficients.[37,38] Changes in soot morphology have been observed for Palas soot exposed to propene ozonolysis products.[39] Also, experiments have been performed to examine the impacts of SOMs from vehicle exhausts on soot particles, when the whole

combustion exhaust from engines was introduced to a chamber, along with oxidants such as OH and/or UV light.[40,41] It has been suggested that particle mass measurements may be more accurate in quantifying organic coating than volume measurements, since condensation of organics may not increase the particle volume significantly but rather fill the voids between primary particles of fresh soot.[40] Hygroscopicity measurements on the basis of particle mobility diameter have been suggested to be strongly affected by changes in morphology of coated soot particles.[41] Those previous results suggest the necessity to evaluate the mass and morphology changes of soot particles, when they are exposed to organic compounds. Note that the previous environmental chamber studies on the effects of organic coating on soot particles have been conducted exclusively using poly-disperse particles, which might lead to complications in assessing the effects of coating on the particle size and other properties. As a result, a modeling procedure was employed to fit the measured size variation to infer the morphology changes of soot particles.[37-39]

Aromatic hydrocarbons are important anthropogenic pollutants, contributing to 20–30% of the total VOCs in urban areas.[42] For example, the urban toluene concentration ranges from 1 to 200 ppb depending on locations and emission sources.[43,44] Aromatics are expected to react exclusively with OH radicals, and numerous experimental and theoretical studied have indicated the formation of a variety of ring-opening (e.g. glyoxal and methylglyoxal) and ring-retaining (e.g. benzaldehyde and cresol) products.[45-49] The SOA formation on pre-existing ammonium sulfate (AS) aerosols from toluene-OH oxidation products has been evaluated with a SOA yield of

30% in low NO_x condition, independent of the initial toluene concentration.[50] Measurements of hygroscopicity of SOAs formed from the toluene-OH reaction have shown a size growth factor of 1.10 at 90% relative humidity (RH).[51]

Since the interaction between soot and oxidation products of toluene represents an important aerosol aging process in the urban atmosphere, experimental studies are required to investigate the SOA formation on soot particles from toluene-OH oxidation products. In the present work, we investigate aging of soot particles because of exposure to the oxidation products from OH-initiated oxidation of toluene. Toluene and monodisperse soot particles are introduced into a collapsible Teflon® chamber, where OH radicals are generated by photolysis of hydrogen peroxide. Particle physical properties, such as mobility size, mass, organic mass fraction, morphology, and hygroscopicity, are determined by two differential mobility analyzers (DMAs), an aerosol particle mass analyzer (APM), and a condensation particle counter (CPC). Aerosol optical properties, including SSA, light absorption and scattering cross sections are measured by a combination of a cavity ring-down spectrometer (CRDS) and a Nephelometer. Real-time monitoring of the particle size and mass is used to derive the dependence of particle effective density and morphology, as a function of the reaction time and thickness of organic coatings on particles. The impacts of organics on the optical and hygroscopic properties of coated soot particles are evaluated.

Experimental

A schematic presentation of the experimental setup is shown in Figure 2. The main components include a soot generation and size-selecting system, an environmental chamber, a gaseous species injection system, an integrated aerosol analytical system, a Nephelometer, and a cavity ring-down spectrometer (CRDS), to measure the particle size, mass, hygroscopicity and optical properties.

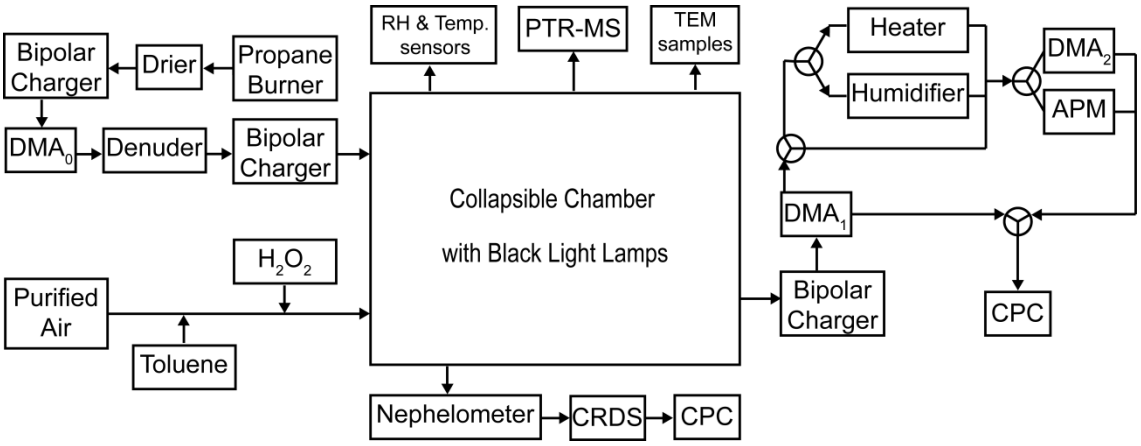

Figure 2. Schematics of the environmental chamber and soot aging experiment setup.

Chamber Experiment Setup

All experiments were performed in a 1.2 m^3 collapsible environmental chamber (Teflon® PFA), equipped with two banks of black light lamps (F30T8/350BL, Sylvania, 18 lamps in total) and surrounded by reflective aluminum sheets to maximize light intensity in the chamber. Between experiments, the chamber was cleaned and flushed

overnight with at least 12 m^3 of purified air (Aadco 737-11, Aadco Inc.), and irradiated by black light lamps to remove any residues. The chamber background conditions were: particles number concentration was less than 0.01 cm^{-3}, NO_x and O_3 concentrations were lower than 1 ppb, and the total hydrocarbons were less than 2 ppb. At the beginning of each experiment, the chamber was filled with ~750 liters purified air.

Soot particles were generated from a modified Santoro-type laminar burner by incomplete combustion of propane.[6] Particles were sampled through a pinhole on the side wall of the chimney, and diluted right away with dried, particle free nitrogen gas. Part of the diluted soot sample was introduced to a size selecting system where particles were dried to < 5% RH via Nafion drier (PD-070-18T-12SS, Perma Pure Inc.), charged by a bipolar ^{210}Po charger, and size-classified by DMA_0 (Model 3081, TSI). The quasi-monodisperse aerosol sample was neutralized by a second bipolar ^{210}Po charger, and passed through two denuders containing Spectrum XB-17 and HS-600 (General Carbon Corp.). The purified soot sample was then introduced into the chamber, with a flow rate of 1.0 lpm for ~1.5 hr to allow the soot particle number concentration to reach ~1000 cm^{-3}. Hydrogen peroxide was introduced into the chamber as the OH radical precursor which was photolyzed as soon as the black lights were turned on. Hydrogen peroxide aqueous solution (16 wt %, 50 μL) was injected into a glass reservoir and then flushed into the chamber with purified air for ~13 min at 20 lpm. Subsequently, appropriate amount (1–10 ml) of purified air saturated with toluene vapor at room temperature was injected into the glass reservoir and was carried into the chamber by 40 liters of purified air. A filter with Teflon liner was placed between the glass reservoir and chamber to

remove any particulate materials. The nominal concentration of H_2O_2 in the chamber was 5 ppm which was found to give a steady OH concentration;[50] initial toluene concentration can be varied from 30 to 300 ppb for each experiment. A mixing fan was turned on for 30 s to thoroughly mix the soot particles and gaseous species, and the black light lamps were turned on to initiate H_2O_2 photolysis and SOA formation process. The concentration of toluene was monitored by a compact proton transfer reaction mass spectrometer (PTR-MS, Ionicon Analytik) during the reaction, and ~5% of the toluene was consumed during each experiment. During the reaction, the RH and temperature in the chamber were 8 % and 302-304 K, respectively.

Blank experiments have been performed under conditions such as soot + black light, soot + toluene + black light and soot + H_2O_2 + black light for one hour. No change in particle size or mass was observed in these experiments. Transmission electron microscope (TEM) samples were taken by sampling from the chamber at 1.0 lpm for 10 min through a low-pressure cascade impactor (Model I-1L, PIXE International Corp.) where aerosols were collected on 200 mesh Copper TEM grids with formvar/carbon film (Model 01800, Ted Pella Inc.). TEM images were examined using a JEM 2010 transmission electron microscope (JEOL Ltd.) operated at 100 kV accelerating voltage.

Measurements of Particle Size, Mass, Hygroscopicity and Organic Mass Fraction

The integrated aerosol analytical system has been described in details earlier,[13] which comprises two DMAs (Model 3081, TSI), an APM (Model 3600, Kanomax Inc., Japan), a CPC (Model 3760A, TSI), a heater and a humidifier, as shown in Figure 2. The

system can be operated as scanning mobility particle sizer (SMPS), tandem differential mobility analyzer (TDMA) , and differential mobility analyzer - aerosol particle mass analyzer-CPC (DMA-APM-CPC) with heat/ humidifying processing options by three-way valves.[13] Aerosols were sampled from the chamber into the system at 1.0 lpm.

The size distribution and number concentration of soot particles in the chamber during the process were monitored with SMPS. The mobility diameter D_p for the quasi-monodisperse particles was then determined. Particle diametric growth factor *Gfd* is expressed as $D_p/D_{p,0}$, where D_p represents the mobility diameter of particles at given reaction time and $D_{p,0}$ is that of the fresh soot particles. The relative uncertainty in *Gfd* measurements was less than 2%. Nucleation was occasionally observed but the peak of newly-formed particles did not overlap with the processed soot particle peak. Particle mass was determined using DMA-APM-CPC, where aerosols sampled from chamber were introduced into the APM and their mass was determined by scanning the APM voltage at certain rotation speeds. Calibration curve was obtained to correct any offsets by using spherical Polystyrene Latex (PSL) particles (Duke Scientific Inc.) with known sizes (46, 81, 97, 151 and 240 nm) and material density (1.05 g cm^{-3}). The particle mass growth factor, *Gfm*, was then calculated as m_p/m_0, where m_0 and m_p represent the mass of particles before and after coated by organics, respectively. The relative uncertainty in *Gfm* measurements was less than 3%. There was a small difference (~5 min) in reaction time when particle size and mass measurements were performed. As a result, the data of particle mass growth was fitted versus reaction time to interpolate the *Gfm* value

corresponding to the reaction time when the *Gfd* value was measured. The effective density, ρ_{eff}, can be then calculated as:

$$\rho_{eff} = \frac{6m_p}{\pi D_p^3} \tag{2.1}$$

Particle organic mass fraction f_m_{org} was determined as $(m_p\text{-}m_0)/m_0$, and the material density ρ_m, was calculated from the material density of soot (ρ_{soot}, 1.77 g cm^{-3})[52] and organic coating (ρ_{org}, 1.34 g cm^{-3}, details in the following experimental section), assuming volume additivity:

$$\frac{1}{\rho_m} = \frac{f\_m_{org}}{\rho_{org}} + \frac{1 - f\_m_{org}}{\rho_{soot}} \tag{2.2}$$

Coated soot particles were processed further by heating experiments (coated-heated soot) to evaluate the impact of organic coatings on the properties of soot core.[13] Thermo-TDMA (DMA_1-heater-DMA_2-CPC) experiments were performed by heating the coated soot particles to 300 °C to remove the organic coatings and measuring the change in mobility size of the coated-heated particles. The thermo diametric growth factor, *TGfd*, is expressed as $D_{p,h}/D_p$, where D_p and $D_{p,h}$ represent the mobility diameters of coated and coated-heated soot, respectively. Similarly, DMA_1-heater-APM-CPC determined the mass of coated-heated soot. It is found that the fresh soot generated by our burner contained less than 5 wt % volatile components. The effective density, $\rho_{eff,h}$, of the coated-heated soot, can be calculated using Equation 2.1. It was found that the mass of coated-heated soot was close to that of fresh soot (within 2%), suggesting that all the organic coatings are removed after the heating.

Particle hygroscopicity was monitored by TDMA coupled with humidifier (HTDMA)[13] where particles with mobility size $D_{p,0}$ were obtained by DMA_1 and subsequently exposed to 90% RH in the humidifier before their mobility size D_p was determined by DMA_2. Hygroscopic diametric growth factor *HGfd* was then calculated as $D_p/D_{p,0}$.

Derivation of Particle Morphology Parameters

Volume equivalent diameter D_{ve} is the diameter of a spherical and compact particle that has the same volume as the particle under investigation.[53,54] It was calculated from the particle mass mp and material density ρ_m:

$$D_{ve} = \sqrt[3]{\frac{6m_p}{\pi\rho_m}} \tag{2.3}$$

The change in particle D_{ve} was expresses as the volume equivalent coating thickness $\Delta r_{ve} = (D_{ve} - D_{ve,0})/2$, where D_{ve} and $D_{ve,0}$ are volume equivalent diameters of fresh and coated soot particles, respectively.[34] The dynamic shape factor χ is employed to evaluate the increase in drag force on an irregular particle compared to a spherical particle with equivalent volume when both are moving at the same speed.[54] It was calculated using the measured mobility diameter D_p, and the calculated volume equivalent diameter D_{ve}, according to

$$\chi = \frac{D_p}{C_p} \cdot \frac{C_{ve}}{D_{ve}} \tag{2.4}$$

where C_{ve} and C_p are the Cunningham slip correction factors for particles with diameter D_{ve} and D_p, respectively. Spherical and compact particles have a χ value of 1.0; whereas fractal ones will have $\chi > 1.0$.

Measurements of Aerosol Optical Properties

The optical system consisted of a commercial integrating Nephelometer (Model 3563, TSI) and a CRDS connected in series.[20] The particles were sampled at 6.0 lpm from the chamber into the system where their light scattering (b_{sca}) and extinction (b_{ext}) coefficients at 532 nm were measured. The b_{sca} at 532 nm was calculated from a power law fit to the scattering coefficients at the three nephelometer wavelengths (450, 550 and 700 nm). The b_{ext} was measured by the CRDS with a Q-switched pulsed laser (QG-532-500, CrystaLaser Inc.) producing light pulse at 532 nm, a stainless steel cell with aerosol inlet in the middle and outlet and two ends, and two high-reflectivity dielectric mirrors (Los Gatos Research, Inc.) mounted on both ends of the cell. A small dry nitrogen flow was constantly purging the mirrors to prevent aerosol contamination. Calibration and correction has been performed on the optical system based on the procedure described in detail elsewhere.[20] The absorption coefficient babs can be calculated from $b_{abs} = (b_{ext} - b_{sca})$. The random error in scattering and absorption coefficients is less than 1%. Aerosol scattering (C_{sca}) and absorption (C_{abs}) cross sections were calculated according to:

$$C = \frac{b}{N} \tag{2.5}$$

where N is particle number concentration in the chamber determined by SMPS, with a standard deviation within 3%.

Measurements of Density and Hygroscopicity of Toluene-OH Oxidation Products

Clean chamber was injected with 300 ppb of toluene and 5 ppm of H_2O_2. Black lights were then turned on to allow oxidation reaction and nucleation to take place. The particles formed were allowed to grow until they reached a stable size distribution, monitored by SMPS. The poly-dispersed aerosols had a long-normal size distribution with peak maximum at ~60 nm. The lights were turned off to allow property measurements.

Particle mass m was determined in DMA-APM-CPC mode for particles with mobility diameter D_p between 70–80 nm. The effective density, ρ_{org}, can then be calculated using Equation 2.1, and there was no obvious difference in ρ_{org} values of different sizes. A ρ_{org} value of (1.34 ± 0.04) g cm^{-3} was determined by averaging density data of different sizes. Hygroscopicity growth was determined for particles with mobility diameters of 50, 80 and 100 nm by HTDMA, similar to the procedure described in the previous sections.

Results and Discussion

Evolution of Soot Properties with Organics

Changes in the particle size (*Gfd*), mass (*Gfm*), mass fraction of organic coatings (f_m_{org}), and volume equivalent coating thickness (Δr_{ve}) are plotted versus the reaction time in Figure 3 for soot with three initial mobility diameters D_p of 80, 100 and 150 nm. After coating with the oxidation products, there is a relatively small change in size

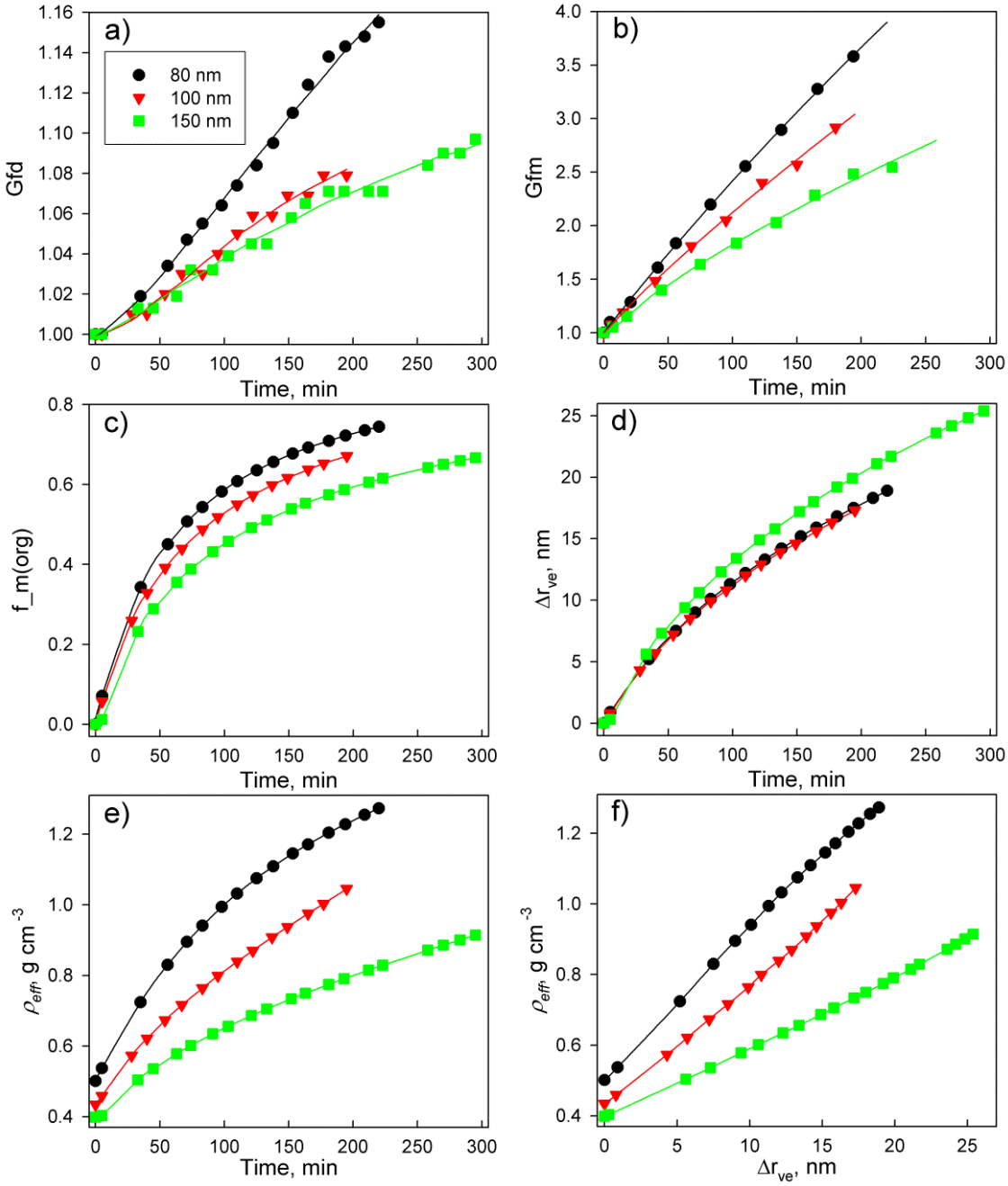

Figure 3. Evolution in properties of soot particles coated by toluene-OH oxidation products. The initial toluene concentration is 250 ppb and initial soot particle number concentration is 750–800 cm^{-3}. Black circles—soot with an initial mobility diameter D_p of 80 nm, red triangles—soot with an initial D_p of 100 nm, and green squares—soot with an initial D_p of 150 nm. a) Particle growth factor of mobility diameter (*Gfd*) as a function of reaction time. b) Particle mass growth factor (*Gfm*) as a function of time. c) Mass fraction of organics (f_m_{org}) on soot particles as a function of time. d) Volume equivalent coating thickness (Δr_{ve}) of organics on soot particles as a function of time. e) Particle effective density (ρ_{eff}) as a function of *T*. f) Particle ρ_{eff} as a function of Δr_{ve}. Solid lines are the best fits of the data.

(Figure 3a), but a large change in particle mass (Figure 3b) and effective density ρ_{eff} (Figure 3e). Those observations are explained by a morphology change of the soot core upon coating of organics, consistent with the notion that it is necessary to monitor the particle mass change during soot aging processes.[6,40] The higher density of the organic coating (1.34 g cm^{-3}) also contributes to the increase in the effective density of coated soot. The time for the mass fraction of organic coatings to reach 50% is about 60, 100, and 145 minutes for soot particles with the initial size of 80, 100 and 150 nm, respectively. The growth rates of size, mass, and organic mass faction decrease as the initial size of soot increases from 80 to 150 nm. The changes in the volume equivalent coating thickness over the reaction time are shown in Figure 3d. Interestingly, particles with the 80 and 100 nm initial sizes exhibit a similar Δr_{ve} growth rate, and the Δr_{ve} value of soot with an initial size of 150 nm increases slightly faster than those of soot with the initial size of 80 or 100 nm.

Table 1. Properties of Fresh Soot Particles.

D_p, nm	m_p, 10^{-16} g	D_{ve}, nm	N_{pp}[a]
82.4	1.47	54.1	20
101	2.34	63.2	32
155	7.77	94.3	105

[a] The number of spherical primary particles in one soot particle, assuming that the primary particle has a density of 1.77 g cm^{-3} and a diameter of 20 nm.

Because of condensation of the oxidation products on primary particle surface during the SOA formation process, the number N_{pp} of primary particles in soot particles, rather than the mobility diameter, is more useful when comparing the particle growth rate. Fresh soot particles used in this study have a primary particle diameter of (20.5 ± 2.2) nm (determined from TEM images), and the N_{pp} values of fresh soot particles with D_p of 80, 100 and 150 nm are 20, 32 and 105, respectively (Table 1). Particles with D_p of 80 and 100 nm have comparable N_{pp} values; the N_{pp} value of particles with D_p of 150 nm is 3–5 times larger than that of particles with D_p of 80 or 100 nm. The sum of primary

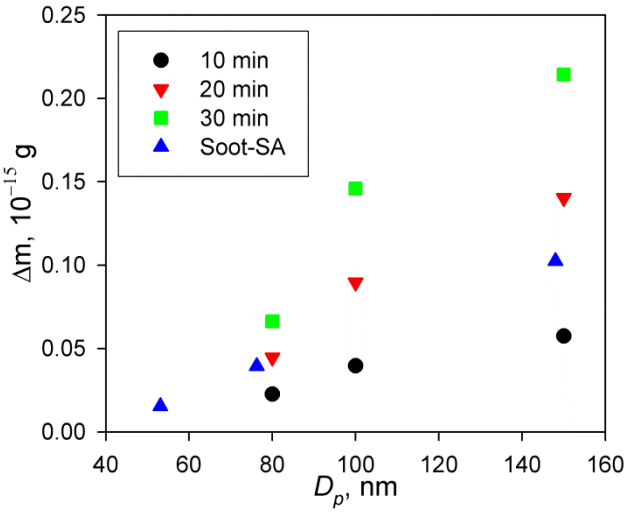

Figure 4. Absolute mass (Δm) of the organic coating of toluene-OH oxidation products as a function of the initial soot particle mobility size D_p. Three different reaction times are plotted: 10 min (black circles), 20 min (red down-triangles), and 30 min (green squares). The absolute mass of sulfuric acid coatings (Soot-SA, blue up-triangles) is adapted from Ref 2. Note that soot particles with larger initial mobility size always show larger increase in absolute mass of the coating.

particle surfaces has been shown as a close estimate for the total surface area of soot,[6] suggesting that particles with D_p of 150 nm have the fastest material condensation rate: as shown in Figure 4, the absolute change in particle mass is the largest for particles with D_p of 150 nm. The observation that the relative increase in mass of 150 nm particles is slower than that of 80 nm particles may be attributed to the larger initial mass of 150 nm particles.

Because of the fractal nature of soot particles, Δr_{ve} represents a spatial parameter to better reflect the change in the particle volume by organic coating and to correlate the change of the particle properties with the thickness of organics, in addition to the reaction time as the temporal parameter. For example, the growth in particle ρ_{eff} is plotted as a function of Δr_{ve} in Figure 3f, by replacing the reaction time in Figure 3e with the corresponding Δr_{ve} values determined from Figure 3d. Figures. 5a–b show the temporal and spatial profiles of the changes in particle mobility diameter. For different initial toluene concentrations (Figure 5a), the temporal profiles of soot particle mobility diameter growth *Gfd* are different, and the growth rate increases with the increasing initial toluene concentration. When plotted against Δr_{ve}, the change in *Gfd* is only dependent of the thickness Δr_{ve} of organic coatings on soot particles (Figure 5b). Similar behaviors are also evident in the particle mass and effective density profiles as a function of Δr_{ve} (Figure 5c–d). Those measurements indicate that the initial toluene concentration determines the time needed to form a certain thickness Δr_{ve} of organics and the Δr_{ve} value subsequently governs the variations in the soot particle properties. As a result,

experiments using higher initial toluene concentrations may be extrapolated to predict the soot properties under relevant ambient conditions.

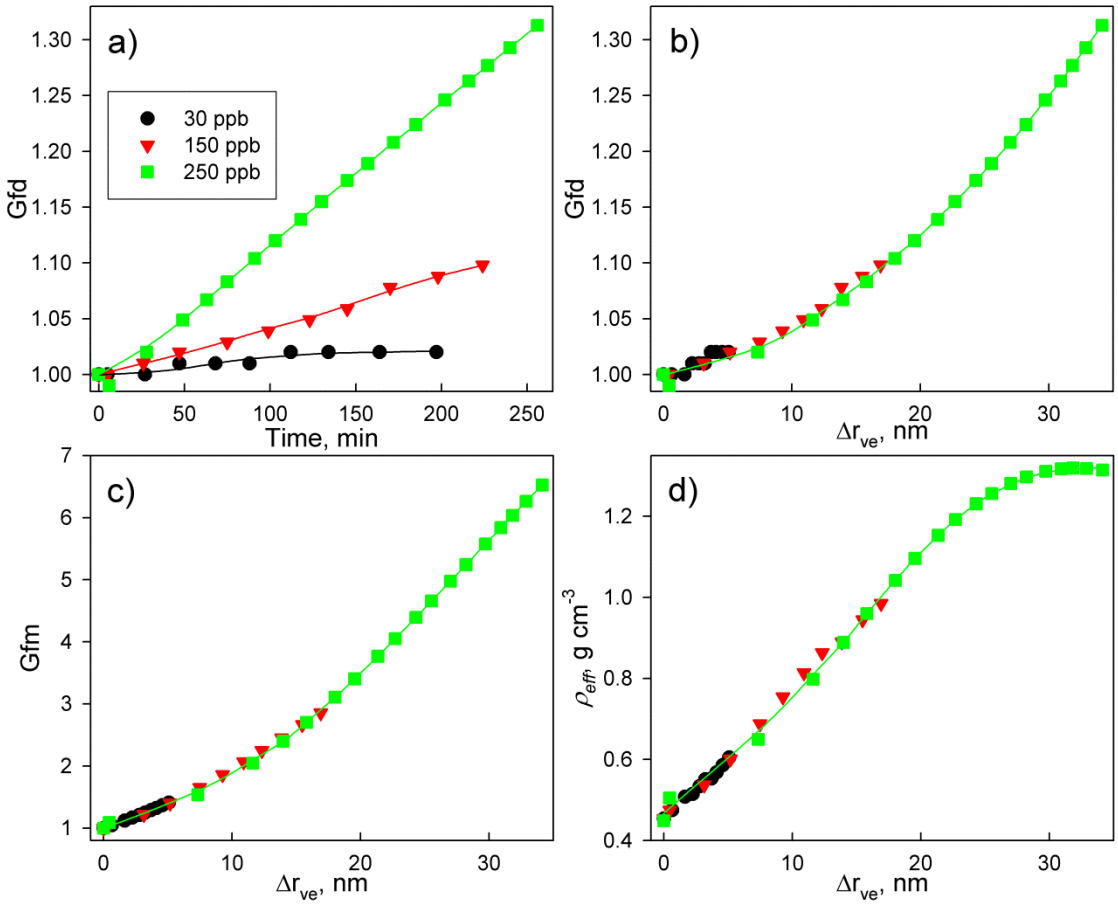

Figure 5. Dependence of soot particle property changes on initial toluene concentrations and the volume equivalent coating thickness (Δr_{ve}) of organics on particles. The initial soot particles have a mobility diameter of 100 nm and particle number concentrations of 1200–1400 cm^{-3}: black circles—an initial toluene concentration of 30 ppb, red triangles—an initial toluene concentration of 150 ppb, and green squares—an initial toluene concentration of 250 ppb. a) Particle growth factor of mobility diameter (*Gfd*) as a function of reaction time *T*. Solid lines are the best fits of the data. b) Particle *Gfd* as a function of Δr_{ve}. c) Particle mass growth factor (*Gfm*) as a function of Δr_{ve}. d) Particle effective density (ρ_{eff}) as a function of Δr_{ve}. For b)–d), the solid green lines are the best fit of the data from experiments with 250 ppb initial toluene concentration.

Changes of Soot Particle Morphology with Organics

To elucidate the morphology change of the soot core, the effective density $\rho_{eff,h}$ of the soot core (coated-heated soot) is determined. Values of $\rho_{eff,h}$ for soot with three initial mobility diameters (D_p=80, 100, and 150 nm) are shown in Figure 6a as a function of Δr_{ve}. In all cases, the $\rho_{eff,h}$ values increase until reaching a steady value. The significant increase in $\rho_{eff,h}$ for coated-heated soot suggests that the organic coatings have restructured the soot core into a more compact form during the SOA formation process. Similar compaction on soot core has been documented when fresh soot was exposed to sulfuric acid,[19] glutaric acid,[35] and α-pinene ozonolysis products,[37] but has not been observed in the case of succinic acid.[35] Previous studies have shown that for soot produced from laboratory burners, coated-heated soot retains the morphology of the original particles if the coating materials do not compact the soot core.[34,35] However, it is still an open question whether coating-heating process will change the morphology of soot particles produced from other sources.

The dynamic shape factor χ represents an important parameter to characterize the shape of soot particles. A particle with an irregular shape has χ larger than 1; the closer χ is to 1, the more spherical the particle is. As depicted in Figure 6b, regardless of the initial size of fresh soot, χ values of coated soot decrease and approach 1.0 when the thickness of organics increases. There are two possibilities for the decrease in χ of coated soot: condensed organics fill the voids between primary particles and smooth the particle surface, and the organics restructure the soot core. Comparison between the TEM images of fresh (Figure 6c) and coated (Figure 6d) soot particles supports the

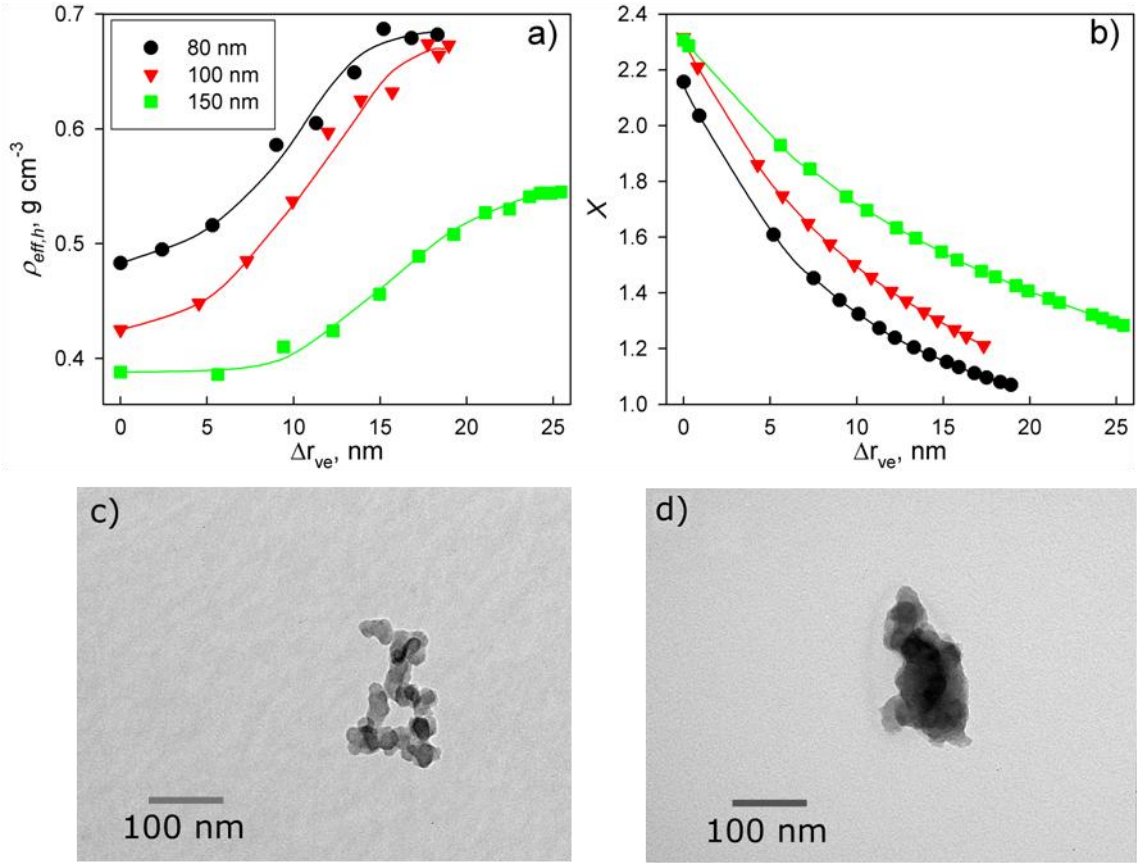

Figure 6. Morphology change and transmission electron microscope (TEM) images of soot particles. For a)–b), the experimental conditions are: an initial toluene concentration of 250 ppb and soot particle number concentration of 750–800 cm^{-3}; black circles—soot with an initial mobility diameter D_p of 80 nm, red triangles—soot with an initial D_p of 100 nm, and green squares—soot with an initial D_p of 150 nm. a) The effective density ($\rho_{eff,h}$) of the soot core (coated-heated soot) as a function of volume equivalent coating thickness (Δr_{ve}). Solid lines are connections through the experimental points. b) Particle dynamic shape factor (χ) as a function of Δr_{ve}. Solid lines are the best fits of the data. TEM images of fresh (c) and coated (d) soot particles are sampled from the experiment with an initial toluene concentration of 250 ppb, and soot particles with an initial D_p of 150 nm. The initial number concentration of fresh soot is 1400 cm^{-3}. The Δr_{ve} of organics on coated soot in (d) was about 40 nm.

explanation that the organic coating effectively restructure the fractal soot core into a more compact shape, resulting in a more spherical shape and lowering χ. On combining the results from $\rho_{eff,h}$ measurements, calculated χ, and TEM images, it can be concluded that toluene-OH oxidation products noticeably restructure the soot core during the SOA

formation. Restructured particles become more compact and have a higher effective density, which contribute to the increase in effective density ρ_{eff} of coated soot particles (Figure 3e–f).

Similar changes in the soot dynamic shape factor have been found in other previous experiments (Table 2). The χ change of soot particles for a similar Δr_{ve} by coating of toluene-OH oxidation products and oleic acid is comparable. The effect of toluene-OH oxidation products coating on χ is much smaller than that of sulfuric acid coating, but toluene-OH oxidation products modify the particle shape more effectively than anthracene. Note that anthracene condenses on soot to decrease χ only by filling the voids between primary particles.[34] Hence, compaction of soot core causes additional decrease in the particle dynamic shape factor.

Table 2. Comparison of the Influence of Different Coatings on Soot Properties.[a]

Coating Compound(s)	Δr_{ve}, nm	χ/χ_0	$C_{sca}/C_{sca,0}$	$C_{abs}/C_{abs,0}$	SSA/SSA$_0$
Sulfuric acid[b]	12.0	0.42	2.8	1.15	2.2
Glutaric acid[c]	-	0.46	2.4	1.06	2.0
Succinic acid[c]	9.3	0.74	2.0	1.05	2.0
Dibutyl phthalate[d]	39.1	-	-	1.33	-
Olelic acid[e]	31.9	0.46	-	-	-
Anthracene[e]	39.0	0.64	-	-	-
α-pinene ozonolysis products[f]	-	-	5.2	1.30	2.5
Toluene-OH oxidation products[g]	39.1	0.48	3.6	1.05	2.4

[a] subscript 0 corresponding to properties of fresh soot; [b] Ref. 6 and 19; [c] Ref. 12 and 35; [d] Ref. 26; [e] Ref. 34; [f] Ref. 37 and 38; [g] This work.

Effect of Organics on Soot Optical Properties

The optical properties of soot particles with an initial mobility diameter D_p of 150 nm are measured during the SOA formation process. Figure 7 illustrates the effect of toluene-OH oxidation products on soot optical properties. Significant variations in the particle optical properties occur as the coating thickness of organics on soot particles increases.

The increase in C_{sca} with organic coating is pronounced: coated soot particles have 3.6 times higher scattering than the fresh ones, attributable to strong scattering of organic coatings and enhanced interactions between compacted primary particles and electromagnetic waves. Similar increase in C_{sca} has been previously observed for soot particles coated with α-pinene ozonolysis products, organic and sulfuric acids (Table 2). A significant increase (2.3 times) in particle SSA is also measured, comparable to previously reported enhancement in SSA for soot particles coated with sulfuric acid[20] or α-pinene ozonolysis products.[38]

The absorption cross section C_{abs} of coated soot with Δr_{ve} = 39 nm increases by ~5% comparing to that of fresh soot. As summarized in Table 2, previous studies have shown that different coating materials on soot enhance light absorption differently (Table 2). For example, a coating of succinic acid (Δr_{ve} = 9 nm) increases light absorption by 5 %, and a coating of sulfuric acid (Δr_{ve} = 12 nm) increases the absorption by 15%. The difference in light absorption enhancement may be explained by the difference in surface tensions of sulfuric acid and toluene-OH oxidation products[20] or the difference in molecule structures of toluene-OH oxidation products and succinic acid.[12]

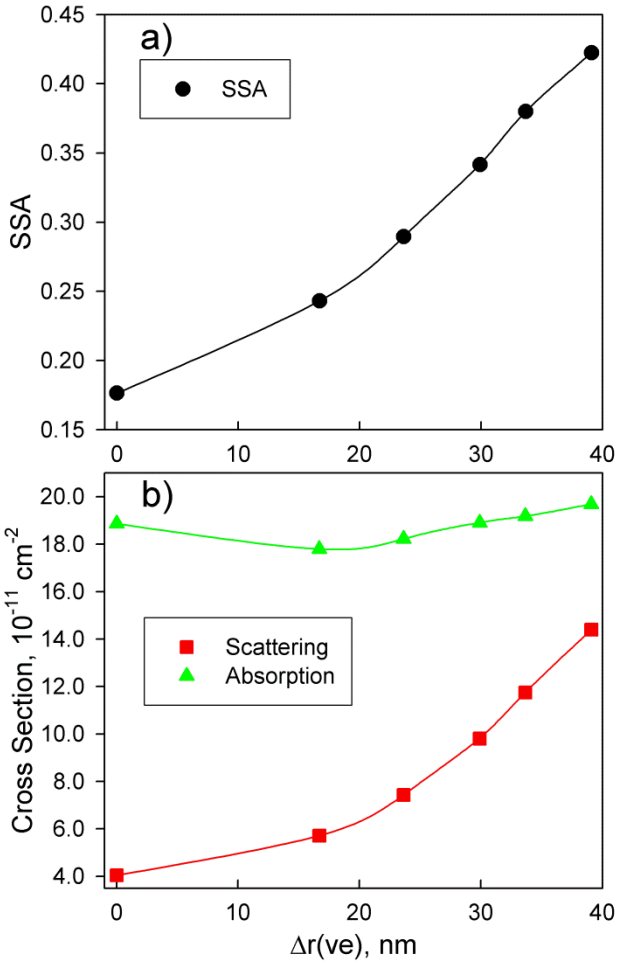

Figure 7. Effects of organic coatings on soot optical properties. The experiment conditions are: the initial toluene concentration 250 ppb, the initial mobility diameter of soot particles 150 nm, and the initial fresh soot number concentration 1300 cm^{-3}. a) Single scattering albedo (SSA, black circles) of soot particles as a function of the volume equivalent coating thickness (Δr_{ve}) of organics. b) Scattering (red squares) and absorption (blue triangles) cross-sections of soot as a function of Δr_{ve}. All values are determined at a light wavelength of 532 nm and the solid lines are connections through the experimental points.

Effect of Organic Coatings on Soot Hygroscopicity

Fresh soot is hydrophobic, since its *HGfd* at 90% RH is measured to be 1.00 ± 0.01, similarly to that from previous studies.[6] For SOA formed from the toluene-OH oxidation products without pre-existing soot particles, the *HGfd* at 90% RH is

determined as (1.09 ± 0.01), consistent with a previously measured value of 1.10 at 90% RH.[51] The change in the mobility diameter D_p of soot particles coated with organics and further processed at 90% RH (coated-wetted soot) is measured with HTDMA and plotted in Figure 8a (black circles) as a function of the volume equivalent coating thickness Δr_{ve} of organics. When particles are processed at 90% RH, the D_p of coated-wetted soot decreases with Δr_{ve} increasing from 0 to 20 nm and then increases as Δr_{ve} further increasing beyond 20 nm. Those changes are attributed to water condensation on coated soot, since soot particles become more hydrophilic with the organic coating. Condensation of water on coated soot further compacts the particles and causes a decrease in particle mobility diameter, explaining the decreasing trend in Figure 8a. When the soot core is fully compacted by organics, water condensation leads to an increase in the particle size, as evident from the increasing trend for $\Delta r_{ve} > 20$ nm in Figure 8a.

HGfd data determined by HTDMA are based on particle mobility diameter D_p which can be significantly different from its volume equivalent diameter D_{ve} for fractal aerosols.[54] The volume equivalent hygroscopic growth factor $HGfd_{ve}$ is defined as the ratio between volume equivalent diameters D_{ve} of coated-wetted and coated soot particles, which have considered the contribution of particle morphology on the hygroscopic measurements.[55]

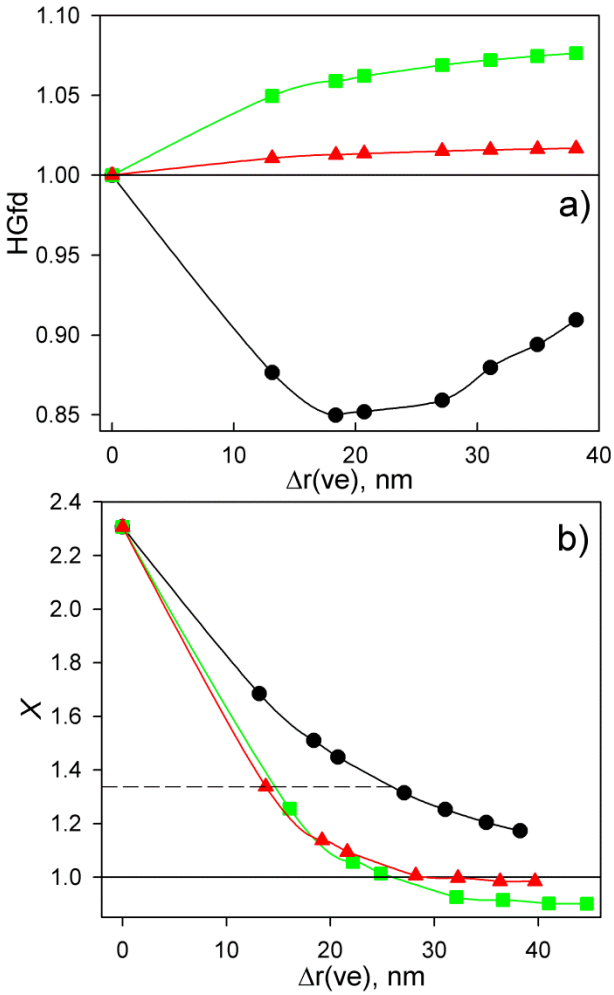

Figure 8. Effects of organic coatings on soot hygroscopicity. The experiment conditions are: the initial toluene concentration is 250 ppb, the initial mobility diameter D_p of soot is 150 nm, and the initial soot number concentration is 1400 cm^{-3}. The coated soot particles are humidified to 90% RH (coated-wetted soot) during the HTDMA measurement cycle. a) hygroscopic growth factor (*HGfd*) of particle size as a function of the volume equivalent coating thickness (Δr_{ve}) of organics: black circles—*HGfd* based on the D_p of the coated-wetted soot particles, red triangles—*HGfd* based on the volume equivalent diameter (D_{ve}) of the coated-wetted soot assuming the mass ratio between water and organic coatings (k_w) is 4.4%, and green squares—*HGfd* based on the D_{ve} of the coated-wetted soot assuming the k_w is 22.0%. b) Particle dynamic shape factors (χ) of coated and coated-wetted soot as a function of the Δr_{ve} of organic coatings: black circles—the χ of coated soot as a function of the Δr_{ve} of organics, red triangles—the χ of coated-wetted soot as a function of the Δr_{ve} of organics and water, assuming the k_w is 4.4%, and green squares—the χ of coated-wetted soot as a function of the Δr_{ve} of organics and water, assuming the k_w is 22.0%. For coated-wetted soot, the corresponding Δr_{ve} represents the coating thickness of organics and water on coated-wetted soot particles. The solid lines are connections through the experimental points.

It is assumed that the mass of condensed water is linearly proportional to that of organic coatings with a factor of k_w. As a result, when a coated soot particle with mass of mp and a organic mass fraction of f_m_{org} is exposed to 90% RH, the resulting coated-wetted particles will have a mass $m_{p,w}$ as:

$$m_{p,w} = \left(1 + k_w \cdot f\_m_{org}\right) m_p \tag{2.6}$$

The organic mass fraction $f\_m_{org,w}$ in the coated-wetted soot is:

$$f\_m_{org,w} = \frac{f\_m_{org}}{1 + k_w \cdot f\_m_{org}} \tag{2.7}$$

Assuming volume additivity for components in coated-wetted soot, its material density $\rho_{m,w}$ can be estimated as:

$$\frac{1}{\rho_{m,w}} = \frac{f\_m_{org,w}}{\rho_{org}} + \frac{k_w \cdot f\_m_{org,w}}{\rho_{water}} + \frac{1 - (1 + k_w) f\_m_{org,w}}{\rho_{soot}} \tag{2.8}$$

The volume equivalent diameter $D_{ve,w}$ for the coated-wetted soot particle is:

$$D_{ve,w} = \sqrt[3]{\frac{6 m_{p,w}}{\pi \rho_{m,w}}} \tag{2.9}$$

And the $HGfd_{ve}$ can then be calculated as $D_{ve.w}/D_{ve}$, where $D_{ve.w}$ and D_{ve} are the volume equivalent diameters of coated-wetted and coated soot particles, respectively (Figure 8a, green squares and red triangles, calculated based on two k_w values, see the discussion below). It is clear that the D_{ve} of coated-wetted soot increases as the Δr_{ve} of organic coating increases, for both k_w values. The dynamic shape factor χ_w of coated-wetted soot is estimated using Eq. (4) and plotted in Figure 8b. Note that for χ_w, the corresponding Δr_{ve} represents the coating thickness of organics and water on coated-wetted soot particles.

Atmospheric Implications

Because of its high absorption cross-section over a broad range of the solar spectrum, soot contributes significantly to climate change by direct radiative forcing and is the second most important climate-warming agent after carbon dioxide.[22] Although internally mixed soot may absorb solar light more efficiently and exert a higher positive direct radiative forcing,[22] the associated increase in light scattering may offset the positive forcing of light absorbing soot particles.[56] Atmospheric aging of soot can dramatically change its composition, morphology, optical properties, and hygroscopicity, impacting its roles in air quality, human health, and radiative forcing. Also, modification of the hygroscopic behavior of soot particles has a positive feedback on aerosol growth, since hydrophilic particles promote water uptake and increase the particle size; higher water content in the particle phase facilitates condensation of water-soluble species or heterogeneous hydrolysis reactions, leading to further growth in the particle mass.[57-60]

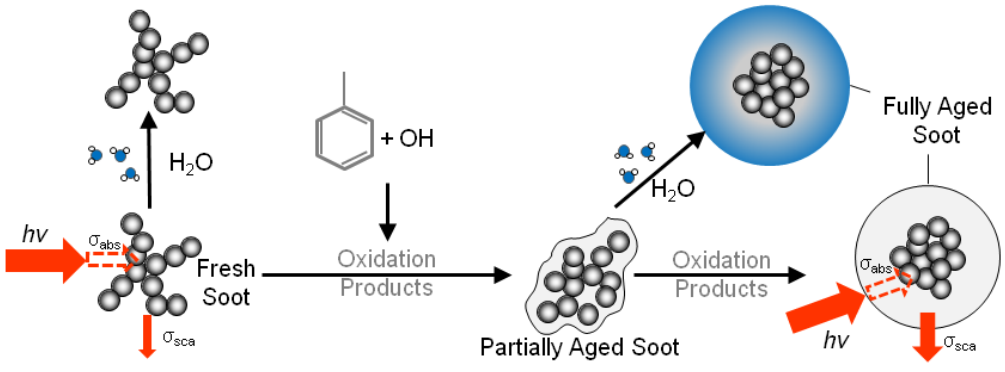

Figure 9. The impacts of toluene-OH oxidation products on soot particles properties.

The impacts of SOA formation on soot properties from the OH-initiated oxidation of toluene have been evaluated (Figure 9). Monodisperse soot particles are exposed to the oxidation products of toluene in an environmental chamber, and the variations in the particle size, mass, organic mass faction, morphology, effective density, hygroscopicity, and optical properties are simultaneously determined by an integrated aerosol analytical system. Our results suggest that the changes in soot properties are closely related to the mass fraction of organic coatings on particles, which are dependent of the reaction time and initial reactant initial concentrations. Furthermore, the particle size and mass growths are associated with the number of primary particles in the soot core. Assuming an atmospheric toluene concentration of 30 ppb (representing a typical concentration of total aromatics in urban areas), it is estimated that toluene-OH oxidation products fully modifies the fractal fresh soot with an initial mobility diameter of 100 nm into a compact shape on a timescale of 2 days. As a result, oxidation of toluene in the atmosphere can contribute to changes in the composition, size, density, and morphology of soot particles, given a typical soot lifetime of ~1 week.[61] It should be pointed out that our estimated aging timescale may represent a lower limit, considering possible loss of the oxidation products on the chamber wall. The timescales of soot aging have been suggested to vary from as short as 3 hr to a few days during atmospheric transport, on the basis of recent field measurements.[62,63]

Our results indicate a significant morphology change during soot aging process, which also correlates with changes in hygroscopicity and optical properties. Compaction of the soot core is evident from the increase in effective density of the soot core and the

decrease in particle dynamic shape factor. The toluene-OH oxidation products considerably restructure soot core, leading to enhanced light scattering and absorption. Organic coatings can change the soot surface from hydrophobic to hydrophilic. Consequential water condensation further changes the particle shape, more effectively than the organic coating. With organic coatings, aged soot particles are more likely to serve as CCN, contributing to cloud formation. An accurate determination of the effects of SOA formation on soot hygroscopicity and optical properties and the associated impacts on solar radiative and cloud formation requires the knowledge of the VOC concentration, timescale of the aging process, and the fraction of coated soot formed in the total ambient aerosol population. Hence, our measurements provide experimental data to better assess the impacts of soot aging on climate.[64] Future directions include experimental studies on how other representative VOCs will affect the aging of soot and modeling works assessing the impact of soot aging on regional and global environment.

CHAPTER III

REACTIONS BETWEEN AMINES AND AEROSOLS WITH AMMONIUM SALTS[*]

Introduction

Overview of Atmospheric Amines

Amines contain a basic nitrogen atom with a lone pair and are derivatives of ammonia, where one or more hydrogen atoms are replaced by a substituent such as an alkyl or aryl group. In the atmosphere amines are emitted to from various biogenic (such as ocean organisms, protein degradation and biomass burning) and anthropogenic (such as animal husbandry, automobiles, industries, and treatment of sewage and waste) sources.[65,66] For example, the gas-phase concentration of alkylamines with low molecular weight (MW) reaches as high as several hundreds μg m^{-3} in the vicinity area of animal husbandry facilities, and the total emission of monomethylamine (MMA), dimethylamine (DMA) and trimethylamine (TMA) is estimated to be ~300 Gg N a^{-1} globally.[66] On the other hand, the typical concentration of atmospheric amines is about 1–2 orders of magnitude smaller than that of ammonia.[66]

Because of the substitution by one or more organic functional groups, amines are of stronger basicity than ammonia and more prone to participation in acid-base reactions in the condensed phase. The atmospheric reaction pathways of amines include gas-phase

[*] Part of this chapter is reprinted with permission from Qiu, C.; Wang, L.; Lal, V.; Khalizov, A. F.; Zhang, R. Heterogeneous Reactions of Alkylamines with Ammonium Sulfate and Ammonium Bisulfate. *Environmental Science & Technology* **2011**, *45*, 4748. Copyright 2011 American Chemical Society. Part of the chapter has been submitted to *Phys. Chem. Chem. Phys.* for the consideration of publication.

reactions with oxidants such as OH, NO_3 and O_3, producing nitrogen-containing organics that can condense on or be partitioned into the particle phase and engage in heterogeneous reactions with acidic or carbonyl compounds, both facilitating the formation and growth of atmospheric aerosols. The subject on research in the kinetics and mechanism of the gas-phase oxidation of amines is not discussed here, and readers are directed to several other recent studies.[67-69] The multi-phase reactions of amines include acid-base neutralization, carbonyl-amine interaction, and particle-phase oxidation reactions (Reactions 3.1–3.4).

$$R_nNH_{3-n} + HX \rightarrow R_nNH_{4-n}X \quad (3.1a)$$

$$2R_nNH_{3-n} + H_2SO_4 \rightarrow (R_nNH_{4-n})_2SO_4 \quad (3.1b)$$

$$R_nNH_{3-n} + NH_4X \rightarrow R_nNH_{4-n}X + NH_3 \quad (3.2a)$$

$$R_nNH_{3-n} + NH_4HSO_4 \xrightarrow{(\alpha)} (R_nNH_{4-n})(NH_4)SO_4 \xrightarrow{(\beta)} (R_nNH_{4-n})_2SO_4 \quad (3.2b)$$

$$R_nNH_{3-n} + NH_4HSO_4 \rightarrow (R_nNH_{4-n})HSO_4 + NH_3 \quad (3.2b')$$

$$2R_nNH_{3-n} + (NH_4)_2SO_4 \rightarrow (R_nNH_{4-n})_2SO_4 + 2NH_3 \quad (3.2c)$$

$$RNH_2 + O{=}CR_2 \rightarrow RN{=}CR_2 \quad (3.3a)$$

$$R_2NH + O{=}CRCHR_2 \rightarrow R_2N{-}CR{=}C\,R_2 + H_2O \quad (3.3b)$$

$$2R_nNH_{3-n}(aerosol) + Oxidants\ (ozone, OH, etc.) \rightarrow products \quad (3.4)$$

where n=1–3, and X=Cl^- or NO_3^-.

Reactions 3.1a–b and 3.2a–c are of acid-base, although the acidity of ammonium salts (except ammonium bisulfate, ABS) is much weaker than hydrochloric, nitric, or sulfuric acid. Typically, these acid-based reactions occur dominantly in the condensed phases.[9,70,71] Recently, reactions 3.2a–c have been shown to take place between gaseous

amines and ammonium salts in clusters and nanoparticles.[72,73] Also, it has been suggested that amines form strong molecular complexes with sulfuric acid and stabilize molecular clusters and freshly nucleated nanoparticles, contributing to new particle formation in the atmosphere (Figure 1).[74-77] The carbonyl-amine reactions (Reaction 3.3 a–b) also lead to the formation of imines, enamines and polymerized products, dependent on the structure of amines and carbonyl compounds.[78,79] Reaction 3.4 represents an additional transformation pathway of aerosols, a research topic that has received increasing attention recently.[11]

The sources, health effects, and gaseous and heterogeneous reactions of atmospheric amines have been discussed in two recent reviews.[65,66] Much more recent progress, however, has been made, reporting results from field observations, theoretical calculations, and laboratory experiments and advancing instrumentation for detection of amine in the gas phase and particles. For example, recent advance in analytical instrumentation allows for both on-line and off-line atmospheric amine detection in gas and particle phase.[80-82] Amines have been scrubbed by acid or water and analyzed using chromatography coupled to mass spectrometry (MS) methods, such as gas chromatography-MS (GC-MS),[81] liquid chromatography-MS (LC-MS),[81,83] and ion chromatography-MS (IC-MS).[82] Particle-phase amines have also been sampled on-line with the Ambient Ion Monitor (total particle composition) or a Micro Orifice Uniform Deposit Impactor (size-resolved particle composition) and analyzed using IC.[84] The chemical Ionization Mass Spectrometer (CIMS) using protonated water clusters,[80]

ethanol or acetone[85] has been employed to detect ambient gaseous amines with concentrations down to the parts per trillion (ppt) level.

Amines have been identified in the particle phase at various locations around the world, including Finland,[86,87] United Kingdom,[88] Mediterranean,[89] megacities in China,[90,91] west North Pacific region,[92] urban and rural areas of Canada,[93-95] western North Atlantic,[96] Southeast U.S.,[97] Colorado[86] and Riverside, California[98] areas of the U.S., and Mexico.[86] Amino acids, as a special type of amines, have been observed in free and combined forms over the Eastern Mediterranean[99] and Italy.[100] It has been suggested that amines may contribute to 10–20% of the organic content of ambient particles[89,98] and frequently over one hundred different amine species have been observed in the particle phase.[88] The amine contents in ambient aerosols have been found to be dependent of relative humidity (RH),[95] particle size,[94] liquid water content,[91,93] season,[90,101] and locations of the observation sites.[92,101]

Contribution of Amines to Nucleation of Nanoparticles

Recent laboratory study results have revealed the involvement of amines in the nucleation and growth of nanoparticles.[75-77] New particle formation involves a distinct two-step process: nucleation to form critical nucleuses and further growth of freshly nucleated particles to larger sizes.[1] Formation of the critical nucleus is entropy-restricted and a Gibbs free energy barrier needs to be overcome prior to spontaneous transformation into the new phase. Furthermore, for small clusters and nanoparticles, there exists a strong Kelvin effect, i.e., elevated equilibrium vapor pressures above

curved surfaces, which acts as another major limitation in the new particle formation process.[3] The nucleation and growth of atmospheric nanoparticles have been thoroughly discussed in a recent review.[3]

Sulfuric acid has been commonly recognized as one of the crucial nucleating species.[102] In addition to sulfuric acid, a number of other nucleating precursors, including atmospheric ions, ammonia, amines, organic acids, and iodine oxides, have been suggested to be involved in the formation of the critical nucleus under different ambient environments.[3,103] Because of their strong basicity, amines may contribute to new particle formation by forming stable molecular complexes with sulfuric acid[104,105] or even possibly with organic acids to help to overcome the free energy nucleation barrier and by neutralizing/stabilizing freshly nucleated acidic particles to overcome the Kelvin barrier.

A recent experimental study has shown that 100 pptv ammonia along with trace amount of amines can enhance nucleation of sulfuric acid-water system by about 500 times.[106] In a fast-flow nucleation tube, nucleation among sulfuric acid, water, and nitrogen-containing species including ammonia, dimethylamine (DMA) and trimethylamine (TMA) has been investigated.[75,76] The ternary nucleation of sulfuric acid-water-TMA is about ten times higher than that of sulfuric acid-water-ammonia system.[75] DMA has been suggested to enhance the nucleation process of sulfuric acid and water by a factor of ~3.5.[76] In those previous studies,[75,76] ammonia has been detected as a contaminant with a concentration of ~80 ppt, and the actual enhancement of amines on the sulfuric acid-water nucleation could be even higher. For example, in a similar

study with ammonia removed from the reaction system, monomethylamine (MMA) has been found to be about 25–100 times more effective in enhancing sulfuric acid-water nucleation than ammonia.[77]

A particle size magnifier (PSM) method recently developed allows for detection of the number concentration of 1–3 nm nanoparticles.[107,108] It has been shown that the presence of amines increase the number concentration of 2 nm nanoparticles significantly in the sulfuric acid-water nucleation system,[76] further supporting that amines enhance the nucleation and growth of acidic nanoparticles.

However, it remains unclear whether amines enhance new particle formation by overcoming the free energy nucleation barrier through forming stable molecular complexes with sulfuric acid or by overcoming the Kelvin barrier through stabilizing freshly nucleated acidic particles, since available experimental studies do not differentiate the role of amines in the two distinct stages of new particle formation. Furthermore, the gaseous concentration of amines in the atmosphere is typically several orders of magnitude lower than that of organic acids, which also form strong hydrogen-bonded complexes with sulfuric acid. It has been suggested that the molecular complexes containing organic acids may represent an important form in aerosol nucleation under atmospheric conditions.[7,8,109,110] Experimental and field studies to directly detect these molecular complexes in the gas phase have yet to be performed. Atmospheric measurements have revealed the presence of neutral molecular clusters containing four H_2SO_4 molecules and one amine molecule with the most abundant form corresponding to those containing a C2- or C4-amine, when sulfuric acid was added to

ambient air to increase signal-to-noise level using cluster CIMS.[111] The presence of alkylaminium salts on nanoparticles has also been supported by field measurements, with particle sizes down to 8–10 nm.[86]

Contribution of Amines to Growth of Aerosol Particles

Considerable progress has been recently made on experimental kinetic and mechanistic measurements on the heterogeneous reactions between amines and ammonium salts.[72,73] The following paragraphs will discuss the current understanding on reactions between amines and clusters and larger particles. A noticeable feature in the heterogeneous interaction between clusters/nanoparticles and sub-micrometer aerosols lies in that the Kelvin effect is much less significant for particles with a diameter of 80 nm and above.[3] As a result, certain changes in reaction mechanism and kinetics take place when the size of particles increases from sub-nanometer to micrometers. Gas uptake on larger particles of sub-micrometers closely resembles those on bulk solutions.[10]

Contribution of Amines to the Growth of Clusters and Nanoparticles

The reactivity of amines with charged ABS clusters $[(NH_4)_{k+1}(HSO_4)_k]^+$, k = 1–10, have been investigated using a Fourier transform iron cyclotron resonance mass spectrometer.[73,112,113] For positively-charged ABS clusters with k = 1–7, alkylamines, including MMA, DMA and TMA, displace out ammonia via Reaction 3.2b' with a near unit uptake coefficient γ (defined as the ratio of the reactive collisions to the total

collisions).[73] The displacement reaction dominates when *k* increases from 1 to 7 with $\gamma \sim$ 1, but the uptake coefficient decreases 10 times for clusters with *k* larger than 8.9 The size of the clusters also appears to play an important role in the reaction mechanism and kinetics.[112] For example, the neutralization pathway [Reaction 3.2b(α)], has been observed in the DMA-ABS cluster reaction, when the positively-charged ABS clusters has more than eight bisulfate ions.[112] The uptake coefficient of the neutralization pathway, however, rarely increases to more than 0.1 for positively-charged ABS clusters,[112] indicating that the proton on the bisulfate ion may be highly localized or not readily accessible to amines.

The effect of charge on the amine-cluster reactions has also been studied between DMA and negatively-charged ABS clusters.[113] Both neutralization and displacement mechanisms have been observed in the reaction.[113] However, the reaction efficiency is generally much lower than that of the reaction DMA with positively-charged ABS clusters.[113] This may be explained by the charge effect. Amines are nucleophiles with stronger affiliation to positively-charged clusters than to negatively-charged ones and thus react faster with positively-charged clusters. Also, more bisulfate ions in the cluster correspond to a larger cluster size and a less negative charge on the unit cluster surface. As a result, DMA reacts more efficiently with larger negatively-charged ABS clusters. Similarly, the reaction between DMA and negatively-charged sulfuric acid clusters increases with increasing cluster sizes.[113]

The kinetics of the reactions of amines with clusters also depends on the cluster compositions and the amine structure. For example, DMA reacts much faster with

negatively-charged ABS clusters than with negatively-charged sulfuric acid clusters.[113] Also, the uptake coefficients of DMA and TMA on positively-charged ammonium nitrate (AN) clusters are smaller than those on positively-charged ABS clusters. The uptake coefficient of DMA on positively-charged ABS clusters is slightly higher than that of TMA.[73]

The reactions between alkylamines and ABS clusters yield alkylaminium sulfate (AAS) clusters that are stable when exposed to ammonia,[73] consistent with theoretical calculations showing that AAS clusters are more stable than the AS ones.[114] There are, however, reactions between amines and aminium sulfate clusters (see Reaction 3.5 and 3.6 as examples):[73]

$$[(HMMA)_k(HSO_4)_{k-1}]^+ + DMA \rightarrow [(HDMA)_k(HSO_4)_{k-1}]^+ + MMA \quad (3.5)$$

$$[(HDMA)_k(HSO_4)_{k-1}]^+ + TMA \rightarrow [(HTMA)_k(HSO_4)_{k-1}]^+ + DMA \quad (3.6)$$

In general, among simple alkylamines (MMA, DMA and TMA), TMA appears to be the most reactive,[73] with the strongest basicity in the gas phase.[115] This suggests that amine may react with small clusters with the kinetics similar to that in the gas phase. While the clusters $[(HTMA)_2(HSO_4)]^+$ practically do not react with DMA, the clusters $[(HTMA)_3(HSO4)_2]^+$ react with DMA with an uptake coefficient of 0.5.[73] DMA has the highest basicity in aqueous solution.[115] When the size of the cluster increases, the reactivity of amines may resemble that in the condensed phase more than that in the gas phase.

It should be pointed out that the reactivity of amines with charged clusters may be distinct from those on neutral clusters and nanoparticles. Recent experimental studies

have been conducted to investigate the contribution of amines to the growth of sulfuric acid nanoparticles from heterogeneous reactions.[9,10] The reaction between TMA and sulfuric acid nanoparticles with the diameters of 4–20 nm has been measured using tandem nano-differential mobility analyzer (nano-TDMA).[9] When exposed to TMA vapor, the size growth factor is 1.10 for sulfuric acid nanoparticles with an initial diameter of 4 nm at 6% RH, and increases slightly when the RH increases.[9] There is also a slight dependence of the particle growth factor on the particle size. For example, the growth factor is 1.1, 1.12, 1.18, and 1.18 at 6% RH for the particle size of 4, 6, 10, and 20 nm, respectively, clearly reflecting the Kelvin effect. The measured size dependence of the neutralization reaction of amines with sulfuric acid nanoparticles is much weaker than those of polymerization and oligomerization reactions of aldehydes and small α-dicarbonyls, since the former reaction is of the first-order, while the latter reactions correspond to the second- or higher orders in the particle phase.[9,10]

Contribution of Amines to the Growth of Sub-micron Aerosols

Heterogeneous reactions of amines likely occur on inorganic/organic acids and ammonium salts (Reaction 3.1 and 3.2). The uptake of alkylamines (MMA, DMA and TMA) on sulfuric acid surface has been investigated in a low-pressure fast-flow reactor coupled to an ion drift-CIMS (ID-CIMS).[71] For all three amines, the uptake process has been characterized by an irreversible neutralization reaction, with the uptake coefficient in the range of (2.0–4.4) × 10^{-2}, about 20 times lower than that of ammonia.[71] The comparable uptake coefficients of the three amines suggest that the reaction is not

limited by the proton transfer step in the solution, since DMA would otherwise exhibit a higher uptake coefficient than those of TMA and MMA because of the difference in the basicity of amines in solution.[115] The uptake coefficients have been shown to increase slightly when the sulfuric acid concentration increases from 59 to 82 wt %, which may be explained by the increase in mass accommodation with the increase in surface acidity.[71]

The reactions of amines with ammonium salts have been measured in a chamber study.[70] When gaseous MMA and AS aerosols are introduced into an environmental chamber, the monomethylaminium ion concentration in the particle phase increases substantially, as detected by an aerosol mass spectrometer (AMS).[70]

Partial displacement of ammonium by trimethylaminium ions has been measured with poly-dispersed AN aerosols exposed to TMA vapor at 20% RH.[72] The uptake coefficient for this process is estimated to be $(2 \pm 2) \times 10^{-3}$. The reaction is not affected by the presence of ammonia gas with a concentration ten times higher than that of TMA.

Organic molecules with the carbonyl function groups are most abundant in the atmosphere, either emitted directly from the sources or formed during the oxidation of organic compounds in the atmosphere. For example, glyoxal and methyl glyoxal are formed from the oxidation of both biogenic[32,116] and anthropogenic[31,49] compounds. The carbonyl group can react with primary and secondary amines (such as MMA and DMA) to form imines (Reaction 3.3a) and enamines (Reaction 3.3b), respectively. The reactions are likely acid-catalyzed, since sulfuric and nitric acids and organic acids are commonly available in the atmospheric particle phase.

The reaction between MMA and glyoxal has been measured in both bulk solution and particle-phase reactions.[78] Imidazole compounds are formed, indicating the contribution of MMA to the particle mass growth, and the presence of MMA in the particle phase is also suggested to enhance the self-oligomerization of glyoxal.[78] Similar reaction is also observed in the system of glyoxal and AS aerosols.[79,117,118] Field measurements have indicated urban aerosols containing high-MW constituents with a large fraction of carbon-nitrogen bonds, suggesting that the carbonyl-amine reaction can be an important source of nitrogen-containing compounds in the aerosol-phase.[119] Experimental studies on the heterogeneous reactions between glyoxal and AS/amino acid particles (100–300 nm) have been performed recently.[79,120] At 50% RH, the uptake of glyoxal on AS and glycine aerosols increases the particle size 1.7 and 1.6 times, respectively. Aerosols containing the mixture of AS and glycine with a mole ratio of 100:1 appear to grow even more in size when exposed to glyoxal vapor.[79]

The reactions between glyoxal and AS/amine aerosols depend largely on the RH, suggesting that the occurrence of those reactions is more efficient on hygroscopic particles. For example, a minimum RH of 35% is required for the occurrence of the reaction of glyoxal on AS, a RH that overlaps with the efflorescence point of AS.[120] The reaction between glycine and glyoxal occurs only when the RH is ~25% or above, which is slightly lower than the 35% RH required for AS-glyoxal reaction.[120] In the presence of water, the following equilibriums may be achieved in the particle phase:

$$H_2O + NH_4^+ \leftrightarrow H_3O^+ + NH_3 \quad (3.7)$$

$$H_2O + NH_2CH_2COOH \leftrightarrow H_3O^+ + NH_2CH_2COO^- \quad (3.8)$$

As a result, water may effectively increase the hydronium ion concentration in particles, which can catalyze the reactions between glyoxal and ammonia/amine.

Amines in the particle phase may react with gas-phase oxidants such as ozone and OH radicals in the atmosphere, a process leading to more oxidized compounds with higher or lower MW and contributing to aging of organic aerosols.[11] For example, the reactions of ozone with particles consisting of aliphatic amines with long-chain alkyl groups have been investigated.[121] The products with various structures have been identified, including organo-nitrites and nitrates. Exposure of particles consisting of the mixture of aliphatic amines and oleic acid to ozone can lead to the formation of amides and imines.[121]

Proteins correspond to a special type of amines with high MW. The ozone uptake on protein compounds has been studied recently, showing that the reaction kinetics depends largely on the property of the semisolid phase of proteins.[122] The uptake process is controlled by the diffusion of ozone in the bulk phase and can be described by a kinetic multilayer flux model.[122] The results from the latter study suggest the importance to understand the phase state (i.e., solid, semisolid, and liquid) of atmospheric aerosols during the aerosol aging process.

Research Objective of this Chapter

In this chapter, we have investigated the heterogeneous uptake of MMA, DMA, and TMA on glass tubes coated with AS or ABS at 293 K to understand the contribution of amines to the growth of sub-micron aerosol particles. The kinetic measurements were

performed in a low-pressure fast flow reactor coupled to an ion drift-chemical ionization mass spectrometer (ID-CIMS). The flow tube technique and cylindrical tubes with the inner wall uniformly coated with solid species have been widely employed to study heterogeneous interactions between gaseous species and solid surfaces.[58,123-125] An advantage of the flow tube experiments is that it allows an extended exposure time to elucidate the kinetic properties of heterogeneous reactions. In addition, such an experimental approach enables simultaneous monitoring of the changes in the concentrations of the reactants and products during the uptake process, providing direct evidence on the reaction mechanisms. Atmospheric implications of our results to the growth and composition of atmospheric aerosols are discussed.

Experimental

Preparation of Glass Tubes Coated with Ammonium Salts

Ammonium sulfate ($(NH_4)_2SO_4$, Sigma-Aldrich, $\geq$ 99.0%) and ammonium bisulfate ($(NH_4)HSO_4$, Fluka, $\geq$ 99.0%) were used as received. Coating of ASe was prepared following a modified denuder preparation protocol.[126] The inner surface of the tube was roughed by sandblasting, and then cleaned by rinsing sequentially with 17% Nitric acid, deionized water (18 mΩ • cm), saturated KOH/Methanol solution, and deionized water. The tube was then dried with a particle-free Nitrogen flow. The tube was coated with a 25 wt % aqueous AS solution: AS solution with this concentration produced a uniform coating without large crystal formation. One opening of the tube was placed vertically into a small beaker containing the coating solution. A vacuum line

with an inline critical orifice was connected to the other opening of the tube. The coating solution was drawn up into the tube to about 12 cm from the solution level. The coating solution was then allowed to slowly drain back into the beaker, and the process was repeated twice. During the whole process, the position of the beaker was adjusted to ensure only ~0.5 cm of the tube was immersed in the coating solution. The tube was then removed from the beaker and its outside surface was wiped with Kimwipe® to remove any excess coating solution droplets. The inner surface of the tube was then kept vertically and dried with a particle-free N_2 flow at ~70 sccm. About 10−30 mg of AS was coated onto the inner surface of the tube for each experiment.

Coating of ABS was made in a similar way except that (1) during the tube cleaning process, methanol, instead of KOH/methanol solution was used, (2) a 48 wt % ABS solution was used to provide uniform coating, and (3) due to the high hydroscopic nature of ABS, after the coated tube was dried with a N_2 flow for 1 h, it was additionally vacuum dried at 1.0×10^{-3} Torr for 1 h. About 10−20 mg of ABS was coated onto the tube.

The tubes after each experiment were rinsed thoroughly with deionized water, heated at 150 °C for 16 h, and cleaned as described previously.

Flow-tube Experiment Procedures

The uptake measurements were performed in a laminar flow reactor coupled to ID-CIMS, similar to those in our previous work.[71,124,125] Briefly, as shown in Figure 10, the 15 cm-long cylindrical glass tube, coated with ammonium sulfate or ammonium

bisulfate (described in the previous section) was placed in a 50 cm-long Pyrex reactor. The inner tube had a radius of 0.94 cm. The temperature of the reaction system was maintained at 293 ± 2 K.

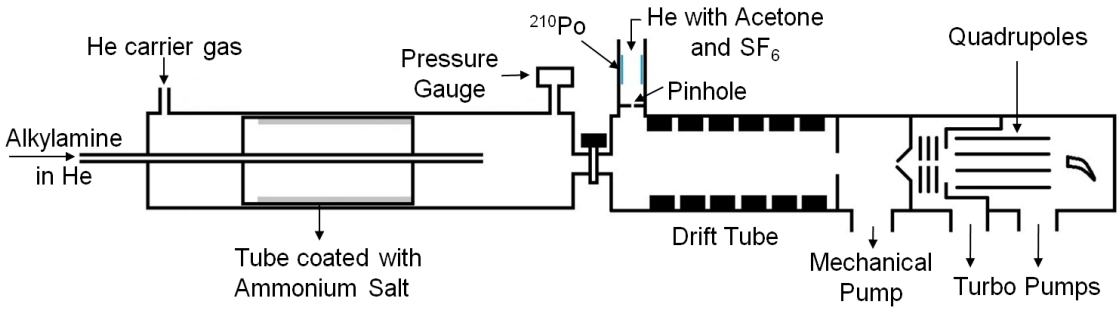

Figure 10. Schematic representation of the laminar-flow reactor coupled to ion drift-chemical ionization mass spectrometer.

Monomethylamine (CH_3NH_2, Aldrich, ≥ 98%), dimethylamine ($(CH_3)_2NH$, Aldrich, ≥ 99%), and trimethylamine ($(CH_3)_3N$, Aldrich, ≥ 99%) were used as received without further purification. Mixtures of individual alkylamines in He gas (80−110 ppm) were prepared by a two-step dilution in a Pyrex bulb and the final pressure was about 920 Torr. A fresh alkylamine/He mixture was prepared after ~20% of alkylamine in the bulb was consumed to ensure a steady flow of alkylamine. The alkylamine vapor in He was introduced into the flow reactor through a movable injector, and its partial pressure in the reactor was estimated to be on the order of 10^{-6} to 10^{-7} Torr. All carrier flows were monitored with calibrated electronic mass flowmeters (Millipore Tylan 260 Series).

The flow reactor was operated under the laminar flow condition at a total pressure of 1.3−2.4 Torr, and a flow velocity of 520−1200 cm s^{-1}. The coated tube was changed after each experiment.

The details of the ID-CIMS instrumentation have been described previously.[7,127] Two complimentary ionization schemes were employed to qualitatively and quantitatively evaluate the kinetics and mechanism of the heterogeneous reactions.

The first detection method involved the reactions of alkylamines and ammonia with protonated acetone dimer ([$(C_3H_6O)_2 \cdot H^+$], PAD, Figure 11a).[128] PAD was used to detect alkylamines (except TMA) and ammonia by the association reaction,

$$A + (C_3H_6O)_2 \cdot H^+ \rightarrow (C_3H_6O)_2 \cdot A \cdot H^+ \quad (3.9)$$

where A denotes MMA, DMA, or ammonia and $(C_3H_6O)_2 \cdot A \cdot H^+$ denotes the corresponding association products. In the case of trimethylamine (TMA), the displacement reaction takes place:

$$TMA + (C_3H_6O)_2 \cdot H^+ \rightarrow (C_3H_6O) \cdot TMA \cdot H^+ + C_3H_6O \quad (3.10)$$

The PAD reagent ion was produced by passing a 3.0 slpm flow of He, containing trace amounts of acetone (C_3H_6O) and SF_6 through 20-mCi ^{210}Po ionization source (NRD), and a pinhole (with a diameter of 0.476 mm) between the ionization source and the ion drift tube was used to increase the pressure in the ionization source to about 90 Torr (Figure 11a).

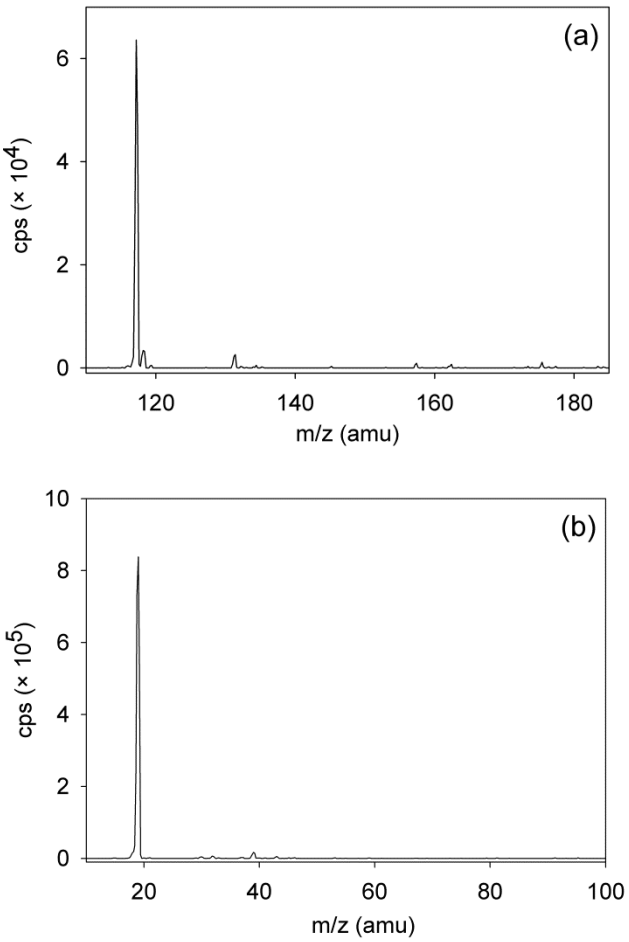

Figure 11. Typical mass spectra for the chemical ionization methods at 293 K. (a) the mass spectrum for protonated acetone dimer (PAD), with P_{total} = 2.38 Torr, and u = 580 cm s^{-1}. (b) the mass spectrum for hydronium ion from proton transfer reaction (PTR), with P_{total} = 1.22 Torr, and u = 1160 cm s^{-1}.

MMA, DMA and ammonia were monitored at their association product peaks, $[(C_3H_6O)_2 \bullet CH_3NH_2 \bullet H]^+$ (m/z = 148), $[(C_3H_6O)_2 \bullet (CH_3)_2NH \bullet H]^+$ (m/z = 162) and $[(C_3H_6O)_2 \bullet NH_3 \bullet H]^+$ (m/z = 134), respectively. TMA was monitored at its displacement product peak, $[C_3H_6O \bullet (CH_3)_3N \bullet H]^+$ (m/z = 118). No protonated hydrated acetone dimer $[(C_3H_6O)_l \bullet H \bullet (H_2O)_y]^+$ or alkylamine-acetone-water cluster $[(C_3H_6O)_l \bullet Y \bullet H \bullet (H_2O)_y]^+$ was observed under our experiment conditions.[128,129] The

measured protonated alkylamine-acetone cluster signal intensities were corrected for the background, which was typically less than 8% of the corresponding alkylamine signals. During the uptake measurements, isotope ion $[(C_3H_6O)_2 \bullet D]^+$ (m/z = 118) was monitored to account for the variation in the protonated alkylamine signal intensity due to minor fluctuation in the reagent ion signal.[71] In the case of TMA, monitoring of reagent ion signal variation is not applicable because the protonated trimethylamine-acetone cluster also had the m/z value of 118.

The second detection method is the proton transfer (PTR) reaction between amines/ammonia and hydronium ion (H_3O^+) was also employed:

$$B + H_3O^+ \rightarrow B \cdot H^+ + H_2O \qquad (3.11)$$

where B and $B \bullet H^+$ denote alkylamines and their corresponding protonated forms, respectively. The details of this method have been reported previously (Figure 11b).[71] Ammonia could not be quantified by this method, because of the overlap between H_3O^+ and NH_4^+ signals.

MMA, DMA, and TMA were monitored at their protonated peaks, $(CH_3NH_2 \bullet H)^+$ (m/z = 32), $[(CH_3)_2NH \bullet H]^+$ (m/z = 46), $[(CH_3)_3N \bullet H]^+$ (m/z = 60), respectively. Similarly to the data process protocol in the PAD method, the measured protonated alkylamine signal intensities were corrected for the background, which was typically less than 4% of the corresponding alkylamine signals, and $H_3{}^{18}O^+$ (m/z = 21) isotope ion was monitored during the uptake measurements for all amines. However, ammonia could not be detected by this method, since the product NH_4^+ had an m/z value of 18, which overlapped with that of H_3O^+ with much higher signal intensity.

The reactions between alkylamines and ammonium sulfate/bisulfate were evaluated by exposing a length of the glass tube coated with a corresponding salt to the alkylamine vapor, while retracting the moveable injector to an upstream position of the tube and selectively monitoring the alkylamine and ammonia signals using the ID-CIMS.

Calculation of the Uptake Coefficient γ

The uptake coefficient (γ), defined by the ratio of gas-surface collisions that result in loss of the alkylamine onto the surface to the total gas-surface collisions, was determined by monitoring the signal change of the alkylamine, as it was exposed to the coated tube.[58,124,125] The uptake coefficient γ was calculated from the first-order rate constant k_r of alkylamine signals:[124,125]

$$\gamma = \frac{2rk_r}{\omega + rk_r} \tag{3.12}$$

where r is the radius of the flow reactor and ω is the mean thermal speed.

We considered two uptake coefficients γ in the reaction between alkylamines and ammonium sulfate, i.e., the initial uptake coefficient γ_0 and steady-state uptake coefficient γ_{ss}.

To determine the initial uptake coefficient γ_0, the observed first-order rate constant k_{obs} for each experiment was measured from the loss of alkylamine during the exposure:[57,71]

$$k_{obs} = \frac{u}{L}\ln\left(\frac{I_0}{I_t}\right) \tag{3.13}$$

where u is the carrier gas flow velocity (cm s^{-1}), L is the exposure distance (i.e., the distance between the injector outlet and the tube outlet, cm), I_0 is the initial alkylamine signal before uptake by ammonium salt, and I_t is the signal at the reaction time when the signal loss of alkylamine reaches maximum.

Gas-phase diffusion correction was determined according to:[130]

$$\frac{1}{k_{obs}} = \frac{1}{k_{diff}} + \frac{1}{k_r} \tag{3.14}$$

where k_{diff} (s^{-1}) represents the radial alkylamine vapor gradients in the reaction chamber due to significant reactive wall loss. k_{diff} was obtained as[130,131]

$$k_{diff} = \frac{3.66 D_{amine-He}}{r^2} \tag{3.15}$$

where $D_{amine\text{-}He}$ represents the binary gas diffusivity between a specific alkylamine and He, at given temperature and pressure (cm^2 s^{-1}). $D_{amine\text{-}He}$ was estimated by an empirical correlation.[132] The typical k_{diff} values for MMA, DMA, and TMA were 641.5, 517.8 and 469.3 s^{-1}, respectively, with the PAD method (2.4 Torr, 293 K) and were 1213, 1029 and 1180 s^{-1}, respectively with the PTR method (1.3 Torr, 293 K).

To determine the steady-state uptake coefficient γ_{ss}, the exposure distance was converted into the contact time between alkylamines and ammonium sulfate, and the natural logarithm of the ratio of alkylamine signal levels before exposure and at the steady-state reaction was plotted as a function of the contact time, t. The observed first-order rate constant k_{obs} for each alkylamine was obtained from the slope of the linear regression of each data set of the corresponding alkylamine, and the first-order rate constant k_r was then obtained employing Equation 3.14 for the gas-diffusion corrections.

The steady-state uptake coefficients γ_{ss} were calculated from Equation 3.12 using the corresponding first-order rate constants k_r.

We estimated that the systematic uncertainty in the uptake coefficient was within 20%, considering sources of the error in temperature and pressure fluctuations and gas flow rate changes.

Results and Discussion

Uptake of Alkylamines on Ammonium Sulfate

Figure 12 illustrates the temporal profile of alkylamines and ammonia signals with the PAD method, showing the loss of MMA on the AS tube (Figure 12a) and formation of ammonia (Figure 12b). The MMA concentration in the gas phase dropped instantly when the injector was withdrawn upstream to expose a 2.7 cm length of the inner surface of the tube to the MMA vapor, accompanied by an increase in the ammonia signal. After about 20 s, the MMA signal slowly recovered to about 70% of the original intensity, and the release of ammonia decreased gradually to a steady state. There was no further change after the reaction system reached this steady state, even after 150 s exposure time. When the injector was slid downstream, the MMA signal recovered after a small desorption of MMA, while the ammonia signal decreased to about its original level. Since the accommodation of gas molecules on a solid surface involves both physical adsorption and surface reaction, such observation likely suggests a slower surface reaction rate than that of accommodation. Because physical adsorption is reversible, the small desorption peak indicates the release of the adsorbed MMA on

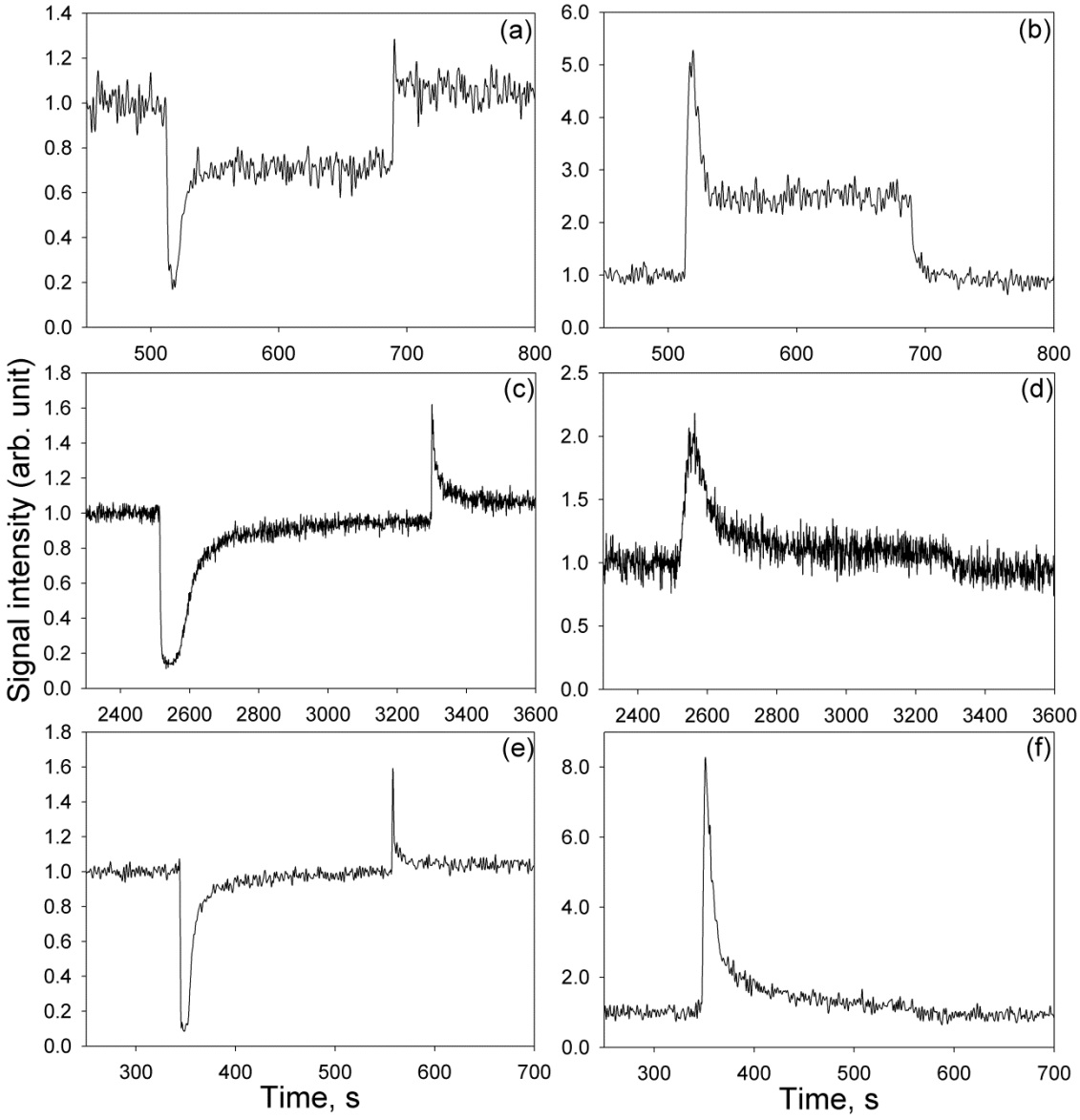

Figure 12. Temporal profiles of the protonated alkylamine-acetone cluster and protonated ammonia-acetone cluster signals when the alkylamine vapor is exposed to ammonium sulfate at 293 K. (a) Signal of MMA-acetone-H^+. (b) Signal of NH_3-acetone-H^+ for the same time interval of (a). (c) Signal of DMA-acetone-H^+. (d) Signal of NH_3-acetone-H^+ for the same time interval of (c). (e) Signal of TMA-acetone-H^+. (f) Signal of NH_3-acetone-H^+ for the same time interval of (e).

the surface back to the gas phase. The release of ammonia upon MMA uptake confirms a displacement reaction between MMA and AS. The reaction was fast during the initial 20

s of the exposure time, but decreased when the system reached the steady state. Similar behaviors were observed in the uptake experiments of DMA and TMA with AS, as depicted in Figures 12c to 12f.

Simple alkylamines react with AS to generate alkylaminium (ammonium) sulfate

$$X + (NH_4)_2SO_4 \rightarrow (HX)_2(NH_4)_{2-n}SO_4 + nNH_3 \qquad (3.16)$$

where *X* denotes MMA, DMA, or TMA and *n* is 1 or 2. The initial uptake coefficients γ_0 for MMA, DMA and TMA are in the range of determined to be $(2.6 \pm 0.4) \times 10^{-2}$, $(3.4 \pm 0.9) \times 10^{-2}$ and $(2.9 \pm 1.5) \times 10^{-2}$, respectively (Table 3), indicating that alkylamines react with AS with a similar rate. The fast reaction is fast during the first 20 s, is probably because of fast reactions on the more reactive sites such as defects and steps of the AS surface. Similar behaviors were observed for the alkylamines using the PTR method, which provided a better S/N ratio, and the initial uptake coefficients γ_0 estimated from the PTR method were similar to those using the PAD method.

Table 3. Measured Uptake Coefficients (γ_{ss}) of Alkylamines on Ammonium Sulfate.[a]

	PTR[b]		PAD[c]	
	γ_0 ($\times 10^{-2}$)	γ_{ss} ($\times 10^{-4}$)	γ_0 ($\times 10^{-2}$)	γ_{ss} ($\times 10^{-4}$)
Monomethylamine	3.4 ± 0.8	60 ± 12	2.6 ± 0.4	42 ± 2.8
Dimethylamine	3.2 ± 1.1	9.4 ± 2.2	3.4 ± 0.9	5.9 ± 0.7
Trimethylamine	2.4 ± 0.4	2.3 ± 0.4	2.9 ± 1.5	2.3 ± 0.7

[a] All experiments are performed at 293 K and the error corresponds to one standard deviation (1σ) for all measurements.
[b] Values are based on at least six independent uptake experiments.
[c] Values are based on at least five independent uptake experiments.

To assess the kinetics of the steady-state reaction, the exposure distance is converted into a contact time between alkylamines and AS, and the decay of alkylamine signal at the steady state was plotted as a function of the contact time (Figure 13). The black circles, blue squares, and red triangles represent the measurements for MMA, DMA and TMA, respectively, under similar experimental conditions, i.e., using the PTR method, T = 293 K, P_{total} = 1.20 − 1.48 Torr, u = 863−1225 cm s^{-1}, and t = 2.5−7.6 × 10^{-3} s. All three decays follow the first-order kinetics, and the reaction rate constant decreased with the increasing number of methyl group on alkylamine. The steady-state uptake coefficients γ_{ss} are calculated from the first-order rate constants, obtained from the slope of the linear regression of each data set with the gas-diffusion corrections.

The steady-state uptake coefficients γ_{ss} for the three alkylamines with AS are summarized in Table 3, with the values obtained with the PAD and PTR methods being comparable. At 293 K, the uptake coefficients γ_{ss} are in the range of (6.0 ± 1.2) × 10^{-3} for MMA, (9.4 ± 2.2) × 10^{-4} for DMA, and (2.3 ± 0.4) × 10^{-4} for TMA using the PTR method, with one standard deviation uncertainty. The value of the steady-state uptake coefficient is the largest for MMA and the smallest for TMA, indicating a decreasing trend when the number of methyl groups in alkylamines increases. This observation can be explained by the bulkiness of the alkylamines molecules: more methyl groups likely correspond to less accessible lone pair electrons on the nitrogen atom, making it to be less reactive. It has been reported that the displacement reaction between TMA and AN aerosols is not affected in the presence of ammonia, with the ratio of about 10 between

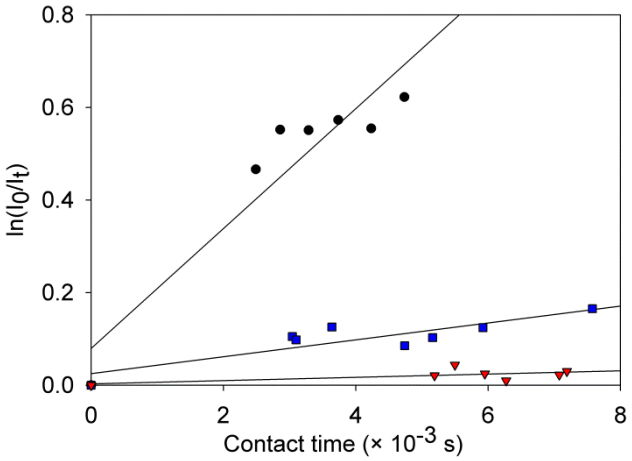

Figure 13. Alkylamine signal as a function of the contact time between amines and ammonium sulfate surface at 293 K. The black circles represent the monomethylamine signal when exposed to ammonium sulfate, with P_{total} = 1.33–1.35 Torr, u = 1205–1225 cm s^{-1}, and a contact time t = 2.5−4.7 × 10^{-3} s; the blue squares represent the dimethylamine signal, with P_{total} = 1.20–1.48 Torr, u = 863–1064 cm s^{-1}, and a contact time t = 3.0−7.6 × 10^{-3} s; the red triangles represent the trimethylamine signal with P_{total} = 1.22–1.29 Torr, u = 1131–1213 cm s^{-1}, and a contact time t = 5.2−7.2 × 10^{-3} s. Ionization method: PTR.

the ammonia and TMA concentrations in the gas phase.[72] Also, it has been shown that ammonia is unable to replace amines in aminium nitrate clusters.[73] Hence, the displacement reaction between alkylamines and ammonia salts is likely irreversible.

A reactive uptake coefficient of 2 × 10^{-3} previously has been determined by Johnston and co-authors for AN aerosols,[72,73] and their value is generally within the range of our measured initial and steady-state uptake coefficients (10^{-2}–10^{-4}). Those previous measurements used AN particles of 20–500 nm diameter and charged ABS clusters, corresponding to a shorter reaction time (~23 s)[72] and a fast depletion of ammonium salt molecules (less than 12 molecules per cluster),[73] respectively.

Our observed steady-state uptake coefficients γ_{ss} for all alkylamines are independent of the mass of AS coated onto the tube, as shown in Figure 14. The

available area for reaction of the AS may not be significantly different from its geometric area, since the value of γ_{ss} will otherwise increase with an increasing mass of AS on the tube.[124,125] For a tube coated with 8 mg AS, the estimated volume of alkylamine to consume all AS is about 1.36 cm^3 at STP, which is larger than all the alkylamine filled in one bulb (for an alkylamine concentration of 100 ppm, a 2 L bulb at 920 Torr contains 0.24 cm^3 alkylamine at STP). Since the tubes used in the uptake experiments are coated with more than 8 mg AS, it is possible that only a small fraction of the outer layer of AS is consumed during the experiment.

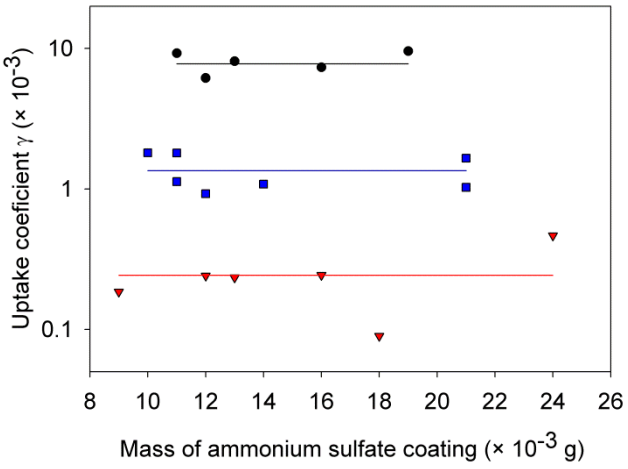

Figure 14. Steady-state uptake coefficient γ_{ss} as a function of ammonium sulfate mass on the tubes. The black circles, blue squares, and red triangles represent monomethylamine, dimethylamine, and trimethylamine, respectively.

Uptake of Alkylamines on Ammonium Bisulfate

A typical uptake of MMA on ABS tube is shown in Figure 15a, and Figure 15b depicts the ammonia signal with the PAD method. Similarly to the uptake on AS, the gas phase MMA concentration drops to 30% of the original level when the MMA vapor is exposed to a 1.7 cm length of the coated ABS. However, there is little change in the signal of ammonia. No recovery of MMA is observed on the time scale of the exposure. When the injector is slid downstream, there is a full recovery of the MMA signal to its original level, but no desorption peak is observed. Similar behaviors are observed for the other two alkylamines (Figures 15c to 15f). Interestingly, for a given exposure time, the loss is identical for all three alkylamines. In Figure 15c, the recovery in the concentration of DMA showed a delay when the injector was changed to the downstream position, probably because of reversible physical adsorption/desorption on the reactor wall. Measurements using the PTR method yield the similar kinetic behaviors.

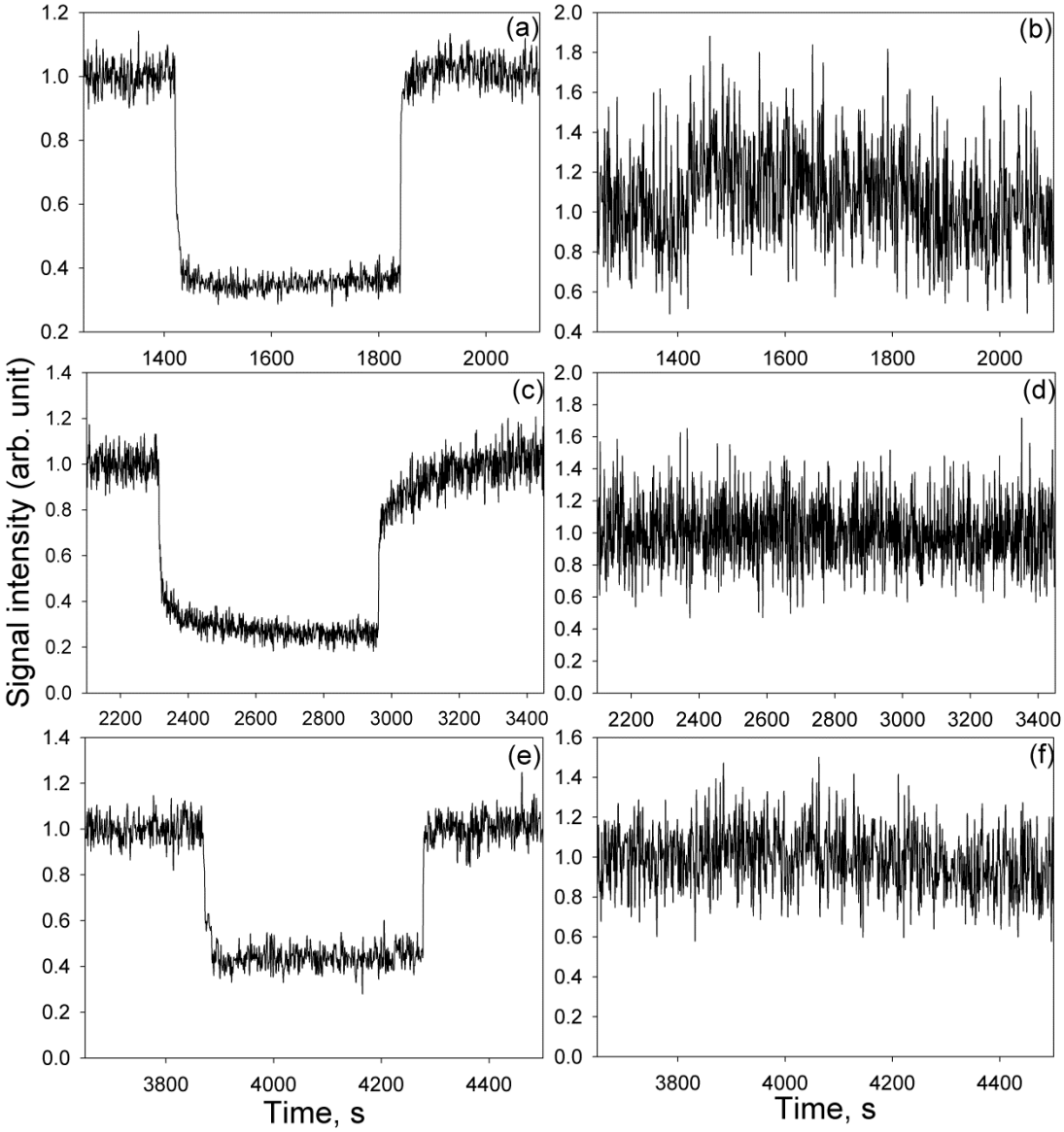

Figure 15. Temporal profiles of the protonated alkylamine-acetone cluster and protonated ammonia-acetone cluster when the alkylamine vapor is exposed to ammonium bisulfate at 293 K. (a) Signal of MMA-acetone-H^+. (b) Signal of NH_3-acetone-H^+ for the same time interval of (a). (c) Signal of DMA-acetone-H^+. (d) Signal of NH_3-acetone-H^+ for the same time interval of (c). (e) Signal of TMA-acetone-H^+. (f) Signal of NH_3-acetone-H^+ for the same time interval of (e).

The uptakes of alkylamines on ABS are similar to those of alkylamines on H_2SO_4, which involve an irreversible alkylamine uptake with no desorption and similar uptake coefficients for all three alkylamines.[71] It is likely that the alkylamines react with ABS to form alkylaminium ammonium sulfates

$$Y + NH_4HSO_4 \rightarrow (HX)(NH_4)SO_4 \quad (3.17)$$

where *Y* represents one of the three alkylamines, MMA, DMA or TMA.

The measured reaction rate constants (k_{obs}) for all alkylamines are close to the diffusion-limited values (k_{diff}), indicating that this type of gas-solid reaction is diffusion-controlled and the uptake coefficients are close to unity. The gas-solid reaction rate is controlled by several factors including mass transfer of alkylamines to the solid surface, adsorption of alkylamines on the surface, and chemical reaction rate.[133] The reaction between alkylamine and ABS is a fast acid-base reaction. The adsorption of alkylamine molecules onto the surface of ABS will not be the rate-limiting step. For one unit cell of ABS crystal (an area of about 1 nm^2), there are four proton atoms which are accessible to the alkylamine molecule to react with.[134] Furthermore, there may be more accessible protons on the defects and steps of the solid surface. When an alkylamine molecule collides on the ABS surface, it is likely that this occurs on an accessible proton. Even if an alkylamine molecule is physically adsorbed on the ABS surface, it reacts promptly with protons in its vicinity. A similar behavior has been observed in the uptake of OH radical on ammonium salts: OH has a larger uptake coefficient on ABS surface than that on AS.[135] Also, theoretical analysis of this reaction system concluded that surface adsorption is not the rate-controlling step.[136]

To confirm the difference in the reactivity between solid and liquid surfaces, an uptake experiment of DMA on 30 wt % ABS solution at 245 K was performed, using a previously reported approach.[71,137] The uptake coefficient of DMA on 30 wt % AS solution is determined to be $(1.8 \pm 0.6) \times 10^{-2}$ with the PTR method, comparable to the uptake coefficient of DMA on sulfuric acid.[71] This result indicates that due to the dilution and solvation effects of water, a longer time is required for alkylamine molecules to diffuse into the solution to react with H_3O^+.[138]

Other Recent Studies of the Amine Uptake on Ammonium Salts

Shortly after this study, several research articles on the reactions between amines and ammonium salts have been published. The purpose of this section is to summarize the recent progress on the heterogeneous reactions between amine and ammonium salts.

The uptake of MMA on a series of ammonium salts has been investigated using a Knudsen cell reactor coupled to a quadrupole MS (QMS).[139] Finely grounded powders of ammonium salts, including sulfate, bisulfate, nitrate and chloride, are exposed to an excess amount of MMA vapor and the decrease in MMA vapor concentration and the formation of NH_3 is monitored by the QMS.[139] The uptake coefficients of MMA on ammonium sulfate and nitrate in the Knudsen cell are comparable to those determined in this chapter and on sub-micron particles.[72] The uptake coefficient of MMA on ABS in Knudsen cell experiments, however, is much lower than the values measured on solid ABS surface in this chapter, but close to that of the alkylamines uptake on the ABS solution determined by us. Since in the later study the MMA vapor is generated from the

aqueous solution of MMA, the ABS surface may also take up water molecules, leading to a decreased uptake coefficient on the ABS surface.

The reactions between triethylamine (TEA) and a series of ammonium salts have been measured using an electrodynamic balance (EDB) coupled with a Raman spectroscopy.[140] Charged particles (solid or aqueous solution, 15–35 μm in diameter) of ammonium salts, including sulfate, bisulfate, nitrate, chloride, and oxalate, are suspended in the EDB chamber and exposed to excess amount of TEA vapor (3 ppm) at a controlled RH of 5, 50 or 75%.40 It has been shown that the uptake of TEA is efficient and nearly complete on the droplet of ammonium salt solutions, including sulfate, bisulfate, nitrate, and chloride. However, there is only a limit reaction (~5% increase in mass) between TEA and dry ammonium sulfate or oxalate solid particles.[140] It is possible that the uptake of TEA on ammonium salts is slow and limits the reaction. It is shown in this chapter that the uptake coefficients of alkylamines on AS decrease as the alkyl groups become larger. As a result, it is possible that the uptake coefficients for TEA may be in the range of 10^{-5}. It can be estimated that it may take ~10^6 seconds (~12 days) for a 20 μm dry AS particle to react with TEA completely, or a mass growth of ~8% in 1 day, which is the timescale of the EDB experiments. The process is further complicated by the diffusion of gas molecules in the condensed phase, which is not well understood especially for the aminium salts produced during the uptake experiments.

Atmospheric Implications

Our experimental results demonstrate that amines react efficiently with solid ammonium sulfate and bisulfate surfaces; the former occurs via a displacement reaction, while the latter takes place by neutralization. Under atmospheric conditions, both amines and ammonia can neutralize acidic aerosols. However, since ammonia is far more abundant than amines under typical atmospheric condition, except at the proximity to the emission source of amines, aerosol neutralization occurs dominantly by ammonia. On the other hand, further reactions of amines can replace out ammonia on AS aerosols, leading to the formation of aminium sulfate.

The uptake coefficients of alkylamines on sulfuric acid are about one order of magnitude lower than that of ammonia.[141] Given that the atmospheric ammonia concentration is normally ten times higher than those of amines, amines may not contribute significantly to neutralization of particle-phase sulfuric acid. However, amines can react effectively with ammonium salts, displacing out ammonia and forming aminium salts in the particle phase. As a result, even if ammonia reacts initially with acidic constituents in the particle phase because of the kinetic preference, the products (ammonium salts) will likely react further with gaseous amines to yield aminium salts in aerosols.

Our measured initial uptake coefficients for the displacement reaction between alkylamines and AS solid are large, indicating that a partial exchange occurs rapidly to alter the composition of the outer layer of the AS particles, followed by a slower steady-state uptake. Both the initial and steady-state uptake can be important pathways to alter

the AS particle composition. Since the displacement reaction between alkylamines and ammonium salt are likely irreversible, the occurrence of such a reaction will not be affected in the presence of ammonia, even if its concentration may be substantially higher than those of amines in the atmosphere. Our findings provide an explanation of atmospheric field measurements, showing that aerosols containing aminium salts were observed even in the presence of high concentration of ammonia.[142]

Field measurements have shown a larger abundance of DMA than MMA in the aerosol phase, despite of their comparable gaseous concentrations.[71] Our results reveal that at steady state DMA reacts with AS solid at a much slower rate than that of MMA, indicating that a selective accumulation of dialkylaminium in the particle phase is unlikely related to a kinetic preference.

Our results reveal that alkylamines react with bulk ABS surface via the neutralization mechanism and this reaction is limited by gas-diffusion diffusion and proceeds efficiently with the uptake coefficient close to unity. In the absence of ammonia, we estimate that a time scale of about 30 seconds is needed to allow 1 ppb DMA to completely react with an ABS particle of a 100 nm diameter (with a density of 1.78 g cm^{-3}), on the basis of a shrinking unreacted core model.[133] On the other hand, ABS is highly hydroscopic with a deliquescence point of 40% RH at 298 K.[137] As a result, at high RH condition, it is plausible likely that the outer layers or the entire ABS particles are aqueous ABS solution. The uptake coefficient of alkylamines on ABS solution is close to that on sulfuric acid solution. Using the uptake coefficient of DMA on ABS solution, it is estimated that ~22 min is needed for 1 ppb of DMA (in the

absence of ammonia) to completely react with a 30 wt % ABS aqueous droplet of 100 nm diameter (with a density of about 1.17 g cm^{-3}).

The findings from this work, along with the recent results by Johnston and co-authors[72,73,112,113] and the previous studies of uptake of alkylamines on sulfuric acid,[71] suggest that alkylamines contribute to acidic particle growth and alternation of ammonium salt particle composition. This conclusion is supported by atmospheric measurements, showing widespread presence of organic nitrogen-containing species in the aerosol-phase.[86,142,143] Accurate kinetic information of uptake of alkylamines on acidic and ammonium salt aerosols will contribute to a better assessment of the evolution and sinks of alkylamines in atmospheric models, along with the knowledge of aerosol properties (i.e., size, number concentration, and chemical composition, etc.) and concentrations of gas-phase oxidants.

Future Research Directions

Accumulating evidences have indicated the contribution of amines to new particle formation in the atmosphere. However, the available experimental studies do not differentiate the roles of amines in the two distinct stages of new particle formation, i.e., whether amines enhance new particle formation by overcoming the free energy nucleation barrier by forming stable molecular complexes with sulfuric acid or by overcoming the Kelvin barrier by stabilizing freshly nucleated acidic particles. Future experimental and field research is required to directly detect these molecular complexes in the gas phase. Also, there exist large discrepancies among available experimental

results on the magnitude in the enhancement of new particle formation by amines, probably because of contaminations of trace ammonia/amines in previous experimental studies. Refined experimental procedures need to be developed to eliminate the interference from contaminations in experimental nucleation studies. Advances in analytical instruments for detecting sub 3-nm particles and clusters and to analyze their chemical compositions are also required to quantitatively assess the role of amines in new particle formation. Analogous to sulfuric acid, amines may form molecular complexes with organic acids to help to overcome the nucleation barrier, and future experimental and theoretical studies are needed to investigate the formation of molecular complexes between amines and organic acids.

The growth of clusters and nanoparticles in the atmosphere remains poorly understood. The heterogeneous reaction between amines and acidic clusters may contribute significantly to this process, on the basis of recent studies using charged clusters. In general, positively-charged clusters are more reactive toward amines than negatively-charged ones, which may be attributed to the nucleophilicity of amines. Although it may be reasonable to assume that the reactivity of neutral clusters with amines is between those of positively- and negatively-charged clusters, direct kinetic experiments are necessary to measure the reactions between amines and neutral clusters and to better assess the contribution of amines to growth of atmospheric clusters and nanoparticles. Also, experimental studies are needed to compare the reactivity for different types of amines (e.g., MMA, DMA and TMA) on acidic clusters to establish the reactivity-structure relation. Furthermore, it has been well recognized that the

atmospheric sulfuric acid concentration is often insufficient to explain the growth of nanoparticles and organic compounds are believed to be largely responsible for the growth of nucleation mode particles.[3] It is plausible that the particle-phase reactions between amines and organic acids and a synergistic effect involving carbonyls may contribute to nanoparticle growth.

Amines may play an essential role in the growth and transformation of submicron aerosols in the atmosphere. One such a reaction pathway involves neutralization with acidic aerosols, similar to ammonia. Since the ambient concentration of ammonia is normally much higher than those of amines, ammonia is anticipated to dominantly neutralize acidic particles, leading to formation of ammonium salts. However, we have shown that amines can replace ammonia from particles containing ammonium salts to form aminium salts. Also, the carbonyl-amine reaction may contribute to particle growth and lead to the formation of high-MW, nitrogen-containing compounds. Further experiments are needed to investigate the uptake of alkylamines on monodispersed neutral ammonium salt nanoparticles, which can elucidate the possible size effects on the reactivity of ammonium salt particles with alkylamines. Also, research is needed to investigate the interactions between organic acids and amines, including the detailed reaction kinetics and mechanism. In particular, a systematic study is recommended to cover a series of representative organic acids and amines that have been frequently observed in the atmosphere, to develop the reactivity-structure relationship between the organic acids and amines. For the uptake of amines on crystalline ammonium salts, discrepancies still exist on whether there is a limitation in

the uptake process because of solid-phase diffusion. Further investigation is needed to address this issue. The interactions between aminium salts and carbonyl compounds are also worth exploring, since even at low RH aminium salts readily absorb water, which may be critical to facilitate the carbonyl-amine reaction in the particle phase.

CHAPTER IV

MODIFICATION OF AEROSOL PROPERTIES BY PARTICLE-PHASE AMINES[*]

Introduction

As discussed in Chapter III, atmospheric amines undergo various heterogeneous reactions with aerosol constituents, and particle-phase amines can be further oxidized by atmospheric oxidants. The major products from heterogeneous reactions of amines include aminium salts (sulfate, nitrate, chloride, and carboxylate), imines/enamines, nitrogen-containing polymers, and organo-nitrites/nitrates. Their presence in the particle phase can significantly impact the aerosol properties, which ultimately influence the direct and indirect climate forcing of aerosols.

Hygroscopicity and Cloud Condensation Nuclei Activation

Several early studies have showed that AASs are highly hygroscopic and absorb water even at low RH.[144] As a result, after aerosols containing ammonium salts (partially) react with gaseous amines, particles may become more hygroscopic and absorb water at low or medium RH. For example, the efflorescence and deliquescence of triethylaminium sulfate (TEAS) microparticles have been studied using EDB.[140] It is found that the reaction between ammonium salts and TEA would change particles

[*] Part of this chapter is reprinted with permission from Qiu, C.; Zhang, R. Physiochemical Properties of Alkylaminium Sulfates: Hygroscopicity, Thermostability, and Density. *Environmental Science & Technology* **2012**, *46*, 4474. Copyright 2012 American Chemical Society. Part of the chapter has been submitted to *Phys. Chem. Chem. Phys.* for the consideration of publication.

deliquescence point to lower RH. Unfortunately, so far there is no systematic study on the hygroscopicity of aminium sulfates.

The hygroscopic growths of 7.5 nm nanoparticles containing aminium carboxylates at 90% RH have also been determined using nano-TDMA.[86] For nanoparticles with the diameter of 7.5 and 10 nm, the acetates and propanoates of MMA, DMA and TMA show a similar size growth (~1.15) at 90% RH, lower than that of AS (~1.33).[86] The size growth of 15 nm nanoparticles of the acetate and propanoate of TMA is larger than those of the acetates and propanoates of MMA and DMA at 90% RH.

The CCN activities of a series of amino acids have been recently investigated.[145] The solubility of amino acids in water appears to be the key factor in controlling their CCN activity. For example, amino acids with a higher water solubility (>100 g/L) are more effective in CCN activation, while particles containing amino acids with intermediate and low solubility exhibit limited CCN activation.[145]

Thermostability

The volatility of several classes of aminium salts have been recently determined, including aminium carboxylates, nitrates and chlorides.[86,139,146] The acetates and propanoates of MMA, DMA and TMA are all thermally more stable than AS above 120 °C, and the carboxylates of DMA is the most stable compounds.[86] Hence, the compounds containing aminium carboxylates are thermally stable in the particle phase. Volatility measurements have also been performed on a series of alkylaminium nitrates and the enthalpies of vaporization of those compounds are comparable to that of AN.[146]

The vapor pressures of alkylaminium nitrates are around 2×10^{-4} Pa, slightly lower than that of AN.[146] Hence, alkylaminium nitrates exhibit comparable stability to that of AN under atmospheric conditions and may exist in atmospheric aerosols as the products of heterogeneous reactions of amines. Under high vacuum conditions, monomethylaminium nitrate and chloride show partial decomposition, similar to ammonium nitrate and chloride.[139]

Phase Transformation

The replacement reactions of amines with AS aerosols may lead to a change in the particle phase, i.e., from crystalline to amorphous or liquid phase. Aminium salts could be typically amorphous or liquid at ambient temperature,[147-149] in contrast to AS that exists in the solid state at atmospheric-relevant temperature. For example, the melting point of ethylaminium nitrate is 9 °C,[147] and the glass transition and melting temperature of ethylaminium sulfate are −67.1 and 39.7 °C, respectively.[148]

Aminium salts are likely hygroscopic and may absorb water at low or intermediate RH. The transition of the particle surface from crystalline to amorphous/liquid also changes the diffusion in particle phase substantially, since the diffusion in solid is normally at least 5–10 orders of magnitude lower than that in amorphous or liquid phase.[122] The phase transition because of the presence of amine derivatives in aerosols may have profound impacts on particle CCN activity and the reactivity towards atmospheric oxidants.

Optical Properties

The heterogeneous reactions between amines and carbonyl compounds yield unsaturated organic compounds, including imines, enamines, oligomers, and polymers. These compounds may absorb light in the UV-Vis range, e.g., 350 nm, as frequently termed as "brown carbon".[59,150-152] For example, the reaction between glyoxal and glycine aerosols enhances the aerosol extinction cross section, σ_{ext}, at 355 nm up to 6 times, depending on the particle sizes. For the reaction between glyoxal and AS aerosols under the similar conditions, the enhancement in σ_{ext} is about 9 times. Interestingly, aerosols containing AS and glycine with a mass ratio of 100:1 exhibit an increase of 10 times in σ_{ext}, suggesting the existence of a synergistic effect when both amino acids and AS are presented in the particle phase to react with glyoxal.[79]

Research Objective of this Chapter

In this chapter, we have conducted laboratory experiments to systematically investigate several important physicochemical properties of aminium sulfates, including hygroscopicity, thermostability and density by an integrated aerosol analytical system. The sulfates of five representative alkylamines were used, including MMA, DMA, TMA, DEA, and TEA, which correspond to those commonly observed in field measurements of atmospheric aerosols. The properties of AAS-AS mixtures were also determined to evaluate the impacts of formation of AASs on the properties of AS aerosols.

Experimental

Five AASs, MMAS, dimethylaminium sulfate (DMAS), trimethylaminium sulfate (TMAS), diethylaminium sulfate (DEAS), and triethylaminium sulfate (TEAS) were prepared by mixing stoichiometric amounts of a diluted alkylamine aqueous solution and a diluted sulfuric acid aqueous solution. The resulting AAS stock solution had a typical concentration of ~1 wt %. AAS-AS mixture with a specific mass ratio was prepared by adding a known amount of AS solid to an appropriate volume of the AAS stock solution; the resulting solution was then diluted to a final total salt concentration of ~1 wt %.

The AAS or AAS-AS mixture solution was then transferred into a constant output atomizer (Model 3076, TSI), where aerosols were generated and diluted with dry Nitrogen. A small fraction (~10%) of aerosols was sampled, dried to RH ~5% by a Nafion drier (PD-070-18T-12SS, Perma Pure), charged by a ^{210}Po bipolar charger, and analyzed by the integrated aerosol analytical system described in Chapter II. A schematic presentation of the experimental setup is shown in Figure 16.

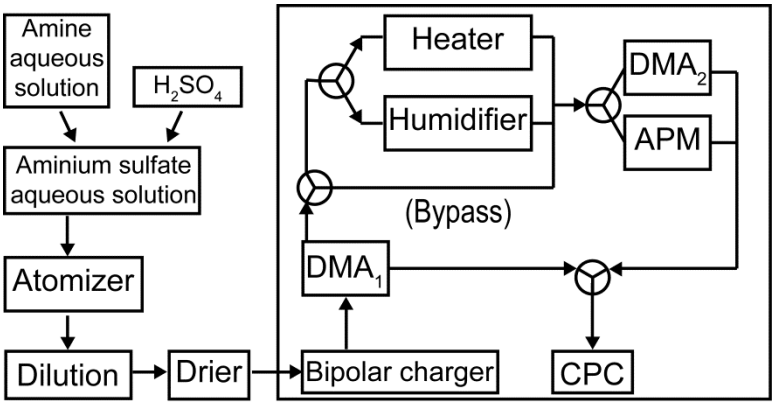

Figure 16. Schematic representation of the experiment procedure to measure the physicochemical properties of aminium sulfates.

The aerosol analytical system, described in detail in Chapter II, was composed of two differential mobility analyzers (DMAs), an APM, a CPC, a heater, and a humidifier (Figure 16). Dependent of the thermodynamic properties to be measured, the aerosol system operated in several modes, including SMPS, TDMA, and DMA-APM-CPC. Additional processing options of the aerosol system included heating and humidifying, selected by means of three-way switching valves. Aerosol samples were analyzed using the SMPS mode to ensure the size distributions for all AAS species to be constant for each measurement.

The hygroscopicity of aminium sulfates was measured by the TDMA mode with a humidifier (HTDMA) and the RH before and after DMA_2 was tuned to be within 2%. The hygroscopic diametric growth factor (*HGfd*) was defined by the ratio of $D_{p,RH}/D_{p,0}$, where $D_{p,RH}$ and $D_{p,0}$ represent the mobility sizes after DMA_2 at an elevated RH and at

RH~12%, respectively. The measured values of *HGfd* for all species corresponded to a random error within ± 1%.

The thermostability measurements were performed using the DMA-APM-CPC mode with the heater. Aerosol sample was size-selected by DMA_1, and processed by the heater. The resulting particles were then transferred into APM to determine the APM voltage V required to balance the centrifugal force on particles in the APM. The APM voltage V was linear to the aerosol mass *m*. The aerosol mass change, denoted as *Gfm*, is determined as:

$$Gfm = \frac{m_T}{m_0} = \frac{V_T}{V_0} \tag{4.1}$$

where m_T and V_T are the particle mass and corresponding APM voltage after particle heating at a temperature of *T*, and m_0 and V_0 correspond to those before heating at room temperature. The random error in APM voltage was found to be within 1.5%. No significant change in the particle mass was observed when the residence time in the tubing was changed, suggesting that AASs were stable at room temperature. After each volatility measurement, the system was properly cleaned and purged with particle free air for an extended period of time to remove possible contaminates from thermal decomposition of AASs.

Density measurements were also performed using the DMA-APM-CPC mode for all AASs. At room temperature, particles with mobility sizes D_p of 81, 97, 151 and 240 nm were measured at least three times for each size to determine the corresponding APM voltages *V* at 10% RH. The APM voltages V_{PSL} for polystyrene latex (PSL, Duke

Scientific) particles with the same sizes was also determined. Since the mass m_{PSL} for PSL particles is known, the mass m of AAS particles can be calculated as:

$$m = m_{PSL} \cdot \frac{V}{V_{PSL}} \tag{4.2}$$

Assuming a spherical shape, the particle effective density ρ is calculated by a linear regression of the mass and volume. Fractal dimension, D_{fm}, is determined by the relation:[6]

$$m \propto D_p^{D_{fm}} \tag{4.3}$$

After particles are heated at ~80 °C, their mass is measured similarly. Furthermore, thermo-TDMA (TTDMA) measurements were performed where mono-dispersed aerosols of size D_{p1} were obtained by DMA_1 and subsequently heated to ~80 °C before their size D_{p2} was determined by DMA_2. The thermo diametric growth factor, *TGfd*, was defined as D_{p2}/D_{p1}, and used to calculate the volume change upon heating. The change in density of the heated aerosols was then determined.

Results and Discussion

Hygroscopicity of Alkylaminium Sulfates

The deliquescent behaviors of five AASs in 10–90% RH range are presented in Figure 17. *HGfd* values for particles with four initial mobility sizes of 80, 100, 150 and 240 nm are measured, and the results reveal no apparent Kelvin effect. Aerosols of all AASs exhibit a monotonic increase in size when exposed to increasing RH without a clear deliquescence point, suggesting that AASs readily absorb water even at low RH to

lead to aerosol volume and mass increases. Interestingly, the *HGfd* values at RH<80% decrease systematically, when the alkyl carbon number in AASs increases from MMAS to TEAS. However, there exists little trend in *HGfd* with respect to the alkyl carbon number among different AASs when RH reaches 90%. For example, the *HGfd* values of MMAS and TMAS are smaller than those of DMAS and DEAS, respectively.

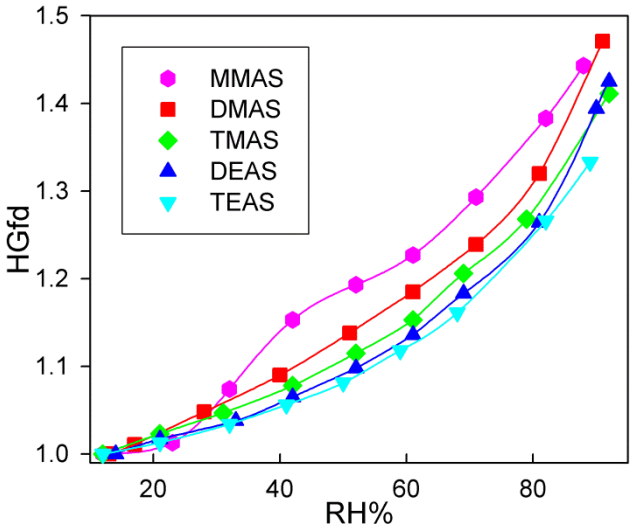

Figure 17. Deliquescent profiles of hygroscopic diametric growth factor (*HGfd*) for alkylaminium sulfates when exposed to increasing RH. Pink hexagons, monomethylaminium sulfate (MMAS); red squares, dimethylaminium sulfate (DMAS); green diamonds, trimethylaminium sulfate (TMAS); blue up-triangles, diethylaminium sulfate (DEAS); cyan down-triangles, triethylaminium sulfate (TEAS). Solid lines are connections through the experimental points.

The aerosol size growth at elevated RH can be estimated from the initial aerosol density ρ_0, final density ρ_1, and salt weight concentration ω of the final solution:

$$HGfd = \left(\frac{\rho_0}{\rho_1 \cdot \omega}\right)^{\frac{1}{3}} \quad (4.4)$$

No previous experiment data are available on the dependence of the density of AAS solutions as a function the salt concentration. However, since solid AASs have a higher density than that of water, it is likely that ρ_1 decreases when ω decreases as observed in AS and ABS solutions,[153,154] resulting in an aerosol size increase as observed. At 90% RH, DMAS may absorb more water than MMAS, causing a larger decrease in ω and ρ_1. As a result, although MMAS has a higher initial density, its *HGfd* is smaller than that of DMAS at 90% RH. Such an explanation is also applicable for the case of TMAS and DEAS: DEAS may uptake more water at 90% RH and have a higher *HGfd*. Further investigation on AAS aqueous solution density is warranted for a quantitative analysis and simulation of the AAS hygroscopic behaviors. Also, hygroscopicity measurements close to the water saturation condition (RH ~ 100%) are necessary to evaluate the contribution of AASs to could droplet activation.

To further assess the impact of AAS on particle hygroscopicity, the deliquescence profiles of pure AS, DMAS-AS and MMAS-AS mixtures with the mass ratios of 1:1 and 1:9 are measured, as shown in Figure 18.

Deliquescence of AS occurs sharply at RH~79%. When 10 wt % of DMAS or MMAS is added to AS particles, there still exists an apparent deliquescence point at ~71% RH when sharp hygroscopic growth occurs, but there is an increase in *HGfd* even at 10–70% RH, suggesting that MMAS and DMAS absorb water even with a low mass fraction in particles. The effect of AAS on aerosol hygroscopic behavior is more pronounced with AAS-AS particles containing 50 wt % of DMAS or MMAS, where no clear deliquescence point is identifiable. Because of the similarity in hygroscopicity for

all AASs, our results suggest that incorporation of AAS into AS aerosols can considerably lower the deliquescence point for AS particles.

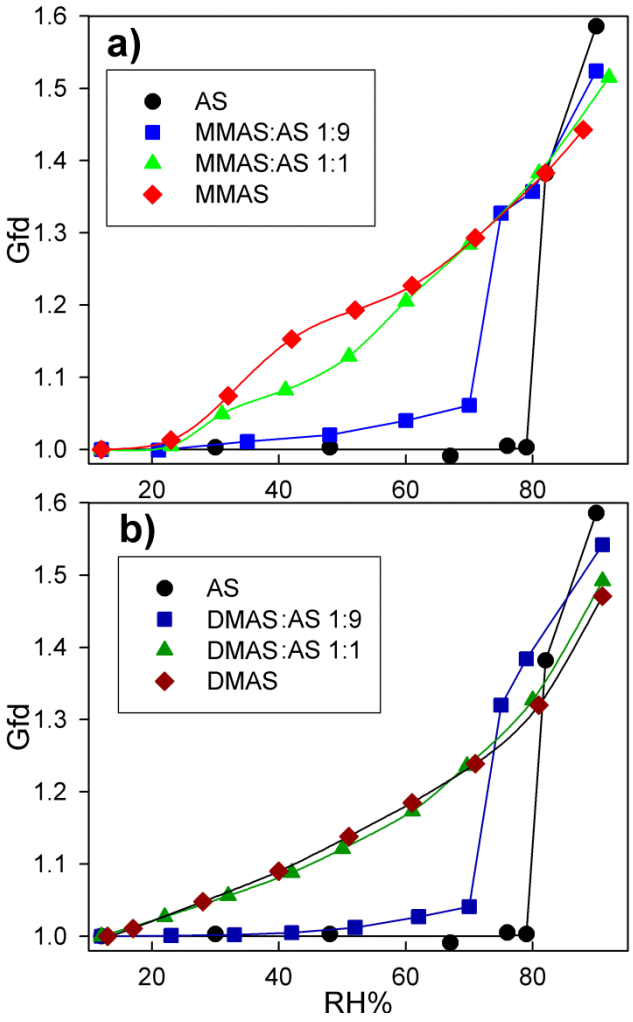

Figure 18. Deliquescent profiles for alkylaminium-ammonium sulfate mixtures. a) Hygroscopic diametric growth factor (*HGfd*) profiles for MMAS and AS mixtures: black circles, AS; blue squares, mixture with MMAS:AS=1:9 by mass; green triangles, mixture with MMAS:AS=1:1 by mass; red diamonds, MMAS. b) *HGfd* profiles for DMAS and AS mixtures: black circles, AS; dark-blue squares, mixture with DMAS:AS=1:9 by mass; dark-green triangles, mixture with DMAS:AS=1:1 by mass; dark red diamonds, DMAS. Solid lines are connections through the experimental points. Values are averages from measurements on aerosols with initial mobility diameters of 80, 100, 150 and 240 nm with a random error of less than ± 1% in *HGfd*.

Thermostability of Alkylaminium Sulfates

Figure 19 depicts the *Gfm* profiles of AASs and AS aerosols with ~100 nm initial diameter in the temperature range of 25–200 °C. For AS aerosols, a small discontinuous step occurs around 100 °C, likely attributed to the formation of ABS.[155] Rapid mass loss takes place in the temperature range of 130–160 °C, higher than that determined for 7.5 nm AS particles.[86] This behavior may be explained by the Kelvin effect that is significant for nanoparticles.[156] All AASs volatilizes rapidly in the temperature range of 130–170 °C. DMAS appears to be the most stable species, followed by MMAS and DEAS, while TMAS and TEAS have a thermostability similar to that of AS. The volatilization temperature range for MMAS aerosols is lower than that determined

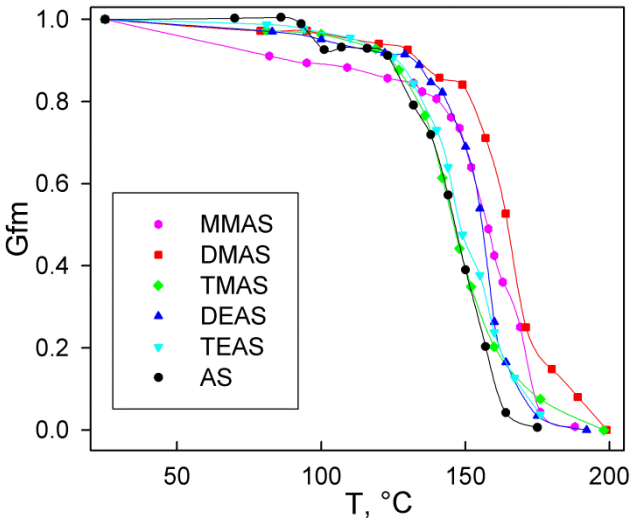

Figure 19. Aerosol mass change (*Gfm*) profiles of alkylaminium sulfates and ammonium sulfate. Pink hexagons, monomethylaminium sulfate (MMAS); red squares, dimethylaminium sulfate (DMAS); green diamonds, trimethylaminium sulfate (TMAS); blue up-triangles, diethylaminium sulfate (DEAS); cyan down-triangles, triethylaminium sulfate (TEAS); black circles, AS. Solid lines are connections through the experimental points. Values are calculated from mass measurements on aerosols with an initial mobility diameter of 97 nm with a random error of within ± 3%.

previously on MMAS crystals, which was estimated by a melting-point apparatus involving a larger sample quantity.[157] This difference may suggest that MMAS aerosols in our experiments are not crystalline but rather amorphous.

For all species, the measured thermostability profile resembles the shape of a reversed sigmoidal curve, which can be described by the expression,

$$Gfm = A_2 + \frac{A_1 - A_2}{1 + \exp\left(\frac{T - T_s}{dT}\right)} \tag{4.5}$$

where A_1 and A_2 denote the upper and lower limits of the data set, T_s represents temperature at which the volatilization rate is the largest, and dT is the temperature range where the volatilization takes place. The four parameters for AASs and AS are determining by fitting the experiment data *Gfm* and *T* with Equation 4.5.

The T_s values for all AASs and AS are determined and listed in Table 4, providing quantitative data for thermostability comparison. The relative thermostability for AASs and AS is in the order as listed below:

DMAS > MMAS > DEAS > TMAS ≈ TEAS ≈ AS

For all AASs, A_1 is close to 0 and dT is about 9 °C. In principle, if particles contain entirely pure AAS, A_2 is expected to be 1. Since A_2 determined from our experiments ranges from 0.91 to 0.99, this suggests that particles measured at room temperature may contain small amount of water, which reflects the hygroscopic nature of AASs.

Table 4. Thermostability and Density of Aminium Sulfates.

Salt	T_s,[a] °C	D_{fm}[b]	ρ,[c] g cm^{-3}	ρ_h,[d] g cm^{-3}
MMAS	161 ± 2	2.9 ± 0.1	1.438 ± 0.027	1.485 ± 0.089
DMAS	165 ± 2	2.9 ± 0.1	1.351 ± 0.026	1.408 ± 0.084
TMAS	146 ± 2	2.9 ± 0.1	1.307 ± 0.026	1.342 ± 0.081
DEAS	156 ± 2	3.0 ± 0.1	1.211 ± 0.023	1.268 ± 0.076
TEAS	150 ± 2	2.9 ± 0.1	1.183 ± 0.023	1.247 ± 0.075
AS	148 ± 2	-	1.778 ± 0.020;[e] 1.77[f]	-

[a] Values with confidence intervals were obtained from fitting the aerosol mass change *Gfm* profiles in 25–200 °C with a reversed-sigmoidal function. Measurements were carried out with aerosol particles with an initial mobility diameter of 97 nm.
[b] All measurements were performed at 298 K on particles with mobility diameters of 81, 97, 151 and 240 nm. At least three measurements were performed for each size and the random error in APM voltage is within 1.5%.
[c] Density values were obtained by linear regression of mass against volume assuming spherical aerosol shape. Random error in density measurements was less than 1.5%.
[d] Density values were determined for particles with initial mobility diameter of 97 nm. The aerosols were heated to 80 °C before the changes in mass and size were measured.
[e] Density value was determined for particles with mobility diameter of 97 nm at room temperature.
[f] Ref. 158.

Densities of Alkylaminium Sulfates

The mass of aerosols with known mobility sizes from 80 to 240 nm is measured using the DMA-APM-CPC mode to establish the mass-mobility relationship. The effective density at room temperature can then be calculated by plotting mass against volume, assuming a spherical shape; the linearity of the plots is high. The fractal dimension D_{fm} can also be determined, which is close to 3.0 for all AASs (Table 4). Hence, AAS aerosols are highly uniform and compact in shape, indicating that the

particles are close to be spherical. As a result, AAS effective density corresponds to their material density.[54]

The AAS density values measured at room temperature are summarized in Table 4, ranging from 1.2 to 1.4 g cm^{-3}. For comparison, the density of 97 nm AS particles is estimated to be 1.778 g cm^{-3} by our system. Interestingly, the density of AASs decreases as the total alkyl carbon number in AAS increases from 2 to 12. This suggests that an increase in the AAS total carbon number may contribute more to increase in particle volume than in mass. AAS can be considered as an AS molecule with the methylene group (-CH_2-) inserted between N-H or N-C bond. For example, MMAS with the structure of (H-CH_2-NH_3)$_2SO_4$ can be treated as AS with two methylene groups, and similarly, DMAS, (H-CH_2-CH_2-NH_3)$_2SO_4$ as AS with four methylene groups. The total alkyl carbon number *n* in the AAS molecule represents the number of methylene groups inserted into an AS molecule to form the corresponding AAS. A semi-empirical model is then developed to predict the density ρ of AASs:

$$\rho = \rho_{AS} \frac{1 + an}{1 + bn} \tag{4.6}$$

where ρ_{AS} is the material density of AS, 1.77 g cm^{-3}, parameter *a* is mass increase factor representing the relative increase in mass when one methylene group is added to an AS molecule and has a constant value of 14.03/132.16=0.106, and parameter *b* is defined as the volume increase factor (VIF), which represents the relative increase in volume when one methylene group is introduced to the compound. On the basis of our density measurements, *b* is determined as (0.210 ± 0.005). The parameterized density curve based on the model is plotted in Figure 20.

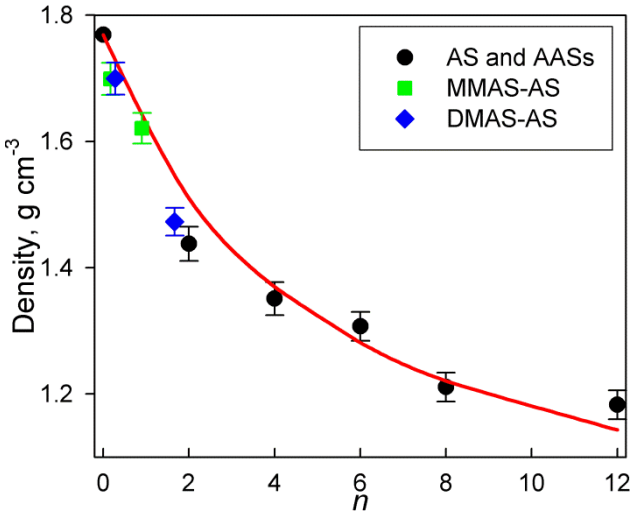

Figure 20. Density of ammonium sulfate and alkylaminium sulfates (black circles) plotted against the alkyl carbon number *n* and the fit curve (red line) based on the density prediction model. Densities of monomethylaminium sulfate-AS (MMAS-AS, green squares) and dimethylaminium sulfate-AS (DMAS-AS, blue diamonds) mixtures are determined by measuring the density of particles with 97 nm mobility diameter at least three times with a random error of within ± 1.5%.

It may be possible to expend our model to predict the density of AAS-AS mixture if the definition of *n* is generalized to the CH_2/total sulfate (AS + AAS) mole ratio in the mixture. To evaluate this hypothesis, the density values of aerosol particles containing MMAS-AS and DMAS-AS mixtures with mass ratios of 1:1 and 1:9 are measured and the results agree with calculated valued based on our model within 5% differences (Figure 20). Since the ammonia concentration is usually 10 times higher than those of alkylamines in the atmosphere, the CH_2/total sulfate ratio is expected to be less than 2. This suggests that the density of AAS-AS mixture can be estimated by our model, if the CH_2/total sulfate ratio is determined.

Our measurements show that AAS aerosols are highly hygroscopic and contain water even at low RH, since after heating to 80 °C, those particles lose about 3–8% in

mass, which is likely due to loss of water. To evaluate the effect of water on our density measurements, TTDMA measurements are carried out where AAS aerosols are heated to about 80 °C and the changes in particle size are monitored. The change in particle volume is combined with our mass measurements at 80 °C to determine the relative change in the effective density due to heating. The effective density of the heated AAS aerosols (ρ_h) is then calculated as shown in Table 4, which is about 5% higher than the room temperature measurement values.

The densities of several alkylaminium nitrates have also been determined recently using the AMS and BET methods.[146] The densities of aminium nitrates are lower than that of AN and decrease as the alkyl carbon number in the aminium nitrates increases. A similar trend also exists among alkylaminium chlorides, on the basis of the density data from literatures.[159,160] Hence, Equation 4.6 can be generalized to aminium nitrates and chlorides (ρ_i):

$$\rho_i = \rho_{0,i} \frac{1 + a_i m}{1 + b_i m} \tag{4.7}$$

where $\rho_{0,i}$ is the material density of AN or ammonium chloride, 1.75 or 1.53 g cm^{-3}, respectively. The value of a_i is 0.175 for aminium nitrates and 0.262 for aminium chloride, and b_i is 0.432 for aminium nitrates and 0.480 for aminium chloride, based on previously reported density values (Figure 21 and Table 5).

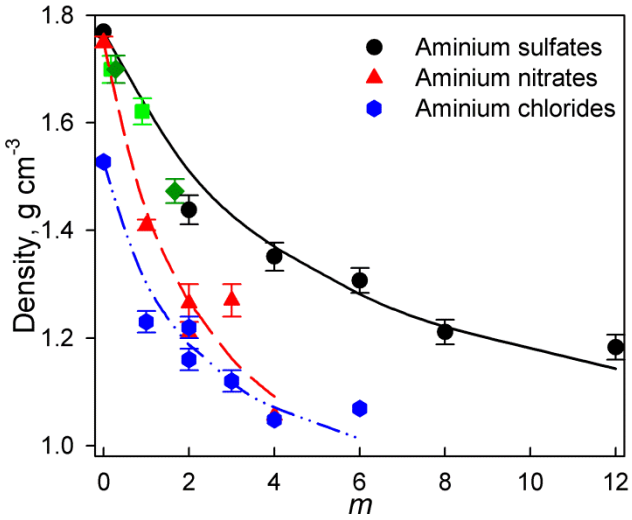

Figure 21. Density values of ammonium sulfate (AS) and alkylaminium sulfates (black circles), ammonium nitrate and alkylaminium nitrates (red triangles), and ammonium chloride and alkylaminium chlorides (blue hexagons) plotted against the alkyl carbon number *m* and the corresponding fit curves (solid black, red dash and blue dot-dash lines, respectively) based on the semi-empirical density prediction model (Equation 4.6). Densities of monomethylaminium sulfate-AS (green squares) and dimethylaminium sulfate-AS (dark-green diamonds) mixtures are also included.

The VIF of aminium nitrates and chlorides is about twice of that of aminium sulfates, suggesting that the charge of the anion in the aminium salts can influence the VIF values (Table 5).

Table 5. The Effect of Anion on the Volume Increase Factor of Aminium Salts.

Anion	Charge *q*	MIF *a*	VIF *b*	$q \times b$
Sulfate	−2	0.106	0.210	−0.420
Nitrate	−1	0.175	0.432	−0.432
Chloride	−1	0.262	0.480	−0.480

Atmospheric Implications

Many of the atmospheric effects of aerosols are dependent of their physiochemical properties. For example, the ability of aerosols to activate as cloud droplets and to scatter and absorb the visible and terrestrial radiation is strongly linked to their hygroscopicity.[13,20] Furthermore, the hygroscopic behaviors of aerosols also have an important feedback on aerosol growth. A more efficient water uptake increases the particle size and, consequently, enhances particle growth processes related to condensation, partitioning, and heterogeneous reactions of organic compounds.[59,60,161]

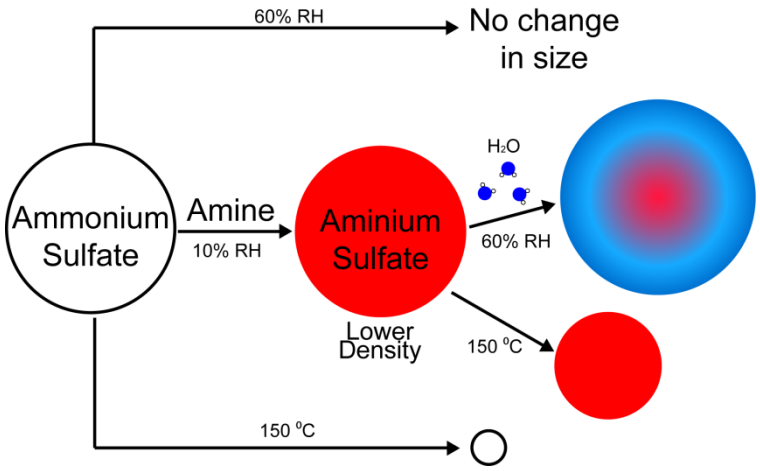

Figure 22. Impacts of particle-phase amines on ammonium sulfate aerosol properties.

Alkylamines are incorporated into the particle phase to form AASs by heterogeneous reactions with sulfuric acid, AS, and ABS in aerosols (Figure 22). It has been estimated that, at 10% RH for 1 ppb DMA and 100 nm diameter AS particles, a

layer of 2 nm and 25 nm DMAS shell can form within 20 s and about 2 h, respectively, and this process is likely irreversible (Chapter III). On the basis of our hygroscopicity measurements, such a change in the aerosol surface composition can significantly alter the particle hygroscopic behaviors. For example, with a change in RH from 10% to 60%, a particle coated with a 25 nm DMAS shell will grow ~12 nm in diameter by absorbing water. Our results show that a small mass fraction (10 wt %) of AAS such as MMAS and DMAS considerably lowers the deliquescence point and enhance water adsorption on AS particles. It has been reported that ambient aerosols exhibit deliquescent profiles that increase monotonically even after exposed to ammonia,[162] but the hygroscopic size growth is too small to be explained alone by the presence of AN. Our laboratory results offer a plausible explanation for the field measurement, indicating that the presence of AASs in aerosols can be responsible for particle growth at low RH. Hence, we conclude that the displacement reaction of alkylamines with AS aerosols leads to a transition from the crystalline to an amorphous phase and an improved water uptake, considerably enhancing their direct and indirect climate forcing.

Our thermostability measurements suggest that AASs have comparable (TMAS and TEAS) or higher thermostability (MMAS, DMAS and DEAS) than AS, indicating that AASs represent a stable form in the particle phase and can account for aminium ions commonly observed in the atmosphere, along with aminium carboxylates and aminium nitrate.[86,146] A minimum temperature of 200 °C is required to fully volatilize AASs from the particle phase in aerosol composition analysis. It has been reported that the aminium nitrate and sulfate content of ambient aerosols only accounted for 1–9% of the total

particle mass after the aerosol sample was heated to 230 °C.[163] It is likely that a high temperature may partially decompose the aminium sulfates in ambient particle phase and lead to an underestimation of the particle amine content. Field measurements have suggested that dialkylaminium ions such as $DMAH^+$ are more abundant in the particle phase that other alkylaminium ions,[142,164,165] which can be attributed to several factors, including the differences in their gas-phase abundance, uptake kinetics, or thermodynamic properties. However, the differences in the concentrations for MMA and DMA may not be significant globally[66] or locally.[166] In laboratory uptake experiments, the reactivity of DMA and MMA with sulfuric acid is comparable,[71] and DMA reacts with AS solid slower than MMA (Chpater III). Those results indicate that a selective accumulation of dialkylaminium ions is not kinetically preferred. On the other hand, our thermostability measurements reveal that DMAS are thermally more stable than other AASs, offering a possible explanation that dialkylaminium ions may be favored in thermodynamic equilibrium, resulting higher concentrations in particles.

Our results reveal that uptake of alkylamines on AS aerosols lowers the aerosol density. For a 100 nm AS particle exposed to 1 ppb of DMA for two hours at 10% RH, we estimate that the aerosol density decreases to 1.43 g cm^{-3}, which is about 80% of the initial density. The semi-empirical model developed in this study can be widely employed to predict the density of AAS-AS mixtures, if the mole ratio of the alkyl carbons to total sulfate (AS + AAS) can be determined.

Future Research Directions

Our measurements of the physical properties of aminium salts have indicated that particles containing aminium salts likely exist in a liquid or amorphous phase. Further experimental and field studies are required to verify that the heterogeneous reactions of amines indeed lead to the phase transition on pre-existing aerosols under atmospherically relevant conditions. It is also plausible that the reaction between aminium salts and carbonyl compounds (such as glyoxal) may lead to a change in particle optical properties, which needs to be quantified in future experimental and field studies.

Previous field measurements have suggested that dialkylaminium salts appear to be the most abundant in the particle phase. Computational work may help to explain this observation and reveal the underlying mechanism.

It is clear that further knowledge is required to better refine the kinetics and mechanism of the multiphase chemistry of amines and to evaluate its roles in aerosol formation and transformation and to predict the particle properties. Also, future effort is needed to develop physically-based parameterizations to represent the heterogeneous processes of amines in atmospheric chemical models and to more accurately assess their roles in air quality, human health, weather, and direct and indirect climate forcings.

CHAPTER V

CONCLUSIONS

In this dissertation, we have evaluated the impacts of soot aging process on particle properties by using products from toluene-OH oxidation as model organic compounds. Using monodisperse soot aerosols, the particle properties, including mobility size and mass can be monitored during the aging process. Information such as organic mass faction and effective density can then be extracted. Significant growth in particle size, mass, organic mass fraction and effective density are observed, dependent largely of the thickness of the organic coating. Compaction on the soot core is evidenced by the increase in effective density of soot core, decrease in particle dynamic shape factor, and changes in TEM images. Aged soot particles are further compacted when exposed to elevated RH, suggesting the increase in particle hygroscopicity with organic coatings. Particle optical properties, including light scattering, absorption and single scattering albedo are all enhanced. Our results suggest that products from oxidation of aromatics in the atmosphere can effectively alter the composition and properties of soot particles within days. Such change in particle composition leads to higher particle density and more compact morphology. Organic coating is found to increase the soot particle hygroscopicity and enhance the aerosol light scattering and absorption.

Amines are emitted into the atmosphere from various biogenic and anthropogenic sources. Amines have been observed in various locations worldwide with large diversity in molecular structures. The atmospheric fate of amines is determined by

several reaction pathways, i.e., gas-phase oxidation and heterogeneous reactions with particle phase acidic/carbonyl compounds to contribute to formation and transformation of aerosols. We have studied the heterogeneous reactions between amines and ammonium sulfate and bisulfate surfaces. The uptake of simple alkylamines on AS is confirmed as a displacement reaction with two kinetic stages, as evidenced by the release of ammonia monitored by mass spectrometer. The initial displacement reaction between amine and AS is fast with the initial uptake coefficients on the order of 10^{-2} for all alkylamines. The steady-state uptake coefficients vary from 6.0×10^{-3} to 2.3×10^{-4} and decrease with increasing number of methyl groups attached to the alkylamine. An acid-base reaction (neutralization) has been observed for the uptake of alkylamines on ABS, with irreversible alkylamine loss and no ammonia generation. The reaction between amines and ABS has a fast rate limited only by the diffusion of gaseous alkylamines.

Furthermore, we have demonstrated that the multiphase reactions of amines on sub-micrometer sized particles may considerably modify the aerosol physiochemical properties, including hygroscopicity, thermostability, and density properties. AAS particles absorb water readily at low RH without well-defined deliquescence points. Aminium sulfates, similar to aminium carboxylates, are thermally more stable than AS, suggesting that aminium sulfates are stable enough at ambient temperature and may exist in the particle phase. The aminium sulfates, nitrates and chlorides have densities lower than those of the corresponding ammonium salts, suggesting that the interactions

between amines and ammonium salts likely lower the particle density in the atmosphere. A semi-empirical formula has been developed to predict the density of aminium salts.

Overall, it is shown in this dissertation that organic compounds can alter the composition and properties of atmospheric aerosols significantly. The changes in aerosol properties consequently influence the direct and indirect effect of ambient particles on our climate change. Several future research directions have been discussed.

REFERENCES

(1) Zhang, R. Y. Getting to the critical nucleus of aerosol formation. *Science* **2010**, *328*, 1366–1367.

(2) Seinfeld, J. H.; Pandis, S. N. *Atmospheric Chemistry and Physics: From Air Pollution to Climate Change*. 2nd ed. Wiley: New York, **2006**.

(3) Zhang, R. Y.; Khalizov, A.; Wang, L.; Hu, M.; Xu, W. Nucleation and growth of nanoparticles in the atmosphere. *Chem. Rev.* **2012**, *112*, 1957–2011.

(4) Seinfeld, J. H.; Pankow, J. F. Organic atmospheric particulate material. *Annu. Rev. Phys. Chem.* **2003**, *54*, 121–140.

(5) Hallquist, M.; Wenger, J. C.; Baltensperger, U.; Rudich, Y.; Simpson, D. et al. The formation, properties and impact of secondary organic aerosol: Current and emerging issues. *Atmos. Chem. Phys.* **2009**, *9*, 5155–5236.

(6) Zhang, R.; Khalizov, A. F.; Pagels, J.; Zhang, D.; Xue, H. et al. Variability in morphology, hygroscopicity, and optical properties of soot aerosols during atmospheric processing. *Proc. Natl. Acad. Sci. USA* **2008**, *105*, 10291–10296.

(7) Zhang, R.; Suh, I.; Zhao, J.; Zhang, D.; Fortner, E. C. et al. Atmospheric new particle formation enhanced by organic acids. *Science* **2004**, *304*, 1487–1490.

(8) Zhang, R.; Wang, L.; Khalizov, A. F.; Zhao, J.; Zheng, J. et al. Formation of nanoparticles of blue haze enhanced by anthropogenic pollution. *Proc. Natl. Acad. Sci.USA* **2009**, *106*, 17650–17654.

(9) Wang, L.; Khalizov, A. F.; Zheng, J.; Xu, W.; Ma, Y. et al. Atmospheric nanoparticles formed from heterogeneous reactions of organics. *Nature Geosci.* **2010**, *3*, 238–242.

(10) Wang, L.; Xu, W.; Khalizov, A. F.; Zheng, J.; Qiu, C. et al. Laboratory investigation on the role of organics in atmospheric nanoparticle growth. *J. Phys. Chem. A* **2011**, *115*, 8940–8947.

(11) Rudich, Y.; Donahue, N. M.; Mentel, T. F. Aging of organic aerosol: Bridging the gap between laboratory and field studies. *Annu. Rev. Phys. Chem.* **2007**, *58*, 321–352.

(12) Xue, H.; Khalizov, A. F.; Wang, L.; Zheng, J.; Zhang, R. Effects of dicarboxylic acid coating on the optical properties of soot. *Phys. Chem. Chem. Phys.* **2009**, *11*, 7869–7875.

(13) Khalizov, A. F.; Zhang, R.; Zhang, D.; Xue, H.; Pagels, J. et al. Formation of highly hygroscopic soot aerosols upon internal mixing with sulfuric acid vapor. *J. Geophys. Res.* **2009**, *114*, D05208.

(14) Kleinstreuer, C.; Zhang, Z.; Donohue, J. F. Targeted drug-aerosol delivery in the human respiratory system. *Annu. Rev. Biomed. Eng.* **2008**, *10*, 195–220.

(15) Pope, C. A.; Ezzati, M.; Dockery, D. W. Fine-particulate air pollution and life expectancy in the United States. *New J. Engl. Med.* **2009**, *360*, 376–386.

(16) Sun, J.; Ariya, P. A. Atmospheric organic and bio-aerosols as cloud condensation nuclei (CCN): A review. *Atmos. Environ.* **2006**, *40*, 795–820.

(17) Li, G.; Zhang, R.; Fan, J.; Tie, X. Impacts of black carbon aerosol on photolysis and ozone. *J. Geophys. Res.* **2005**, *110*, D23206.

(18) Solomon, S., D.; Qin, M.; Manning, Z.; Chen, M.; Marquis, K. B. et al. *IPCC Fourth Assessment Report: Climate Change 2007*. Cambridge University Press: New York, USA, **2007**.

(19) Pagels, J.; Khalizov, A. F.; McMurry, P. H.; Zhang, R. Y. Processing of soot by controlled sulphuric acid and water condensation — mass and mobility relationship. *Aerosol Sci. Technol.* **2009**, *43*, 629–640.

(20) Khalizov, A. F.; Xue, H.; Wang, L.; Zheng, J.; Zhang, R. Enhanced light absorption and scattering by carbon soot aerosol internally mixed with sulfuric acid. *J. Phys. Chem. A* **2009**, *113*, 1066–1074.

(21) Fuller, K. A.; Malm, W. C.; Kreidenweis, S. M. Effects of mixing on extinction by carbonaceous particles. *J. Geophys. Res.* **1999**, *104*, 15941–15954.

(22) Jacobson, M. Z. Strong radiative heating due to the mixing state of black carbon in atmospheric aerosols. *Nature* **2001**, *409*, 695–697.

(23) Adachi, K.; Chung, S. H.; Buseck, P. R. Shapes of soot aerosol particles and implications for their effects on climate. *J. Geophys. Res.* **2010**, *115*, D15206.

(24) Adler, G.; Riziq, A. A.; Erlick, C.; Rudich, Y. Effect of intrinsic organic carbon on the optical properties of fresh diesel soot. *Proc. Natl. Acad. Sci. USA* **2010**, *107*, 6699–6704.

(25) Mikhailov, E. F.; Vlasenko, S. S.; Podgorny, I. A.; Ramanathan, V.; Corrigan, C. E. Optical properties of soot-water drop agglomerates: An experimental study. *J. Geophys. Res.* **2006**, *111*, D07209.

(26) Bueno, P. A.; Havey, D. K.; Mulholland, G. W.; Hodges, J. T.; Gillis, K. A. et al. Photoacoustic measurements of amplification of the absorption cross section for coated soot aerosols. *Aerosol Sci. Technol.* **2011**, *45*, 1217–1230.

(27) Schwarz, J. P.; Spackman, J. R.; Fahey, D. W.; Gao, R. S.; Lohmann, U. et al. Coatings and their enhancement of black carbon light absorption in the tropical atmosphere. *J. Geophys. Res.* **2008**, *113*, D03203.

(28) Chan, T. W.; Brook, J. R.; Smallwood, G. J.; Lu, G. Time-resolved measurements of black carbon light absorption enhancement in urban and near-urban locations of Southern Ontario, Canada. *Atmos. Chem. Phys.* **2011**, *11*, 10407–10432.

(29) Fan, J.; Zhang, R.; Tao, W.-K.; Mohr, K. I. Effects of aerosol optical properties on deep convective clouds and radiative forcing. *J. Geophys. Res.* **2008**, *113*, D08209.

(30) Fan, J. W.; Zhang, R. Y.; Collins, D.; Li, G. H. Contribution of secondary condensable organics to new particle formation: A case study in Houston, Texas. *Geophys. Res. Lett.* **2006**, *33*, L15802.

(31) Lei, W.; Zhang, R.; Sean McGivern, W.; Derecskei-Kovacs, A.; North, S. W. Theoretical study of isomeric branching in the isoprene–OH reaction: Implications to final product yields in isoprene oxidation. *Chem. Phys. Lett.* **2000**, *326*, 109–114.

(32) Zhang, D.; Lei, W. F.; Zhang, R. Y. Mechanism of OH formation from ozonolysis of isoprene: Kinetics and product yields. *Chem. Phys. Lett.* **2002**, *358*, 171–179.

(33) Zhang, R.; Suh, I.; Lei, W.; Clinkenbeard, A. D.; North, S. W. Kinetic studies of OH-initiated reactions of isoprene. *J. Geophys. Res.* **2000**, *105*, 24627–24635.

(34) Slowik, J. G.; Cross, E. S.; Han, J.-H.; Kolucki, J.; Davidovits, P. et al. Measurements of morphology changes of fractal soot particles using coating and denuding experiments: Implications for optical absorption and atmospheric lifetime. *Aerosol Sci. Technol.* **2007**, *41*, 734–750.

(35) Xue, H.; Khalizov, A. F.; Wang, L.; Zheng, J.; Zhang, R. Effects of coating of dicarboxylic acids on the mass — mobility relationship of soot particles. *Environ. Sci. Technol.* **2009**, *43*, 2787–2792.

(36) Barnes, I.; Rudzinski, K. J. *Environmental Simulation Chambers: Application to Atmospheric Chemical Processes*. Springer: Dordrecht, Netherlands, **2006**.

(37) Saathoff, H.; Naumann, K. H.; Schnaiter, M.; Schöck, W.; Möhler, O. et al. Coating of soot and $(NH_4)_2SO_4$ particles by ozonolysis products of [alpha]-pinene. *J. Aerosol Sci* **2003**, *34*, 1297–1321.

(38) Schnaiter, M.; Linke, C.; Möhler, O.; Naumann, K. H.; Saathoff, H. et al. Absorption amplification of black carbon internally mixed with secondary organic aerosol. *J. Geophys. Res.* **2005**, *110*, D19204.

(39) Lu, Z.; Hao, J.; Hu, L.; Takekawa, H. The compaction of soot particles generated by spark discharge in the propene ozonolysis system. *J. Aerosol Sci.* **2008**, *39*, 897–903.

(40) Nakao, S.; Shrivastava, M.; Nguyen, A.; Jung, H.; Cocker, D. Interpretation of secondary organic aerosol formation from diesel exhaust photooxidation in an environmental chamber. *Aerosol Sci. Technol.* **2011**, *45*, 964–972.

(41) Torsten, T.; Zsófia, J.; Maria, M.; Roberto, C.; Martin, G. et al. Changes of hygroscopicity and morphology during ageing of diesel soot. *Environ. Res. Lett.* **2011**, *6*, 034026.

(42) Atkinson, R. Atmospheric chemistry of VOCs and NO_x. *Atmos. Environ.* **2000**, *34*, 2063–2101.

(43) Fortner, E. C.; Zheng, J.; Zhang, R.; Berk Knighton, W.; Volkamer, R. M. et al. Measurements of volatile organic compounds using proton transfer reaction-mass spectrometry during the MILAGRO 2006 campaign. *Atmos. Chem. Phys.* **2009**, *9*, 467–481.

(44) Wang, M.; Zhu, T.; Zheng, J.; Zhang, R. Y.; Zhang, S. Q. et al. Use of a mobile laboratory to evaluate changes in on-road air pollutants during the Beijing 2008 Summer Olympics. *Atmos. Chem. Phys.* **2009**, *9*, 8247–8263.

(45) Molina, M. J.; Zhang, R.; Broekhuizen, K.; Lei, W.; Navarro, R. et al. Experimental study of intermediates from OH-initiated reactions of toluene. *J. Am. Chem. Soc.* **1999**, *121*, 10225–10226.

(46) Suh, I.; Zhang, D.; Zhang, R.; Molina, L. T.; Molina, M. J. Theoretical study of OH addition reaction to toluene. *Chem. Phys. Lett.* **2002**, *364*, 454–462.

(47) Atkinson, R.; Arey, J. Atmospheric degradation of volatile organic compounds. *Chem. Rev.* **2003**, *103*, 4605–4638.

(48) Suh, I.; Zhang, R.; Molina, L. T.; Molina, M. J. Oxidation mechanism of aromatic peroxy and bicyclic radicals from OH−toluene reactions. *J. Am. Chem. Soc.* **2003**, *125*, 12655–12665.

(49) Zhao, J.; Zhang, R. Y.; Misawa, K.; Shibuya, K. Experimental product study of the OH-initiated oxidation of m-xylene. *J. Photochem. Photobiol. A* **2005**, *176*, 199–207.

(50) Ng, N. L.; Kroll, J. H.; Chan, A. W. H.; Chhabra, P. S.; Flagan, R. C. et al. Secondary organic aerosol formation from m-xylene, toluene, and benzene. *Atmos. Chem. Phys.* **2007**, *7*, 3909–3922.

(51) Prenni, A. J.; Petters, M. D.; Kreidenweis, S. M.; DeMott, P. J.; Ziemann, P. J. Cloud droplet activation of secondary organic aerosol. *J. Geophys. Res.* **2007**, *112*, D10223.

(52) Park, K.; Kittelson, D. B.; Zachariah, M. R.; McMurry, P. H. Measurement of inherent material density of nanoparticle agglomerates. *J. Nanopart. Res.* **2004**, *6*, 267–272.

(53) Baron, P. A.; Willeke, K. *Aerosol Measurement — Principles, Techniques, and Applications*. 2nd ed. John Wiley & Sons: New York, USA, **2001**.

(54) DeCarlo, P. F.; Slowik, J. G.; Worsnop, D. R.; Davidovits, P.; Jimenez, J. L. Particle morphology and density characterization by combined mobility and aerodynamic diameter measurements. Part 1: Theory. *Aerosol Sci. Technol.* **2004**, *38*, 1185–1205.

(55) Kreidenweis, S. M.; Koehler, K.; DeMott, P. J.; Prenni, A. J.; Carrico, C. et al. Water activity and activation diameters from hygroscopicity data — Part I: Theory and application to inorganic salts. *Atmos. Chem. Phys.* **2005**, *5*, 1357–1370.

(56) Ramana, M. V.; Ramanathan, V.; Feng, Y.; Yoon, S. C.; Kim, S. W. et al. Warming influenced by the ratio of black carbon to sulphate and the black-carbon source. *Nature Geosci.* **2010**, *3*, 542–545.

(57) Zhang, R.; Jayne, J. T.; Molina, M. J. Heterogeneous interactions of nitryl hypochlorite and hydrogen chloride with sulfuric acid tetrahydrate: Implications for the stratosphere. *J. Phys. Chem.* **1994**, *98*, 867–874.

(58) Zhang, R.; Leu, M.; Taun; Molina, M. J. Formation of polar stratospheric clouds on preactivated background aerosols. *Geophys. Res. Lett.* **1996**, *23*, 1669–1672.

(59) Zhao, J.; Levitt, N. P.; Zhang, R. Heterogeneous chemistry of octanal and 2, 4-hexadienal with sulfuric acid. *Geophys. Res. Lett.* **2005**, *32*, L09802.

(60) Zhao, J.; Levitt, N. P.; Zhang, R.; Chen, J. Heterogeneous reactions of methylglyoxal in acidic media: Implications for secondary organic aerosol formation. *Environ. Sci. Technol.* **2006**, *40*, 7682–7687.

(61) Jacobson, M. Z. A physically-based treatment of elemental carbon optics: Implications for global direct forcing of aerosols. *Geophys. Res. Lett.* **2000**, *27*, 217–220.

(62) Moffet, R. C.; Prather, K. A. In-situ measurements of the mixing state and optical properties of soot with implications for radiative forcing estimates. *Proc. Natl. Acad. Sci. USA* **2009**, *106*, 11872–11877.

(63) Subramanian, R.; Kok, G. L.; Baumgardner, D.; Clarke, A.; Shinozuka, Y. et al. Black carbon over Mexico: The effect of atmospheric transport on mixing state, mass absorption cross-section, and BC/OC ratios. *Atmos. Chem. Phys.* **2010**, *10*, 219–237.

(64) Zhang, R.; Li, G.; Fan, J.; Wu, D. L.; Molina, M. J. Intensification of Pacific storm track linked to Asian pollution. *Proc. Natl. Acad. Sci. USA* **2007**, *104*, 5295–5299.

(65) Cape, J. N.; Cornell, S. E.; Jickells, T. D.; Nemitz, E. Organic nitrogen in the atmosphere - where does it come from? A review of sources and methods. *Atmos. Res.* **2011**, *102*, 30–48.

(66) Ge, X.; Wexler, A. S.; Clegg, S. L. Atmospheric amines — Part I. A review. *Atmos. Environ.* **2011**, *45*, 524–546.

(67) Tuazon, E. C.; Martin, P.; Aschmann, S. M.; Arey, J.; Atkinson, R. Kinetics of the reactions of OH radicals with 2-methoxy-6-(trifluoromethyl)pyridine, diethylamine, and 1,1,3,3,3-pentamethyldisiloxan-1-ol at 298 +/- 2 K. *Int. J. Chem. Kinet.* **2011**, *43*, 631–638.

(68) Karl, M.; Dye, C.; Schmidbauer, N.; Wisthaler, A.; Mikoviny, T. et al. Study of OH-initiated degradation of 2-aminoethanol. *Atmos. Chem. Phys.* **2012**, *12*, 1881–1901.

(69) Onel, L.; Blitz, M. A.; Seakins, P. W. Direct determination of the rate coefficient for the reaction of OH radicals with monoethanol amine (MEA) from 296 to 510 k. *J. Phys. Chem. Lett.* **2012**, *3*, 853–856.

(70) Murphy, S. M.; Sorooshian, A.; Kroll, J. H.; Ng, N. L.; Chhabra, P. et al. Secondary aerosol formation from atmospheric reactions of aliphatic amines. *Atmos. Chem. Phys.* **2007**, *7*, 2313–2337.

(71) Wang, L.; Lal, V.; Khalizov, A. F.; Zhang, R. Heterogeneous chemistry of alkylamines with sulfuric acid: Implications for atmospheric formation of alkylaminium sulfates. *Environ. Sci. Technol.* **2010**, *44*, 2461–2465.

(72) Lloyd, J. A.; Heaton, K. J.; Johnston, M. V. Reactive uptake of trimethylamine into ammonium nitrate particles. *J. Phys. Chem. A* **2009**, *113*, 4840–4843.

(73) Bzdek, B. R.; Ridge, D. P.; Johnston, M. V. Amine exchange into ammonium bisulfate and ammonium nitrate nuclei. *Atmos. Chem. Phys.* **2010**, *10*, 3495–3503.

(74) Berndt, T.; Stratmann, F.; Sipilä, M.; Vanhanen, J.; Petäjä, T. et al. Laboratory study on new particle formation from the reaction OH + SO_2: Influence of experimental conditions, H_2O vapour, NH_3 and the amine tert-butylamine on the overall process. *Atmos. Chem. Phys.* **2010**, *10*, 7101–7116.

(75) Erupe, M. E.; Viggiano, A. A.; Lee, S. H. The effect of trimethylamine on atmospheric nucleation involving H_2SO_4. *Atmos. Chem. Phys.* **2011**, *11*, 4767–4775.

(76) Yu, H.; McGraw, R.; Lee, S.-H. Effects of amines on formation of sub-3 nm particles and their subsequent growth. *Geophys. Res. Lett.* **2012**, *39*, L02807.

(77) Zollner, J. H.; Glasoe, W. A.; Panta, B.; Carlson, K. K.; McMurry, P. H. et al. Sulfuric acid nucleation: Power dependencies, variation with relative humidity, and effect of bases. *Atmos. Chem. Phys.* **2012**, *12*, 4399–4411.

(78) De Haan, D. O.; Tolbert, M. A.; Jimenez, J. L. Atmospheric condensed-phase reactions of glyoxal with methylamine. *Geophys. Res. Lett.* **2009**, *36*, L11819.

(79) Trainic, M.; Abo Riziq, A.; Lavi, A.; Rudich, Y. Role of interfacial water in the heterogeneous uptake of glyoxal by mixed glycine and ammonium sulfate aerosols. *J. Phys. Chem. A* **2012**, *116*, 5948–5957.

(80) Hanson, D. R.; McMurry, P. H.; Jiang, J.; Tanner, D.; Huey, L. G. Ambient pressure proton transfer mass spectrometry: Detection of amines and ammonia. *Environ. Sci. Technol.* **2011**, *45*, 8881–8888.

(81) Key, D.; Stihle, J.; Petit, J. E.; Bonnet, C.; Depernon, L. et al. Integrated method for the measurement of trace nitrogenous atmospheric bases. *Atmos. Meas. Tech.* **2011**, *4*, 2795–2807.

(82) Verriele, M.; Plaisance, H.; Depelchin, L.; Benchabane, S.; Locoge, N. et al. Determination of 14 amines in air samples using midget impingers sampling followed by analysis with ion chromatography in tandem with mass spectrometry. *J. Environ. Monit.* **2012**, *14*, 402–408.

(83) Samy, S.; Robinson, J.; Hays, M. D. An advanced LC-MS (Q-TOF) technique for the detection of amino acids in atmospheric aerosols. *Anal. Bioanal. Chem.* **2011**, *401*, 3103–3113.

(84) VandenBoer, T. C.; Markovic, M. Z.; Petroff, A.; Czar, M. F.; Borduas, N. et al. Ion chromatographic separation and quantitation of alkyl methylamines and ethylamines in atmospheric gas and particulate matter using preconcentration and suppressed conductivity detection. *J. Chromatogr. A* **2012**, *1252*, 74–83.

(85) Yu, H.; Lee, S.-H. Chemical ionisation mass spectrometry for the measurement of atmospheric amines. *Environ. Chem.* **2012**, *9*, 190–201.

(86) Smith, J. N.; Barsanti, K. C.; Friedli, H. R.; Ehn, M.; Kulmala, M. et al. Observations of aminium salts in atmospheric nanoparticles and possible climatic implications. *Proc. Natl. Acad. Sci. USA* **2010**, *107*, 6634–6639.

(87) Ruiz-Jimenez, J.; Parshintsev, J.; Laitinen, T.; Hartonen, K.; Riekkola, M.-L. et al. A complete methodology for the reliable collection, sample preparation, separation and determination of organic compounds in ultrafine 30 nm, 40 nm and 50 nm atmospheric aerosol particles. *Anal. Methods* **2011**, *3*, 2501–2509.

(88) Ozel, M. Z.; Ward, M. W.; Hamilton, J. F.; Lewis, A. C.; Raventos-Duran, T. et al. Analysis of organic nitrogen compounds in urban aerosol samples using GCxGC-TOF/MS. *Aerosol Sci. Technol.* **2010**, *44*, 109–116.

(89) Hildebrandt, L.; Kostenidou, E.; Lanz, V. A.; Prevot, A. S. H.; Baltensperger, U. et al. Sources and atmospheric processing of organic aerosol in the mediterranean: Insights from aerosol mass spectrometer factor analysis. *Atmos. Chem. Phys.* **2011**, *11*, 12499–12515.

(90) Huang, Y.; Chen, H.; Wang, L.; Yang, X.; Chen, J. Single particle analysis of amines in ambient aerosol in Shanghai. *Environ. Chem.* **2012**, *9*, 202–210.

(91) Zhang, G.; Bi, X.; Chan, L. Y.; Li, L.; Wang, X. et al. Enhanced trimethylamine-containing particles during fog events detected by single particle aerosol mass spectrometry in urban Guangzhou, China. *Atmos. Environ.* **2012**, *55*, 121–126.

(92) Miyazaki, Y.; Kawamura, K.; Jung, J.; Furutani, H.; Uematsu, M. Latitudinal distributions of organic nitrogen and organic carbon in marine aerosols over the western North Pacific. *Atmos. Chem. Phys.* **2011**, *11*, 3037–3049.

(93) Rehbein, P. J. G.; Jeong, C. H.; McGuire, M. L.; Yao, X. H.; Corbin, J. C. et al. Cloud and fog processing enhanced gas-to-particle partitioning of trimethylamine. *Environ. Sci. Technol.* **2011**, *45*, 4346–4352.

(94) VandenBoer, T. C.; Petroff, A.; Markovic, M. Z.; Murphy, J. G. Size distribution of alkyl amines in continental particulate matter and their online detection in the gas and particle phase. *Atmos. Chem. Phys.* **2011**, *11*, 4319–4332.

(95) Jeong, C. H.; McGuire, M. L.; Godri, K. J.; Slowik, J. G.; Rehbein, P. J. G. et al. Quantification of aerosol chemical composition using continuous single particle measurements. *Atmos. Chem. Phys.* **2011**, *11*, 7027–7044.

(96) Zamora, L. M.; Prospero, J. M.; Hansell, D. A. Organic nitrogen in aerosols and precipitation at Barbados and Miami: Implications regarding sources, transport and deposition to the western subtropical North Atlantic. *J. Geophys. Res.* **2011**, *116*, D20309.

(97) Lin, M.; Walker, J.; Geron, C.; Khlystov, A. Organic nitrogen in PM2.5 aerosol at a forest site in the Southeast U.S. *Atmos. Chem. Phys.* **2010**, *10*, 2145–2157.

(98) Docherty, K. S.; Aiken, A. C.; Huffman, J. A.; Ulbrich, I. M.; DeCarlo, P. F. et al. The 2005 study of organic aerosols at riverside (SOAR-1): Instrumental intercomparisons and fine particle composition. *Atmos. Chem. Phys.* **2011**, *11*, 12387–12420.

(99) Mandalakis, M.; Apostolaki, M.; Tziaras, T.; Polymenakou, P.; Stephanou, E. G. Free and combined amino acids in marine background atmospheric aerosols over the Eastern Mediterranean. *Atmos. Environ.* **2011**, *45*, 1003–1009.

(100) Barbaro, E.; Zangrando, R.; Moret, I.; Barbante, C.; Cescon, P. et al. Free amino acids in atmospheric particulate matter of Venice, Italy. *Atmos. Environ.* **2011**, *45*, 5050–5057.

(101) Ruiz-Jimenez, J.; Parshintsev, J.; Laitinen, T.; Hartonen, K.; Petaejae, T. et al. Influence of the sampling site, the season of the year, the particle size and the number of nucleation events on the chemical composition of atmospheric ultrafine and total suspended particles. *Atmos. Environ.* **2012**, *49*, 60–68.

(102) Yue, D. L.; Hu, M.; Zhang, R. Y.; Wang, Z. B.; Zheng, J. et al. The roles of sulfuric acid in new particle formation and growth in the mega-city of Beijing. *Atmos. Chem. Phys.* **2010**, *10*, 4953–4960.

(103) Yu, F.; Turco, R. P. From molecular clusters to nanoparticles: Role of ambient ionization in tropospheric aerosol formation. *J. Geophys. Res.* **2001**, *106*, 4797–4814.

(104) Loukonen, V.; Kurtén, T.; Ortega, I. K.; Vehkamäki, H.; Pádua, A. A. H. et al. Enhancing effect of dimethylamine in sulfuric acid nucleation in the presence of water – a computational study. *Atmos. Chem. Phys.* **2010**, *10*, 4961–4974.

(105) Nadykto, A.; Yu, F.; Jakovleva, M.; Herb, J.; Xu, Y. Amines in the Earth's atmosphere: A density functional theory study of the thermochemistry of pre-nucleation clusters. *Entropy* **2011**, *13*, 554–569.

(106) Kirkby, J.; Curtius, J.; Almeida, J.; Dunne, E.; Duplissy, J. et al. Role of sulphuric acid, ammonia and galactic cosmic rays in atmospheric aerosol nucleation. *Nature* **2011**, *476*, 429–433.

(107) Kuang, C.; Chen, M.; McMurry, P. H.; Wang, J. Modification of laminar flow ultrafine condensation particle counters for the enhanced detection of 1 nm condensation nuclei. *Aerosol Sci. Technol.* **2011**, *46*, 309–315.

(108) Vanhanen, J.; Mikkilä, J.; Lehtipalo, K.; Sipilä, M.; Manninen, H. E. et al. Particle size magnifier for nano-CN detection. *Aerosol Sci. Technol.* **2011**, *45*, 533–542.

(109) Nadykto, A. B.; Yu, F. Strong hydrogen bonding between atmospheric nucleation precursors and common organics. *Chem. Phys. Lett.* **2007**, *435*, 14–18.

(110) Zhao, J.; Khalizov, A.; Zhang, R.; McGraw, R. Hydrogen-bonding interaction in molecular complexes and clusters of aerosol nucleation precursors. *J. Phys. Chem. A* **2009**, *113*, 680–689.

(111) Zhao, J.; Smith, J. N.; Eisele, F. L.; Chen, M.; Kuang, C. et al. Observation of neutral sulfuric acid-amine containing clusters in laboratory and ambient measurements. *Atmos. Chem. Phys.* **2011**, *11*, 10823–10836.

(112) Bzdek, B. R.; Ridge, D. P.; Johnston, M. V. Size-dependent reactions of ammonium bisulfate clusters with dimethylamine. *J. Phys. Chem. A* **2010**, *114*, 11638–11644.

(113) Bzdek, B. R.; Ridge, D. P.; Johnston, M. V. Amine reactivity with charged sulfuric acid clusters. *Atmos. Chem. Phys.* **2011**, *11*, 8735–8743.

(114) DePalma, J. W.; Bzdek, B. R.; Doren, D. J.; Johnston, M. V. Structure and energetics of nanometer size clusters of sulfuric acid with ammonia and dimethylamine. *J. Phys. Chem. A* **2011**, *116*, 1030–1040.

(115) Anslyn, E. V.; Dougherty, D. A. *Modern Physical Organic Chemistry*. 1st ed. University Science: Herdon, VA, USA, **2005**.

(116) Zhao, J.; Zhang, R.; Fortner, E. C.; North, S. W. Quantification of hydroxycarbonyls from OH−isoprene reactions. *J. Am. Chem. Soc.* **2004**, *126*, 2686–2687.

(117) Liggio, J.; Li, S.-M.; McLaren, R. Heterogeneous reactions of glyoxal on particulate matter: Identification of acetals and sulfate esters. *Environ. Sci. Technol.* **2005**, *39*, 1532–1541.

(118) Galloway, M. M.; Chhabra, P. S.; Chan, A. W. H.; Surratt, J. D.; Flagan, R. C. et al. Glyoxal uptake on ammonium sulphate seed aerosol: Reaction products and reversibility of uptake under dark and irradiated conditions. *Atmos. Chem. Phys.* **2009**, *9*, 3331–3345.

(119) Wang, X.; Gao, S.; Yang, X.; Chen, H.; Chen, J. et al. Evidence for high molecular weight nitrogen-containing organic salts in urban aerosols. *Environ. Sci. Technol.* **2010**, *44*, 4441–4446.

(120) Trainic, M.; Abo Riziq, A.; Lavi, A.; Flores, J. M.; Rudich, Y. The optical, physical and chemical properties of the products of glyoxal uptake on ammonium sulfate seed aerosols. *Atmos. Chem. Phys.* **2011**, *11*, 9697–9707.

(121) Zahardis, J.; Geddes, S.; Petrucci, G. A. The ozonolysis of primary aliphatic amines in fine particles. *Atmos. Chem. Phys.* **2008**, *8*, 1181–1194.

(122) Shiraiwa, M.; Ammann, M.; Koop, T.; Pöschl, U. Gas uptake and chemical aging of semisolid organic aerosol particles. *Proc. Natl. Acad. Sci. USA* **2011**, *In press*, DOI: 10.1073/pnas.1103045108.

(123) Molina, M. J.; Molina, L. T.; Zhang, R.; Meads, R. F.; Spencer, D. D. The reaction of $ClONO_2$ with HCl on aluminum oxide. *Geophys. Res. Lett.* **1997**, *24*, 1619–1622.

(124) Zhang, D.; Zhang, R. Y. Laboratory investigation of heterogeneous interaction of sulfuric acid with soot. *Environ. Sci. Technol.* **2005**, *39*, 5722–5728.

(125) Levitt, N. P.; Zhang, R.; Xue, H.; Chen, J. Heterogeneous chemistry of organic acids on soot surfaces. *J. Phys. Chem. A* **2007**, *111*, 4804–4814.

(126) Landis, M. S.; Stevens, R. K.; Schaedlich, F.; Prestbo, E. M. Development and characterization of an annular denuder methodology for the measurement of divalent inorganic reactive gaseous mercury in ambient air. *Environ. Sci. Technol.* **2002**, *36*, 3000–3009.

(127) Fortner, E. C.; Zhao, J.; Zhang, R. Development of ion drift-chemical ionization mass spectrometry. *Anal. Chem.* **2004**, *76*, 5436–5440.

(128) Nowak, J. B.; Neuman, J. A.; Kozai, K.; Huey, L. G.; Tanner, D. J. et al. A chemical ionization mass spectrometry technique for airborne measurements of ammonia. *J. Geophys. Res.* **2007**, *112*, D10S02.

(129) von Bobrutzki, K.; Braban, C. F.; Famulari, D.; Jones, S. K.; Blackall, T. et al. Field inter-comparison of eleven atmospheric ammonia measurement techniques. *Atmos. Meas. Tech.* **2010**, *3*, 91–112.

(130) Gershenzon, Y. M.; Grigorieva, V. M.; Ivanov, A. V.; Remorov, R. G. O_3 and OH sensitivity to heterogeneous sinks of HO and CH_3O_2 on aerosol particles. *Faraday Discuss.* **1995**, *100*, 83–100.

(131) Hanson, D. R.; Burkholder, J. B.; Howard, C. J.; Ravishankara, A. R. Measurement of hydroxyl and hydroperoxy radical uptake coefficients on water and sulfuric acid surfaces. *J. Phys. Chem.* **1992**, *96*, 4979–4985.

(132) Fuller, E. N.; Schettler, P. D.; Giddings, J. C. New method for prediction of binary gas-phase diffusion coefficients. *Ind. Eng. Chem.* **1966**, *58*, 18–27.

(133) Szekely, J.; Evans, J. W.; Sohn, H. Y. *Gas-solid Reactions*. Academic Press: New York, USA, **1976**.

(134) Nelmes, R. An x-ray diffraction determination of the crystal structure of ammonium hydrogen sulphate above the ferroelectric transition. *Acta Crystallogr. B* **1971**, *27*, 272–281.

(135) Cooper, P. L.; Abbatt, J. P. D. Heterogeneous interactions of OH and HO_2 radicals with surfaces characteristic of atmospheric particulate matter. *J. Phys. Chem.* **1996**, *100*, 2249–2254.

(136) Remorov, R. G.; Bardwell, M. W. Model of uptake of OH radicals on nonreactive solids. *J. Phys. Chem. B* **2005**, *109*, 20036–20043.

(137) Tang, I. N.; Munkelwitz, H. R. Water activities, densities, and refractive indices of aqueous sulfates and sodium nitrate droplets of atmospheric importance. *J. Geophys. Res.* **1994**, *99*, 18801–18808.

(138) Davidovits, P.; Kolb, C. E.; Williams, L. R.; Jayne, J. T.; Worsnop, D. R. Mass accommodation and chemical reactions at gas−liquid interfaces. *Chem. Rev.* **2006**, *106*, 1323–1354.

(139) Liu, Y.; Han, C.; Liu, C.; Ma, J.; Ma, Q. et al. Differences in the reactivity of ammonium salts with methylamine. *Atmos. Chem. Phys.* **2012**, *12*, 4855–4865.

(140) Chan, L. P.; Chan, C. K. Displacement of ammonium from aerosol particles by uptake of triethylamine. *Aerosol Sci. Technol.* **2011**, *46*, 236–247.

(141) Angelino, S.; Suess, D. T.; Prather, K. A. Formation of aerosol particles from reactions of secondary and tertiary alkylamines: Characterization by aerosol time-of-flight mass spectrometry. *Environ. Sci. Technol.* **2001**, *35*, 3130–3138.

(142) Sorooshian, A.; Murphy, S. M.; Hersey, S.; Gates, H.; Padro, L. T. et al. Comprehensive airborne characterization of aerosol from a major bovine source. *Atmos. Chem. Phys.* **2008**, *8*, 5489–5520.

(143) Smith, J. N.; Dunn, M. J.; VanReken, T. M.; Iida, K.; Stolzenburg, M. R. et al. Chemical composition of atmospheric nanoparticles formed from nucleation in Tecamac, Mexico: Evidence for an important role for organic species in nanoparticle growth. *Geophys. Res. Lett.* **2008**, *35*, L04808.

(144) Tereshchenko, O. V.; Tereshchenko, A. G.; Shlyafer, I. V.; Khlevnoi, I. S.; Shved, V. S. et al. Effect of monomethylamine sulfate addition on the caking tendency of ammonium sulfate. *Coke Chem. USSR* **1985**, *28*, 23–26.

(145) Kristensson, A.; Rosenorn, T.; Bilde, M. Cloud droplet activation of amino acid aerosol particles. *J. Phys. Chem. A* **2010**, *114*, 379–386.

(146) Salo, K.; Westerlund, J.; Andersson, P. U.; Nielsen, C.; D'Anna, B. et al. Thermal characterization of aminium nitrate nanoparticles. *J. Phys. Chem. A* **2011**, *115*, 11671–11677.

(147) Greaves, T. L.; Weerawardena, A.; Fong, C.; Krodkiewska, I.; Drummond, C. J. Protic ionic liquids: Solvents with tunable phase behavior and physicochemical properties. *J. Phys. Chem. B* **2006**, *110*, 22479–22487.

(148) Nakamoto, H.; Watanabe, M. Bronsted acid-base ionic liquids for fuel cell electrolytes. *Chem. Commun.* **2007**, 2539–2541.

(149) Greaves, T. L.; Weerawardena, A.; Krodkiewska, I.; Drummond, C. J. Protic ionic liquids: Physicochemical properties and behavior as amphiphile self-assembly solvents. *J. Phys. Chem. B* **2008**, *112*, 896–905.

(150) Andreae, M. O.; Gelencsér, A. Black carbon or brown carbon? The nature of light-absorbing carbonaceous aerosols. *Atmos. Chem. Phys.* **2006**, *6*, 3131–3148.

(151) Moosmüller, H.; Chakrabarty, R. K.; Arnott, W. P. Aerosol light absorption and its measurement: A review. *J. Quant. Spectrosc. Radiat. Transfer* **2009**, *110*, 844–878.

(152) Zarzana, K. J.; De Haan, D. O.; Freedman, M. A.; Hasenkopf, C. A.; Tolbert, M. A. Optical properties of the products of α-dicarbonyl and amine reactions in simulated cloud droplets. *Environ. Sci. Technol.* **2012**, *46*, 4845–4851.

(153) Tans, A. M. P. A new type of nomogram: Aqueous ammonium sulfate solutions. *Ind. Eng. Chem.* **1958**, *50*, 971–972.

(154) Stelson, A. W.; Seinfeld, J. H. Prediction of the density of ammonium bisulfate solutions. *J. Phys. Chem.* **1981**, *85*, 3730–3733.

(155) Kiyoura, R.; Urano, K. Mechanism, kinetics, and equilibrium of thermal decomposition of ammonium sulfate. *Ind. Eng. Chem. Proc. Des. Dev.* **1970**, *9*, 489–494.

(156) Zhang, R.; Khalizov, A.; Wang, L.; Hu, M.; Xu, W. Nucleation and growth of nanoparticles in the atmosphere. *Chem. Rev.* **2012**, *112*, 1957–2011.

(157) Vilminot, S.; Cot, L.; Avinens, C.; Maurin, M. Existence and comparative crystallography of hydroxylammonium and monomethylammonium sulfates and orthofluoroberyllates. *Mater. Res. Bull.* **1971**, *6*, 189–197.

(158) Haynes, W. M. *CRC Handbook of Chemistry and Physics*. 92nd ed. CRC Press/ Talyor and Francis: Boca Raton, FL, USA, **2011**.

(159) Stammler, M. Polymorphism of salts containing complex ions—I: The halides of ammonium and methyl-substituted ammonium. *J. Inorg. Nucl. Chem.* **1967**, *29*, 2203–2221.

(160) O'Neil, M. J.; Heckelman, P. E.; Koch, C. B.; Roman, K. J. *The Merck Index: An Encyclopedia of Chemicals, Drugs, and Biologicals*. 14th ed. Merck: Whitehouse Station, NJ, USA, **2006**.

(161) Levitt, N. P.; Zhao, J.; Zhang, R. Heterogeneous chemistry of butanol and decanol with sulfuric acid: Implications for secondary organic aerosol formation. *J. Phys. Chem. A* **2006**, *110*, 13215–13220.

(162) Charlson, R. J.; Vanderpol, A. H.; Covert, D. S.; Waggoner, A. P.; Ahlquist, N. C. $H_2SO_4/(NH_4)_2SO_4$ background aerosol: Optical detection in St. Louis region. *Atmos. Environ.* **1974**, *8*, 1257–1267.

(163) Pratt, K. A.; Hatch, L. E.; Prather, K. A. Seasonal volatility dependence of ambient particle phase amines. *Environ. Sci. Technol.* **2009**, *43*, 5276–5281.

(164) Sorooshian, A.; Ng, N. L.; Chan, A. W. H.; Feingold, G.; Flagan, R. C. et al. Particulate organic acids and overall water-soluble aerosol composition measurements from the 2006 Gulf of Mexico atmospheric composition and climate study (GOMACCS). *J. Geophys. Res.* **2007**, *112*, D13201.

(165) Facchini, M. C.; Decesari, S.; Rinaldi, M.; Carbone, C.; Finessi, E. et al. Important source of marine secondary organic aerosol from biogenic amines. *Environ. Sci. Technol.* **2008**, *42*, 9116–9121.

(166) Schade, G. W.; Crutzen, P. J. Emission of aliphatic amines from animal husbandry and their reactions: Potential source of N_2O and HCN. *J. Atmos. Chem.* **1995**, *22*, 319–346.